# STEM-EDS sur échantillon mince et Microanalyse du Li

***Pr. Raynald Gauvin***, Ph.D.
Nicolas Brodusch, M.Sc.A
Stéphanie Bessette, M.Sc.A

McGill

Montréal, Québec, Canada.

# Microanalyse des Films Minces Sans Absorption et Fluorescence

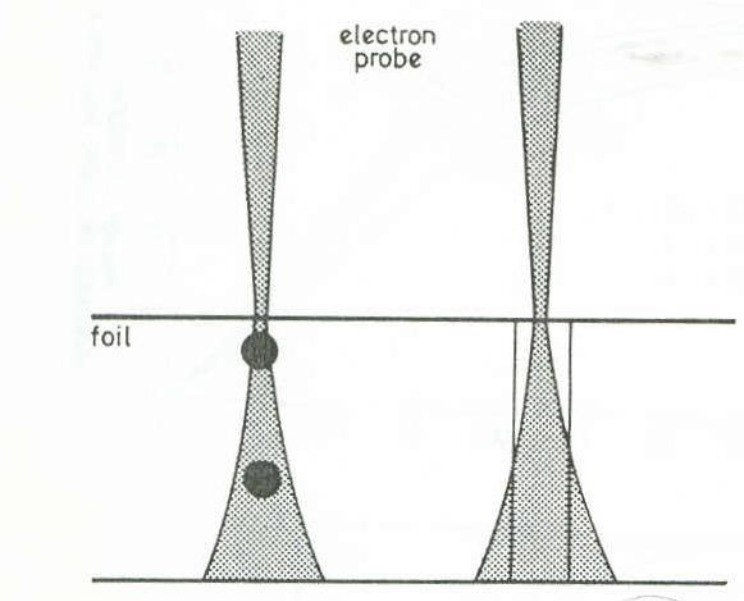


$$I_A = \left(\frac{\Omega}{4\pi}\right) D_e \frac{Q_A \varpi_A \alpha_A \varepsilon_A}{A_A} N_0 \rho t C_A$$

$$D_e = \frac{it^*}{e}$$

# Cliff and Lorimer (1975)

$$\frac{C_A}{C_B} = K_{AB}\frac{I_A}{I_B}$$

$$C_A + C_B = 1$$

Pas de besoin de mesurer le courant.

Pas de besoin de mesurer l'épaisseur si l'absorption est négligeable.

$K_{AB}$ mesuré expérimentalement.

# Goldstein, Costley, Lorimer and Reed (1977)

$$K_{AB} = \frac{Q_B \varpi_B \alpha_B \varepsilon_B A_A}{Q_A \varpi_A \alpha_A \varepsilon_A A_B}$$

Les facteurs $K_{AB}$ mesurés expérimentalement sont beaucoup plus précis que ceux calculés.

*Journal of Microscopy*, *Vol.* 163, *Pt* 3, *September* 1991, *pp.* 295–306. ADONIS002272091001O9W
*Received* 5 *August* 1988; *revised* 7 *November* 1990; *accepted* 20 *December* 1990

# Determination of the $C_{nl}$ parameter in the Bethe formula for the ionization cross-section by the use of Cliff–Lorimer $K_{AB}$ factors obtained at different accelerating voltages in a TEM

*by* R. GAUVIN* *and* G. L'ESPÉRANCE, *Center for Characterization and Microscopy of Materials, Department of Metallurgical Engineering, École Polytechnique de Montréal, Box* 6079, *Station A, Montréal, Québec, Canada H3C 3A7*

$$R = \frac{(K_{AB})^{E_2}}{(K_{AB})^{E_1}} = \left(\frac{Q_B}{Q_A}\right)^{E_2} \left(\frac{Q_B}{Q_A}\right)^{E_1}$$

# Ratio des Facteurs $K_{AB}$

$$Q = 6.51 \times 10^{-20} z_{nl} b_{nl} \frac{ln(c_{nl}\, U)}{(E_{nl})^2 U} \quad (cm^2)$$

$$U = \frac{E_0}{E_{nl}}$$

$$c_{nl} = exp\left(\sqrt{\frac{\psi^2}{4} - \frac{R\alpha - \beta}{R-1}} - \frac{\psi}{2}\right)$$

$$\psi = ln\left(U_B^{E_1} U_A^{E_2}\right) = ln\left(U_B^{E_2} U_A^{E_1}\right)$$

$$\alpha = ln\left(U_B^{E_1}\right) ln\left(U_A^{E_2}\right)$$

$$\beta = ln\left(U_B^{E_2}\right) ln\left(U_A^{1}\right)$$

**Table 1.** $C_k$ calculated from Eqs. (3) and (9)–(12) using experimental $K_{AB}$ factors obtained by Schreiber & Wims (1981) at 100 and 200 kV.

| $K_{AB}$ | $R_{AB}^{100-200}$ | $C_k$ |
|---|---|---|
| Zn–S | 0·91 | 0·90 |
| Cd–S | 0·67 | 0·62 |
| Ba–S | 0·61 | 0·76 |
| | | Average 0·76 |

$$\frac{Q_B}{Q_A} \cong \frac{ln(c_{nl}U_B)}{ln(c_{nl}U_A)}\left(\frac{E_{nl}^B}{E_{nl}^A}\right)^2 \frac{U_A}{U_B}$$

Microsc. Microanal. 18, 915–940, 2012
doi:10.1017/S1431927612001468

Microscopy AND Microanalysis



REVIEW ARTICLE

# What Remains to Be Done to Allow Quantitative X-Ray Microanalysis Performed with EDS to Become a True Characterization Technique?

Raynald Gauvin*

*Department of Materials Engineering, McGill University, M.H. Wong Building, 3610 University Street, Montréal, Québec H3A 2B2, Canada*

# Watanabe et Williams (2006)
# Les Zeta Factors

$$\zeta_A = \frac{A_A}{N_0 Q_A \varpi_A \alpha_A \varepsilon_A \left(\frac{\Omega}{4\pi}\right)} = \frac{C_A D_e \rho t}{I_A}$$

$$K_{AB} = \frac{\zeta_A}{\zeta_B}$$

# Watanabe et Williams (2006)
# Les 3 Équations

Avec $C_A + C_B = 1$

$$\rho t = \frac{\zeta_A I_A + \zeta_B I_B}{D_e}$$

$$C_A = \frac{\zeta_A I_A}{\zeta_A I_A + \zeta_B I_B} \; et \; C_B = \frac{\zeta_B I_B}{\zeta_A I_A + \zeta_B I_B}$$

# Watanabe (2016) sur la correction d'absorption

In Chap. 35 of W&C, different approaches to quantitative X-ray
analysis are described for thin specimens in the AEM. Since the
development of the ratio method by Cliff and Lorimer (**1995**),
this particular method has become the standard approach and
is widely used due to its simplicity. Unfortunately, even in thin specimens, X-ray absorption may need to be corrected for
quantification and **the simple Cliff–Lorimer approach is found
wanting**.

Philibert (1962)

$$A = \frac{\left.\frac{\mu}{\rho}\right|_{Spec}^{i} \rho t \operatorname{cosec}\psi}{1 - e^{-\left.\frac{\mu}{\rho}\right|_{Spec}^{i} \rho t \operatorname{cosec}\psi}}$$

# Goldstein, Costley, Lorimer and Reed (1977)

$$\frac{C_A}{C_B} = K_{AB} \frac{\int_0^{\rho t} \varphi(\rho z)_B e^{-\chi_B \rho z} d\rho z}{\int_0^{\rho t} \varphi(\rho z)_A e^{-\chi_A \rho z} d\rho z} \frac{I_A}{I_B}$$

$$\chi_i = \frac{\mu}{\rho}\Big|_{Spec}^{i} cosec\psi$$

# Goldstein, Costley, Lorimer and Reed (1977)

$$\varphi(\rho z)_A = \varphi(\rho z)_A \cong 1$$

$$\frac{C_A}{C_B} = K_{AB} A_G \frac{I_A}{I_B}$$

$$A_G = \frac{\left.\frac{\mu}{\rho}\right|_{Spec}^{A}}{\left.\frac{\mu}{\rho}\right|_{Spec}^{B}} \left[\frac{1 - e^{-\chi_B \rho t}}{1 - e^{-\chi_A \rho t}}\right]$$

# 50 B - 50 Fe (%At.), 10 000 000 e

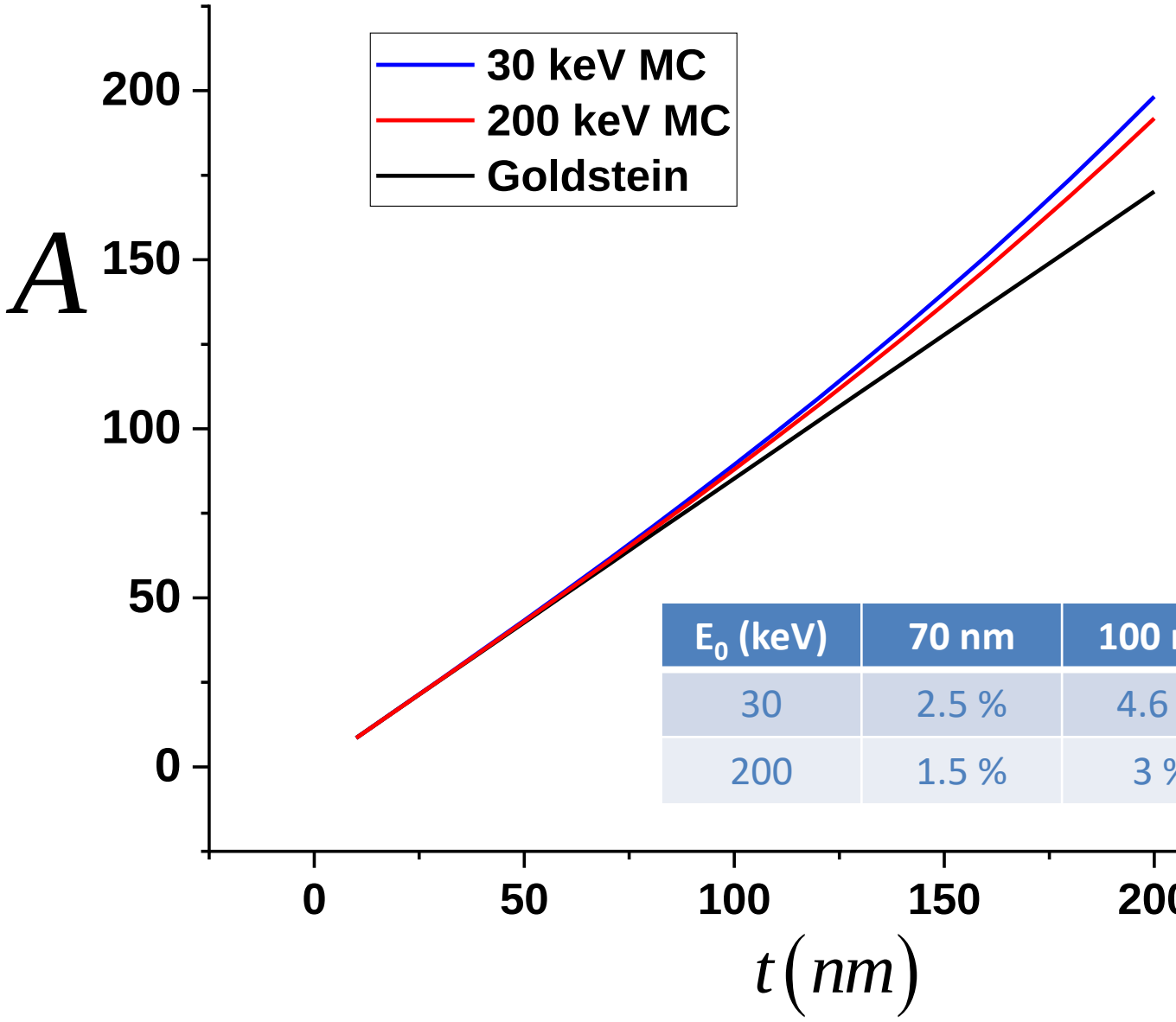


| $E_0$ (keV) | 70 nm | 100 nm | 200 nm |
|---|---|---|---|
| 30 | 2.5 % | 4.6 % | 14.2 % |
| 200 | 1.5 % | 3 % | 11 % |

# Les Zeta Factors et Cliff and Lorimer

$$\frac{C_A}{C_B} = K_{AB}\frac{I_A}{I_B}$$

$$\frac{C_A}{1 - C_A} = K_{AB}\frac{I_A}{I_B}$$

$$C_A = \frac{1}{1 + K_{BA}\frac{I_B}{I_A}}$$

$$C_A = \frac{\zeta_A I_A}{\zeta_A I_A + \zeta_B I_B}$$

# Quantitative X-Ray Microanalysis

$$\frac{C_i}{C_{(i)}} = Z_i A_i F_i \frac{I_i}{I_{(i)}}$$

$$Z_i = \frac{\int_0^\infty \varphi(\rho z)_{(i)} d\rho z}{\int_0^\infty \varphi(\rho z)_i \, d\rho z}$$

$$A_i = \frac{f(\chi_{(i)})}{f(\chi_i)}$$

$$f(\chi_i) = \frac{\int_0^\infty \varphi(\rho z)_i e^{-\chi_i \rho z} d\rho z}{\int_0^\infty \varphi(\rho z)_i d\rho z}$$

$$F_i = \frac{\left(1 + \left\{\sum_{j=1}^{m} f_{c,j}\right\} + f_{Br}\right)_{(i)}}{\left(1 + \left\{\sum_{j=1}^{m} f_{c,j}\right\} + f_{Br}\right)_i}$$

# The f Ratio Method

$$f_A = \frac{I_A}{I_A + I_B}$$

P. Horny, E. Lifshin, H. Campbell and R. Gauvin (2010), “Development of a New Quantitative X-Ray Microanalysis Method for Electron Microscopy”, Microscopy & Microanalysis, Vol. 16, No. 6, pp. 821-830.

# The f Ratio Method

$$f_A = \frac{I_A}{I_A + I_B}$$

$$f_A = \frac{1}{1 + \frac{I_B}{I_A}} = \frac{1}{1 + K_{AB}\frac{(1 - C_A)}{C_A}}$$

$$C_A = \frac{1}{\frac{f_B}{f_A}K_{BA} + 1} = \frac{\zeta_A I_A}{\zeta_A I_A + \zeta_B I_B}$$

# The f Ratio Method

Microsc. Microanal. 18, 915–940, 2012
doi:10.1017/S1431927612001468

Microscopy AND Microanalysis



REVIEW ARTICLE

## What Remains to Be Done to Allow Quantitative X-Ray Microanalysis Performed with EDS to Become a True Characterization Technique?

Raynald Gauvin*

# f Ratio Method

# Standardless

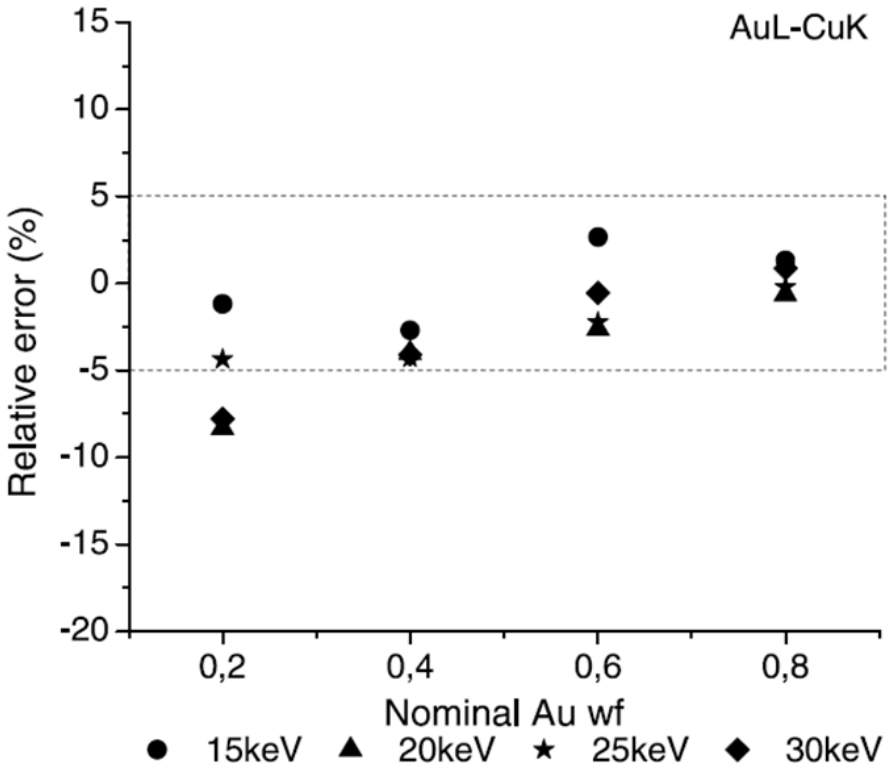


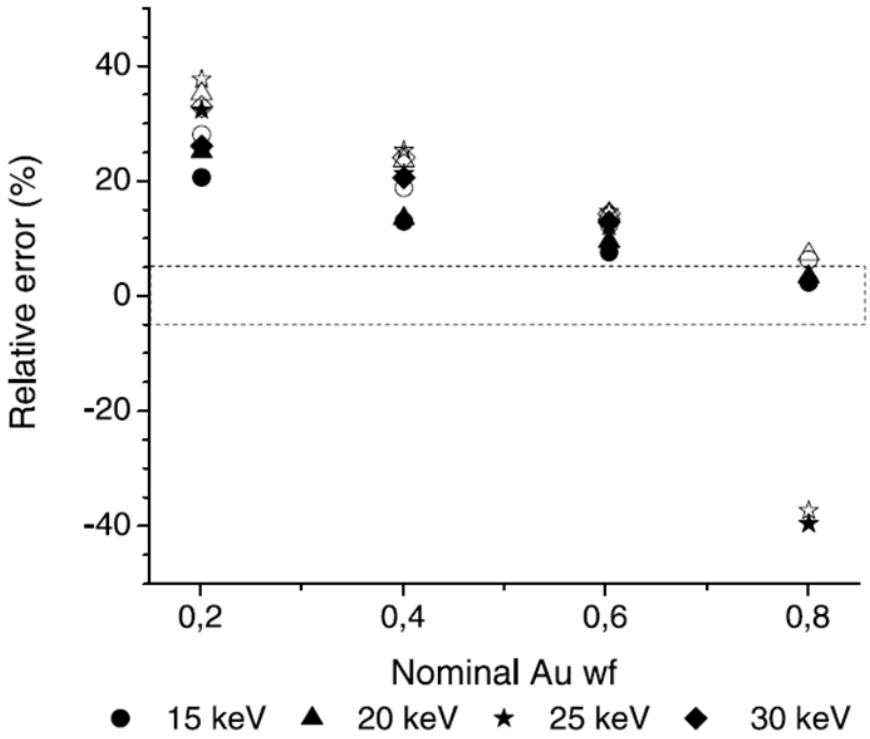


P. Horny, E. Lifshin, H. Campbell and R. Gauvin (2010), “Development of a New Quantitative X-Ray Microanalysis Method for Electron Microscopy”, Microscopy & Microanalysis, Vol. 16, No. 6, pp. 821-830.

# Cold Field Scanning Electron Microscopes, Gauvin's Group

**Hitachi SU-8000 (2010)**

0.5 nm at 30 keV
2 nm at 0.2 keV

**Hitachi SU-8230 (2014)**

0.4 nm at 30 keV,
1.8 nm at 0.2 keV

# Quantitative X-ray mapping of Mg-Al-Zn casting alloy

BSE images

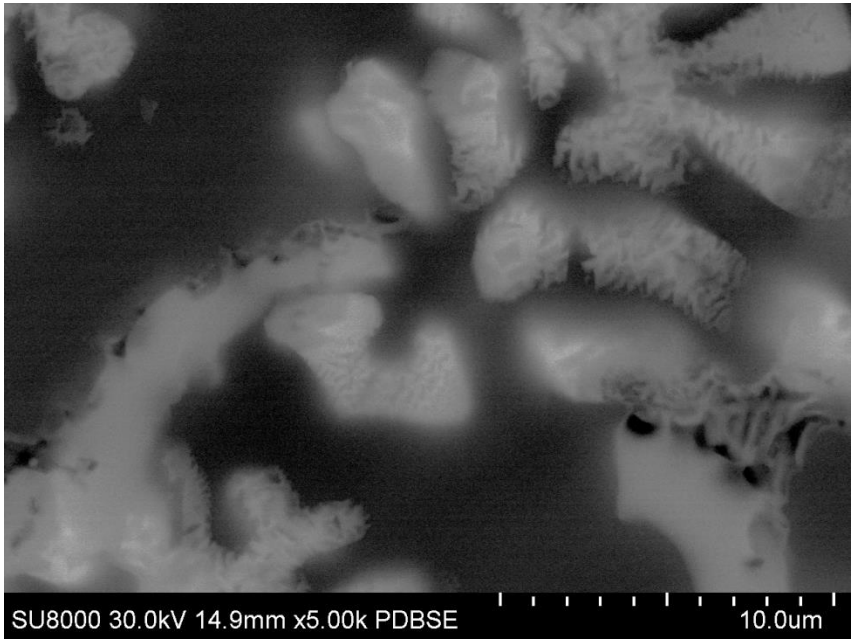


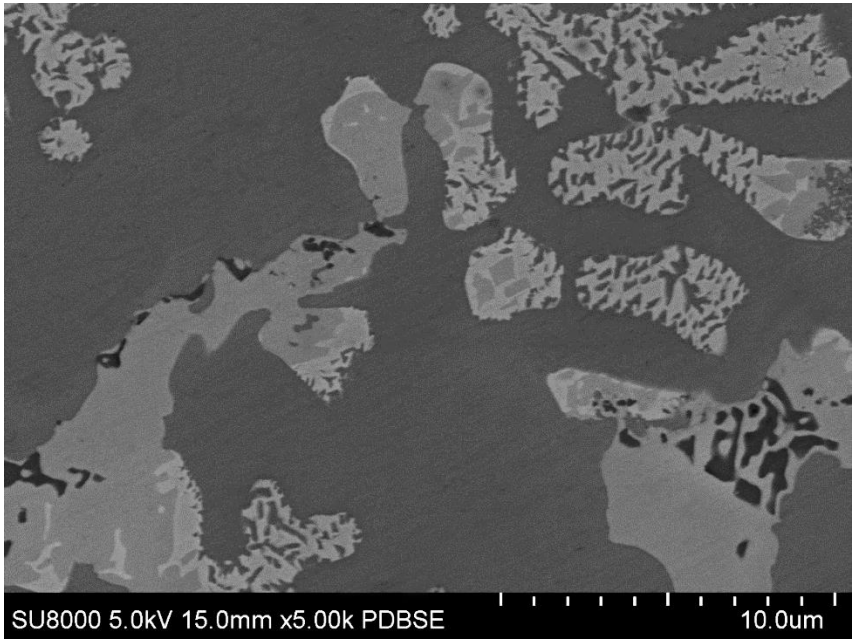


30 kV

5 kV

# High Resolution X-ray mapping 5 keV

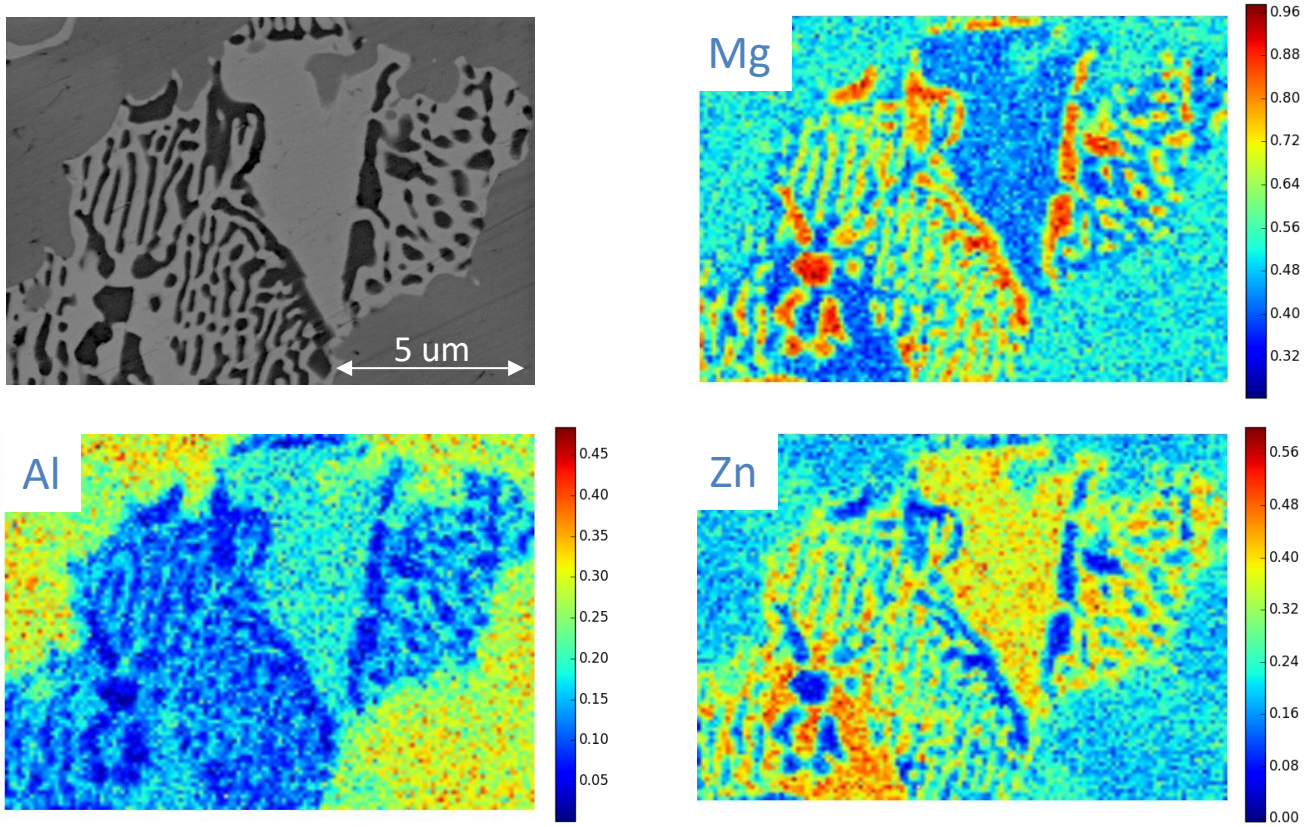


C. Teng, H. Demers, X. Chu, R. Gauvin (2019),Microscopy and Microanalysis, 25, (1), pp. 58-69.

# SU-9000EA STEM (2017)


# SU-9000EA STEM (2017)

- Premier au Monde avec EELS 30 keV fabriqué par Hitachi – Naka Factory.
  - Détection du Li
- EDS SDD Extreme Detector de Oxford:
  - Détection du Li
  - 0.7 Sr d'angle solide
  - TOA 16 Degrés

# $Fe_2O_3$ Nanocubes

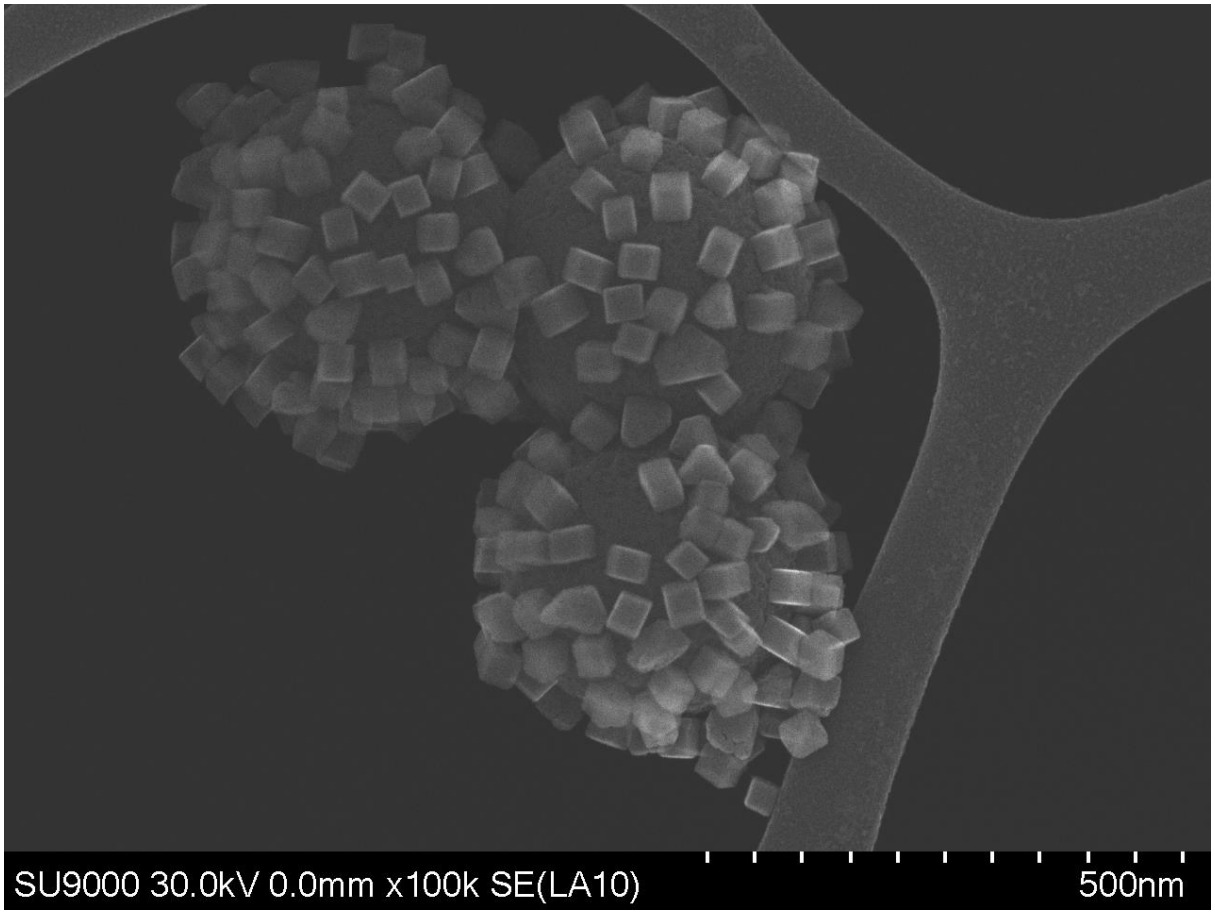

# $Fe_2O_3$ Nanocubes

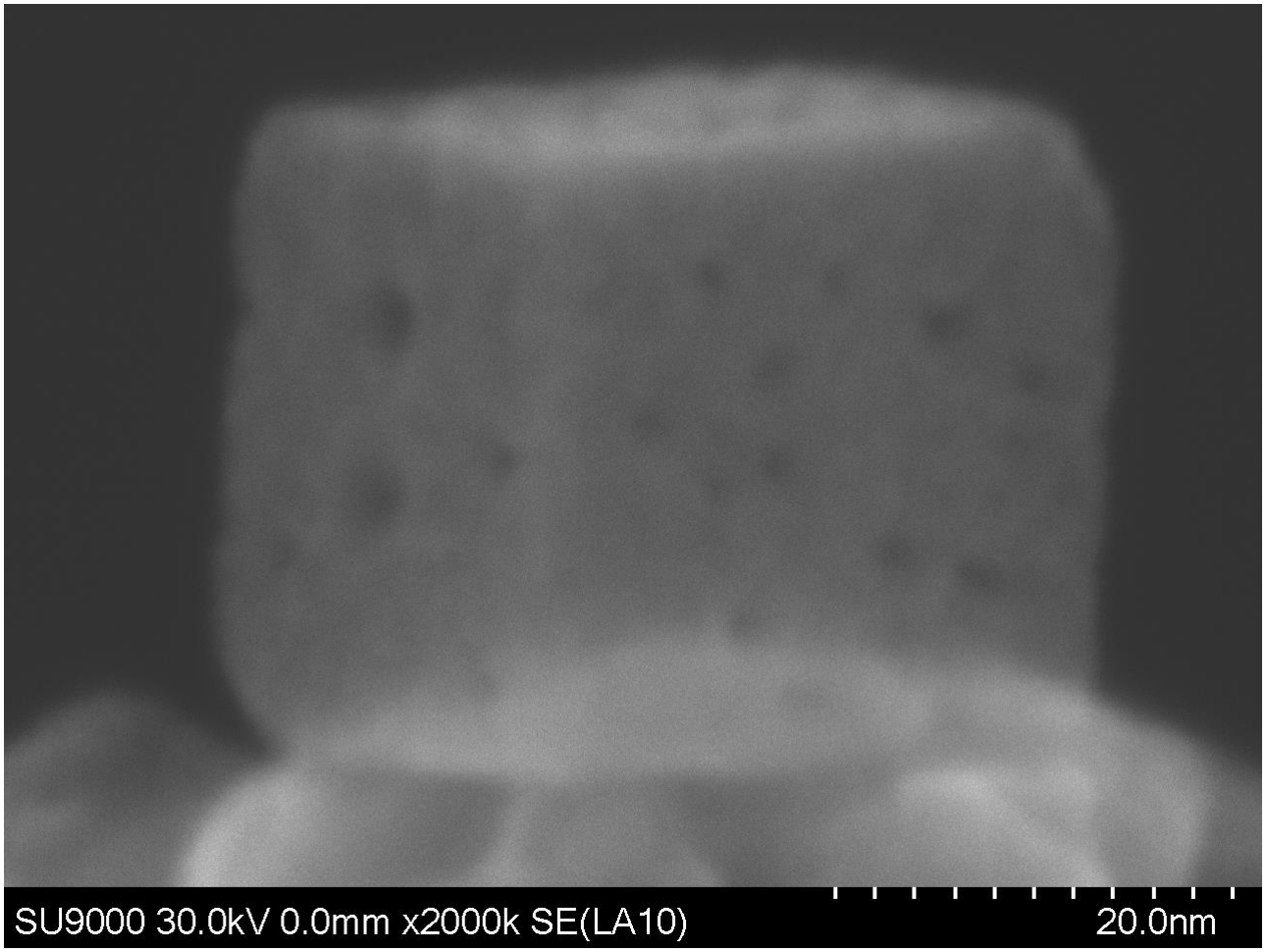

# X-ray detector transmission

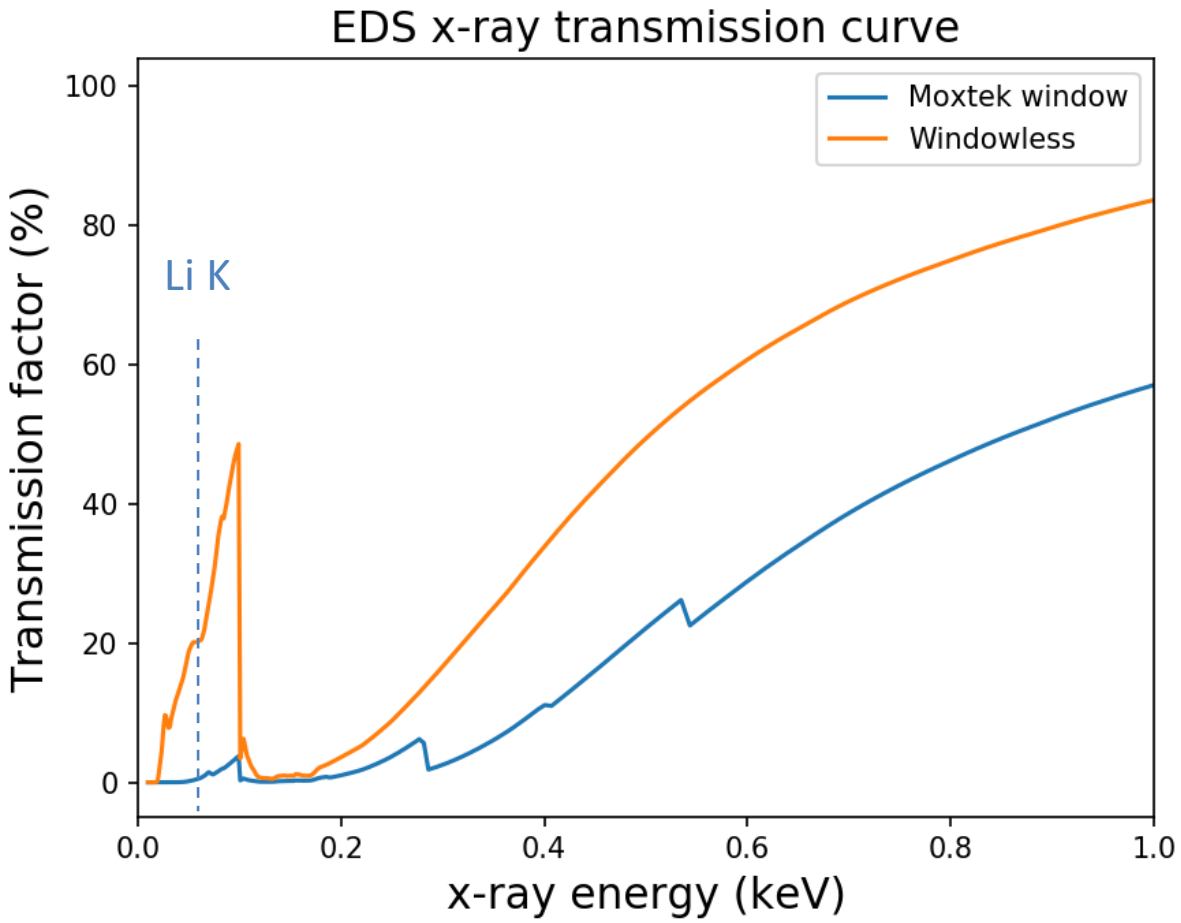

# Core-shell nanocomposite

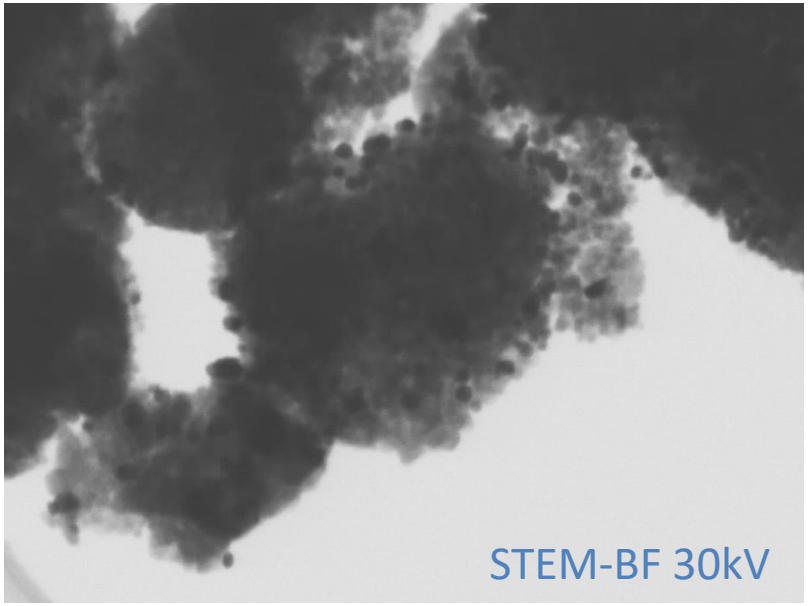


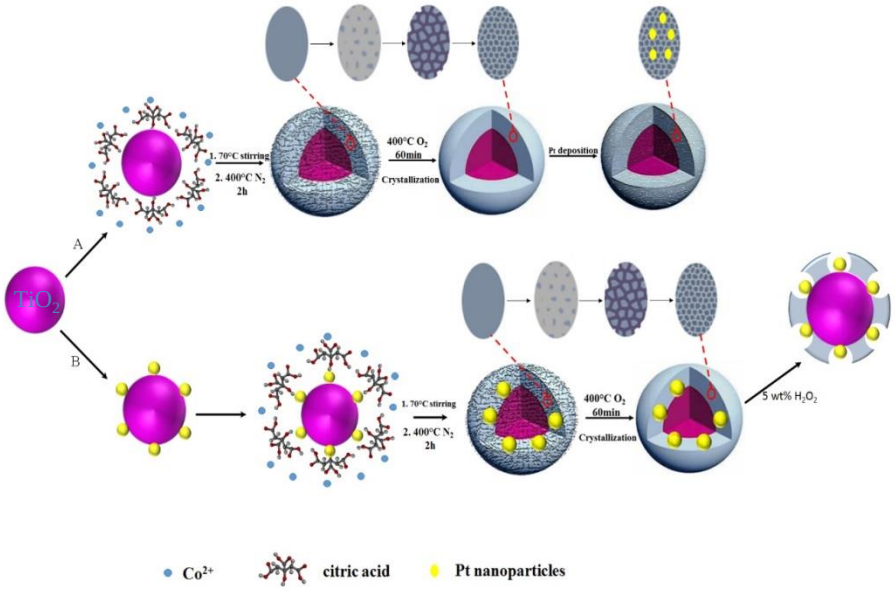


Ti K series

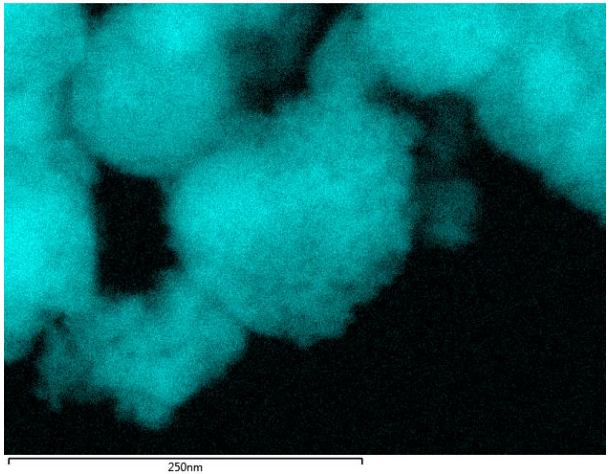


Co K series

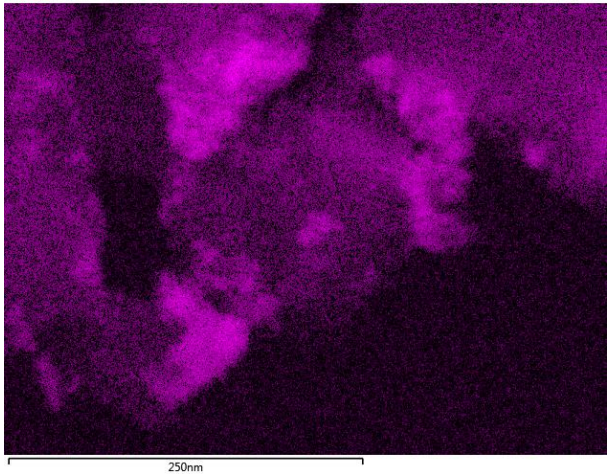


Pt L series

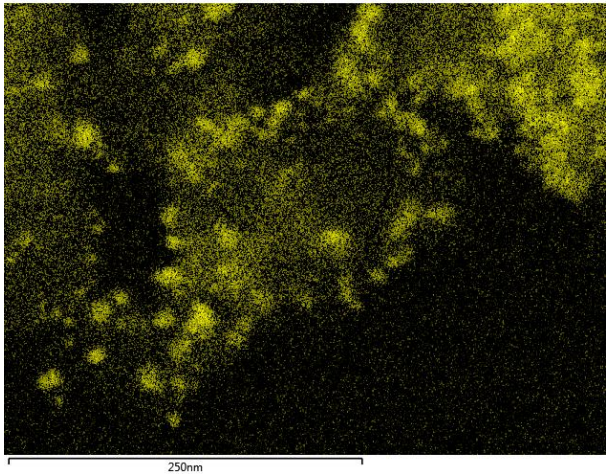

# Spatial Resolution with x-rays – 30 kV

- T1 ($Al_2CuLi$) precipitates in Al-Li-Cu alloys ≈ 1 – 2 nm thick
- 1.6 nm in BF imaging
- 1.9 nm across a T1 precipitate at 30 kV with Cu Kα

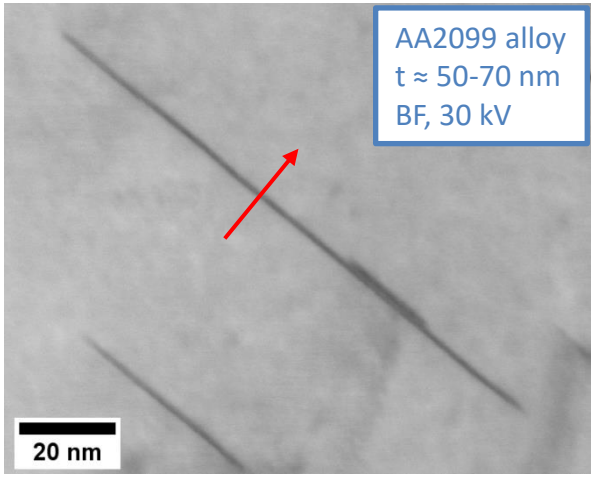


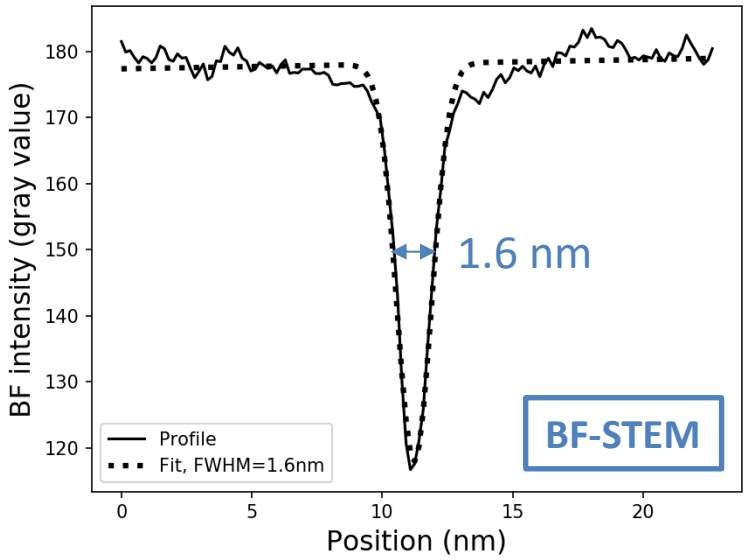


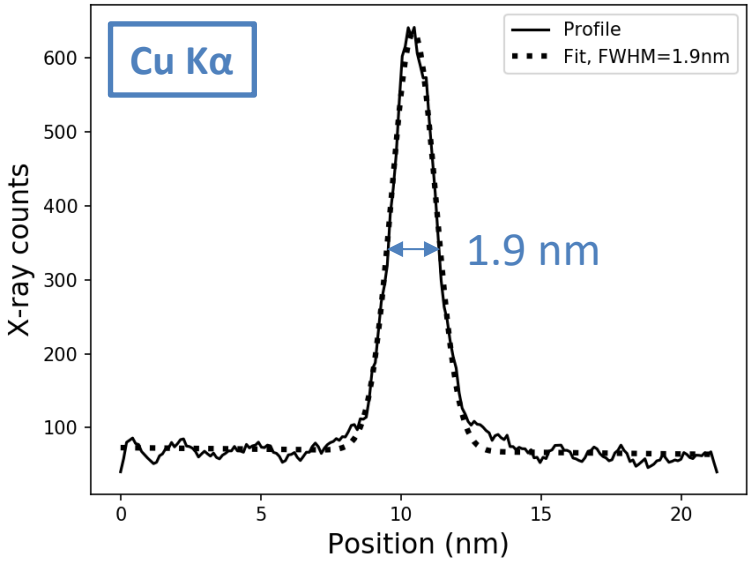

ACS APPLIED NANO MATERIALS

www.acsanm.org Article

# Plasmon-Enhanced Hydrogenation of 1-Dodecene and Toluene Using Ruthenium-Coated Gold Nanoparticles

Luis Carlos de la Garza, Nicolas Brodusch, Raynald Gauvin,* and Audrey Moores*

Cite This: *ACS Appl. Nano Mater.* 2021, 4, 1596−1603 Read Online

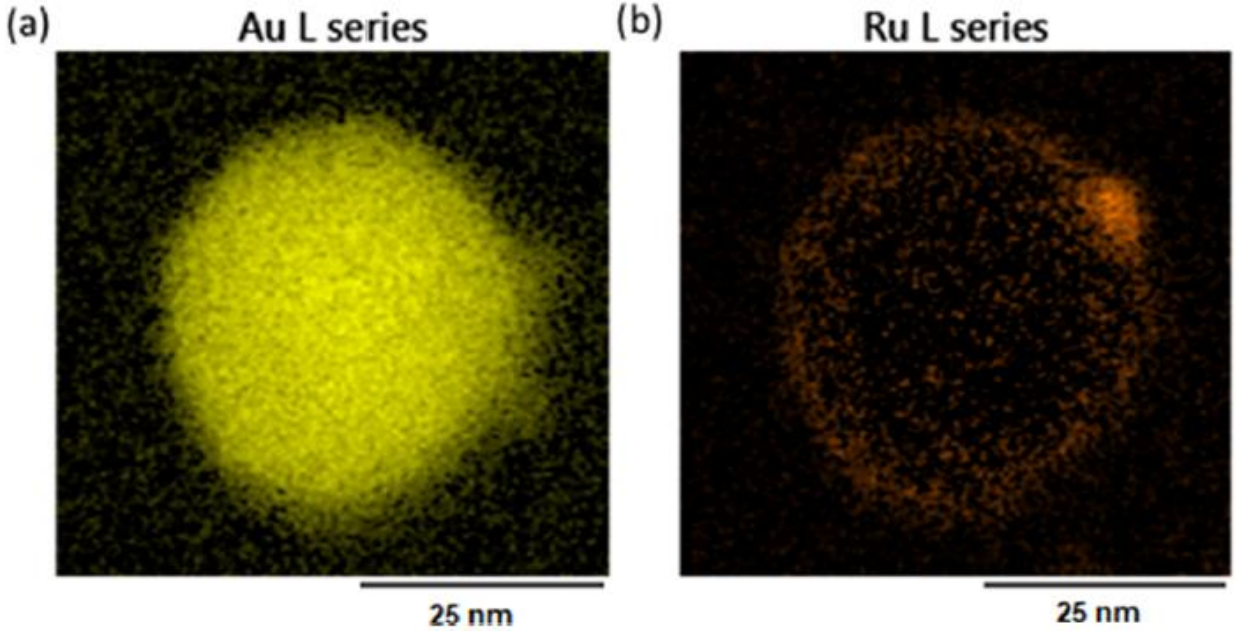


**Figure 3.** STEM-EDS images of Au@Ru NP. (a) Au L signal, (b) Ru L signal.

# Lithium X-ray production

- Maximum emission at low voltage ($E_0$ < 5 kV)
- Different intensity for similar Li weight fractions
- Complex emission process

| Compound | Theoretical Lithium minimum weight fraction |
|---|---|
| $LiO_2$ | 0.1782 |
| LiF | 0.2676 |
| LiCl | 0.1637 |

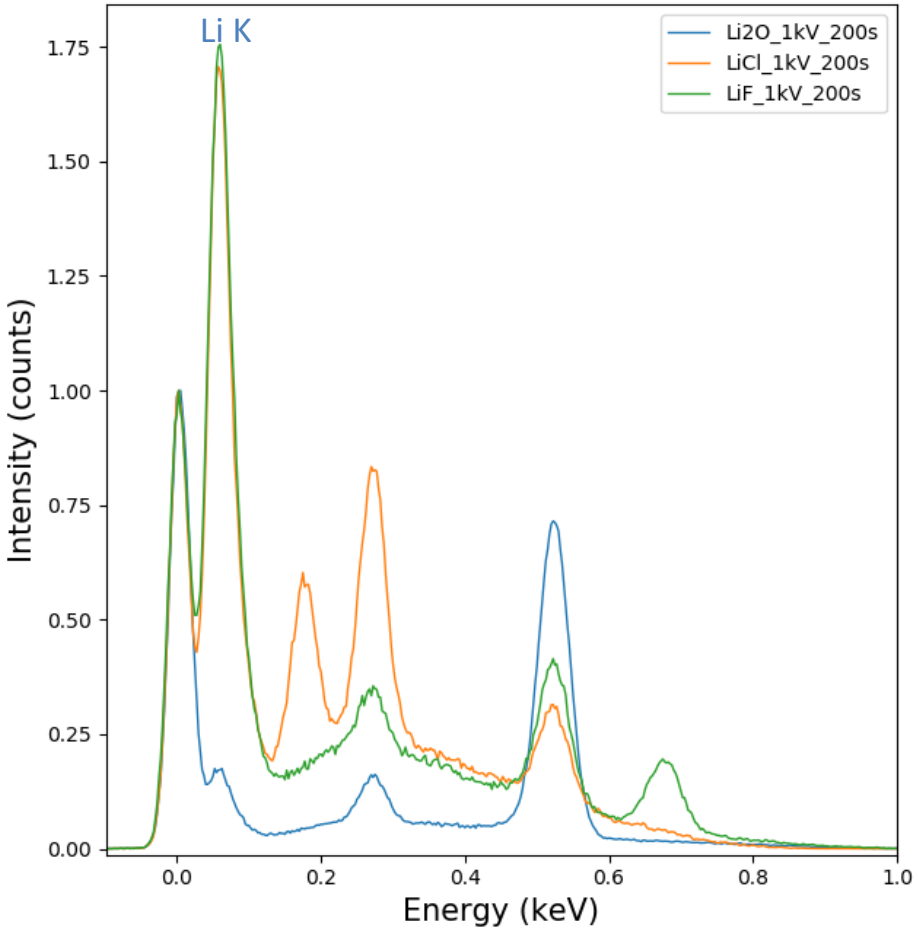

# Lithium Chloride: Intensities vs irradiation time

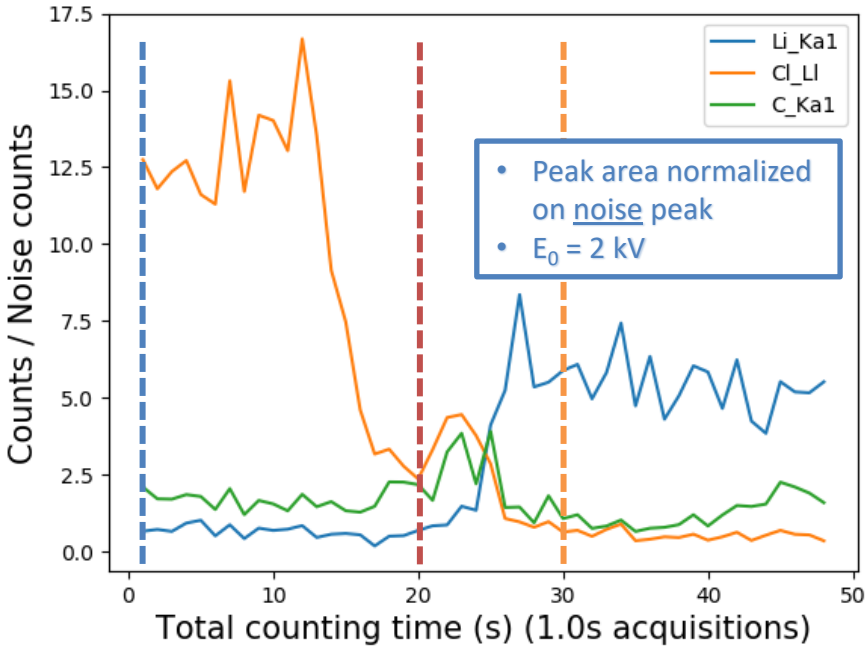


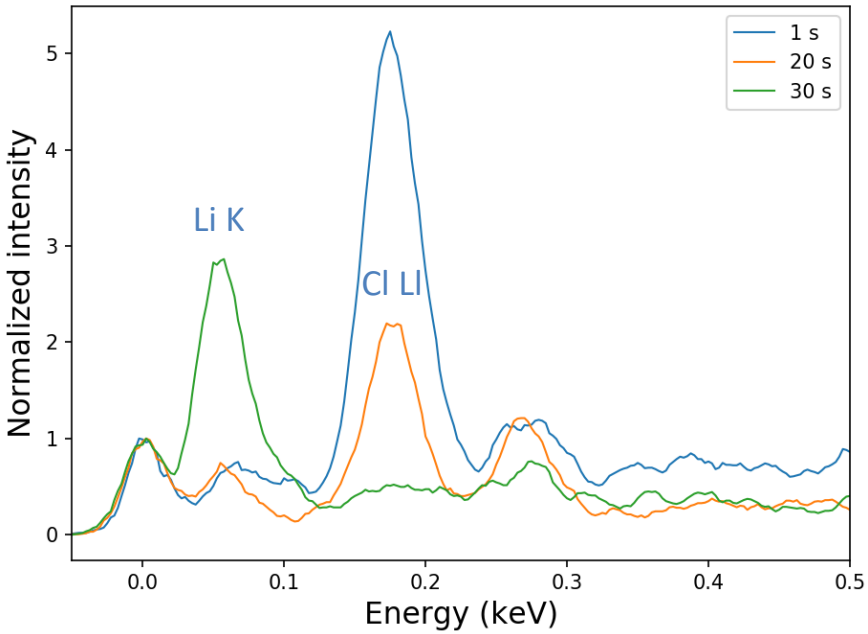

# Beam damage on lithium chloride

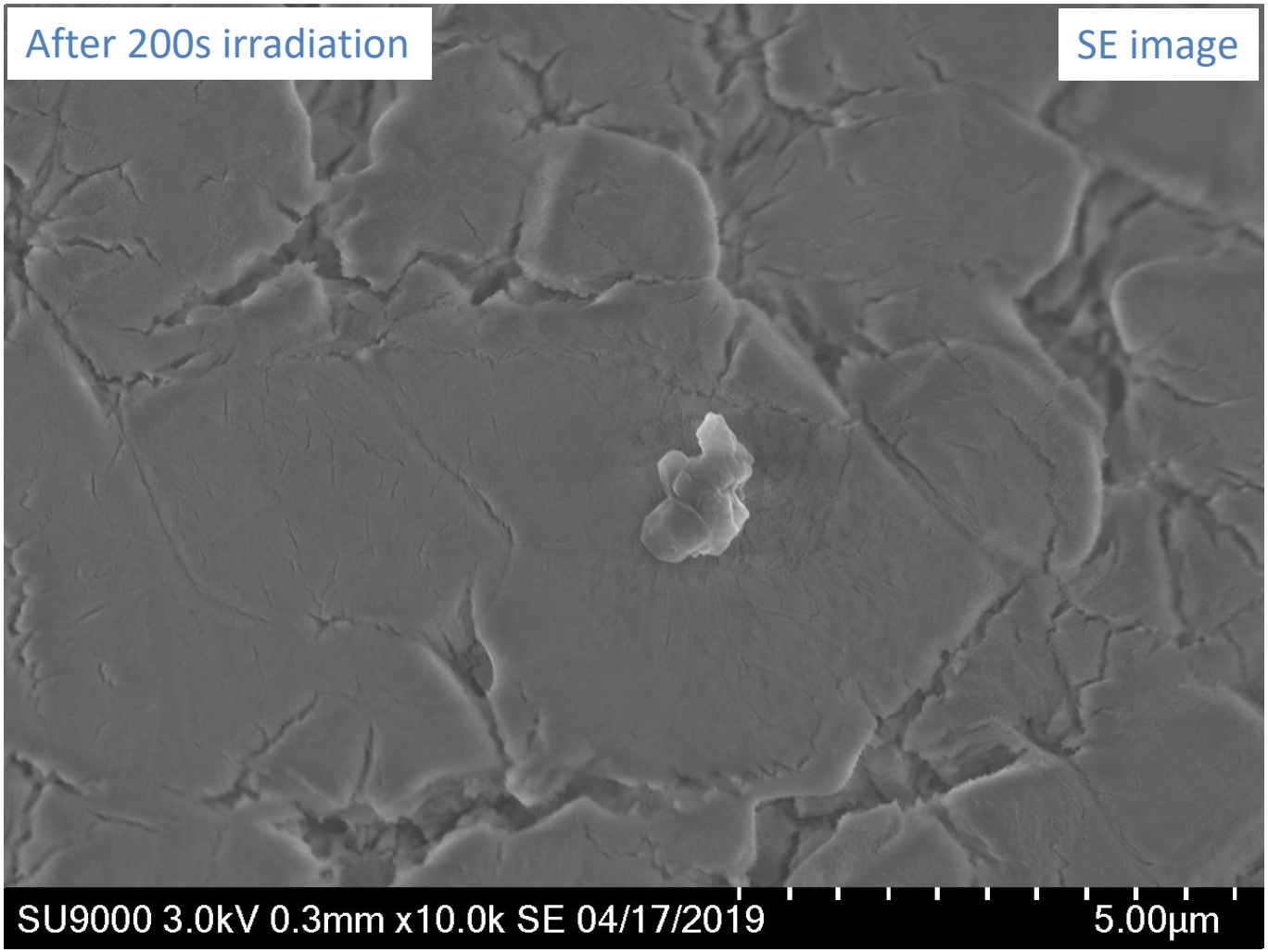

# EDS Extreme (SU-9000) on cycled Lithium Lanthanum Zirconate (LLZ)

- Ion milling cross-section (IM-4000plus) 6 kV
- $E_0$ = 3 kV
- Processing: Richardson-Lucy deconvolution*

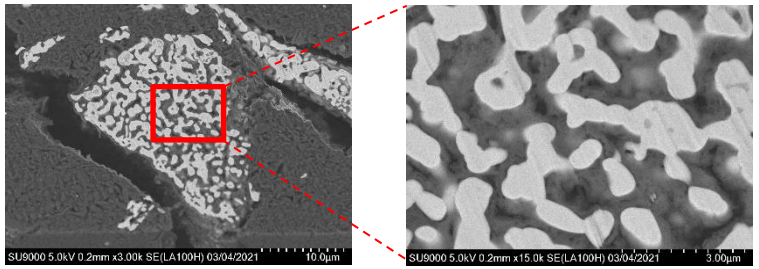


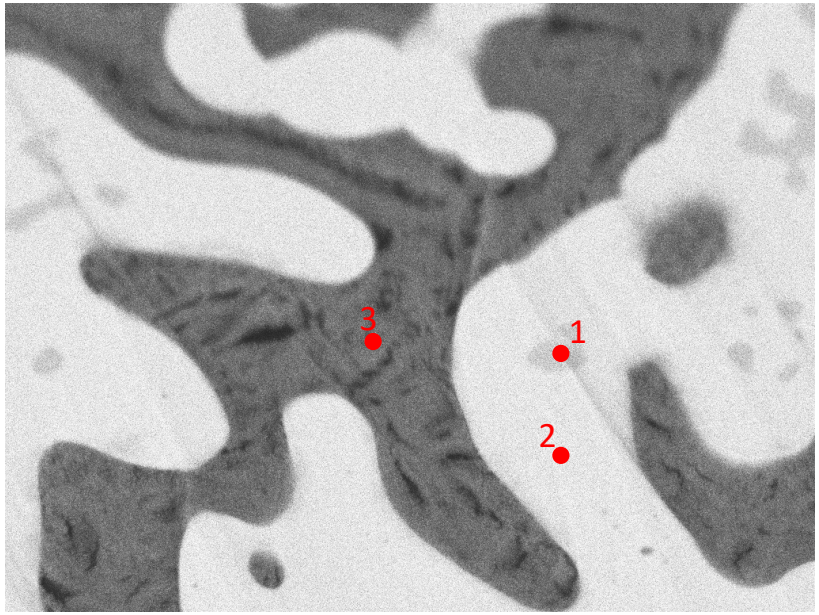


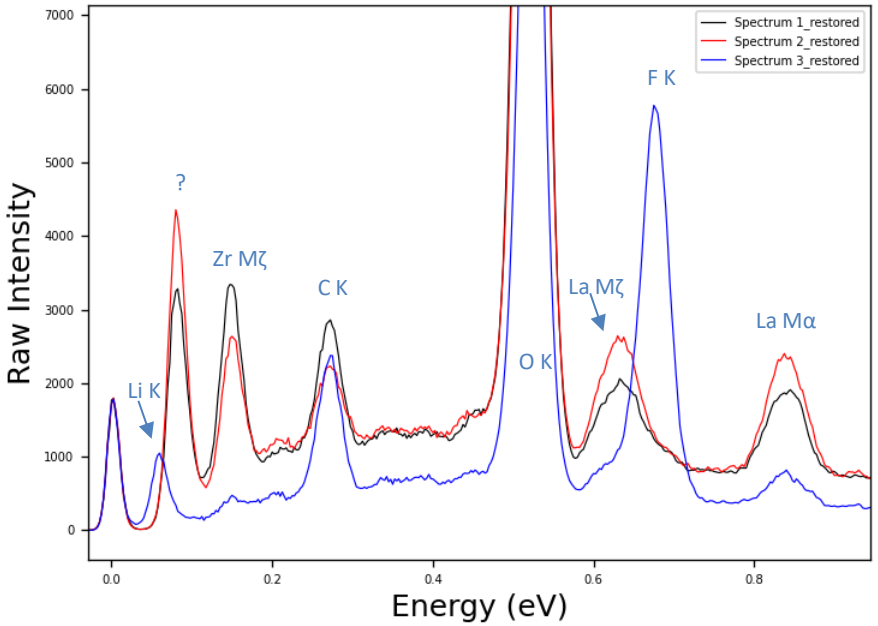


* Brodusch, N.; Zaghib, K. & Gauvin, R.; Improvement of the energy resolution of energy dispersive spectrometers (EDS) using Richardson-Lucy deconvolution; Ultramicroscopy, 2020, 209, 112886

# Chapter 4

- Effect of pressure
- Dendrite chemical analysis
- Dendrite morphology

NANO LETTERS

Letter

Cite This: Nano Lett. 2018, 18, 7583−7589

pubs.acs.org/NanoLett

## In Situ Scanning Electron Microscopy Detection of Carbide Nature of Dendrites in Li−Polymer Batteries

Maryam Golozar,[†,‡] Pierre Hovington,[§] Andrea Paolella,[‡] Stéphanie Bessette,[†,‡] Marin Lagacé,[‡] Patrick Bouchard,[‡] Hendrix Demers,[‡] Raynald Gauvin,[†] and Karim Zaghib*[,‡]

[†]Department of Mining and Materials Engineering, McGill University, Montréal, Quebec H3A 0C5, Canada

[‡]Center of Excellence in Transportation Electrification and Energy Storage, Hydro-Québec's Research Institute, Varennes, Québec J0L 1N0, Canada

[§]Hovington's Consulting, Boucherville, Québec J4B 5E6, Canada

Supporting Information

**ABSTRACT:** Li metal batteries suffer from dendrite formation which causes short circuit of the battery. Therefore, it is important to understand the chemical composition and growth mechanism of dendrites that limit battery efficiency and cycle life. In this study, in situ scanning electron microscopy was employed to monitor the cycling behavior of all-solid Li metal batteries with $LiFePO_4$ cathodes. Chemical analyses of the dendrites were conducted using a windowless energy dispersive spectroscopy detector, which showed that the dendrites are not metallic lithium as universally recognized. Our results revealed the carbide nature of the dendrites with a hollow morphology and hardness greater than that of pure lithium. These carbide-based dendrites were able to perforate through the polymer, which was confirmed by milling the polymer using focused ion beam. It was also shown that applying pressure on the battery can suppress growth of the dendrites.

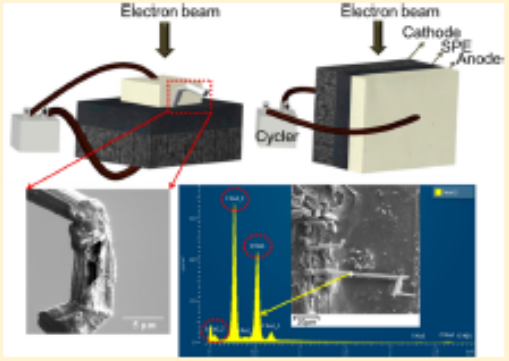


**KEYWORDS:** *In situ, scanning electron microscope, all-solid Li metal batteries, polymer, dendrite*

# Exterior of needle dendrite wall

Needle morphology dendrites are hollow

nanomanipulato

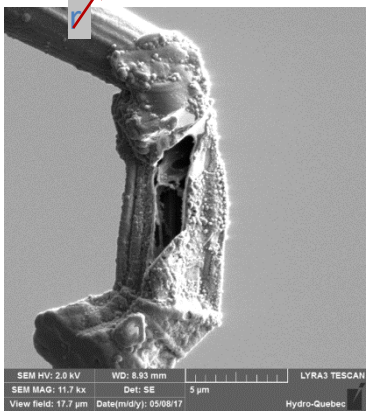


- Dendrite lift out with the nanomanipulator
- Milling dendrite using gallium source FIB
- Observing hollow morphology


Exte

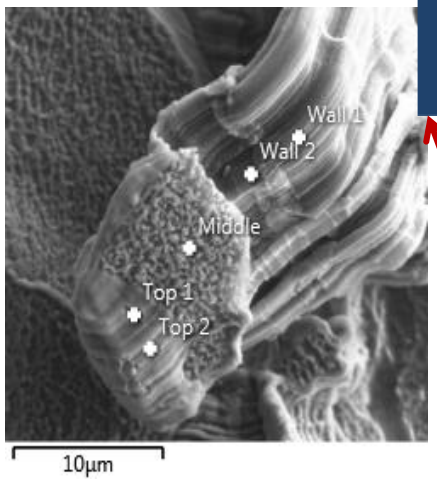


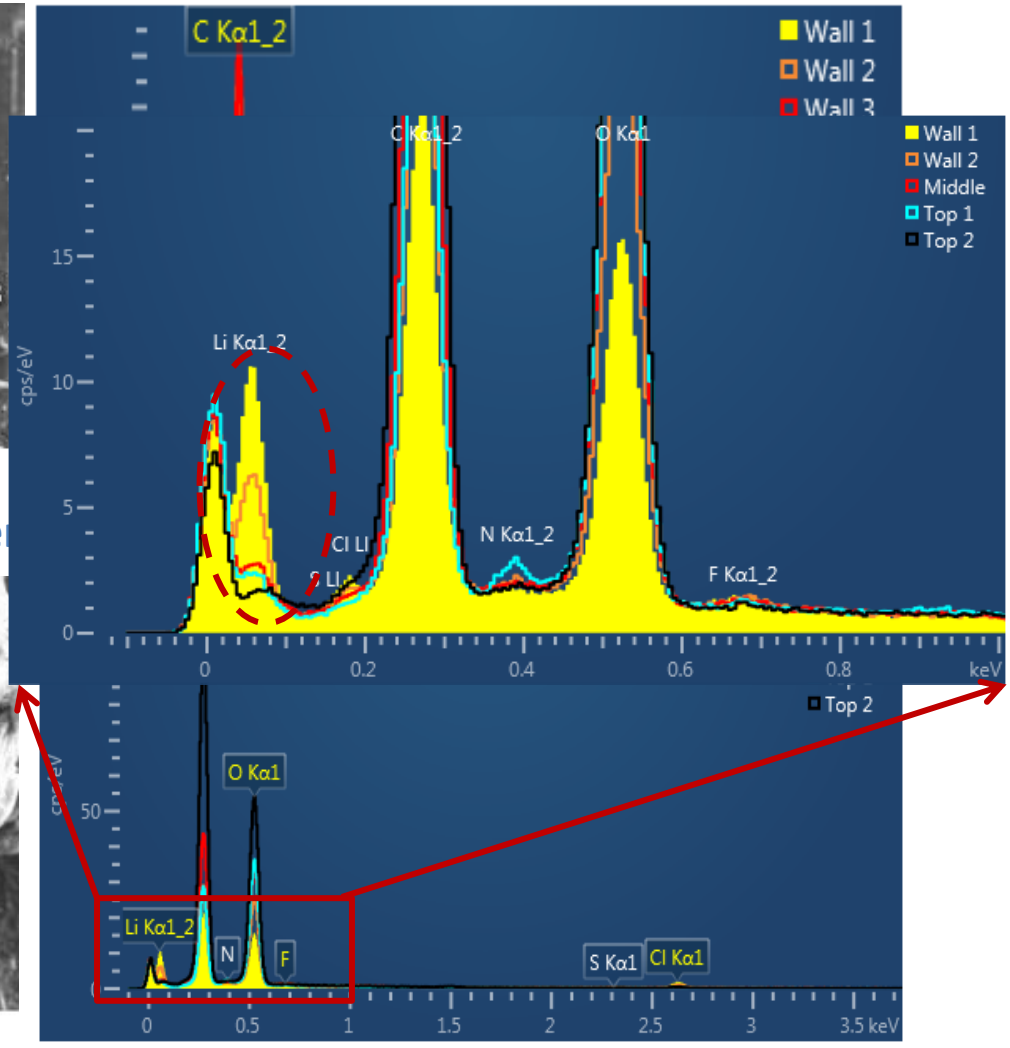

*Journal of Microscopy, Vol.* 128, *Pt* 2, *November* 1982, *pp. RP*1–*RP*2.
*Received* 7 *September* 1982; *accepted* 14 *September* 1982

# THE ROLE OF FAST SECONDARY ELECTRONS IN DEGRADING SPATIAL RESOLUTION IN THE ANALYTICAL ELECTRON MICROSCOPE

D.C.Joy, Bell Laboratories, Murray Hill, NJ 07974, USA
D.E.Newbury and R.L.Myklebust, NBS Washington DC 20234, USA

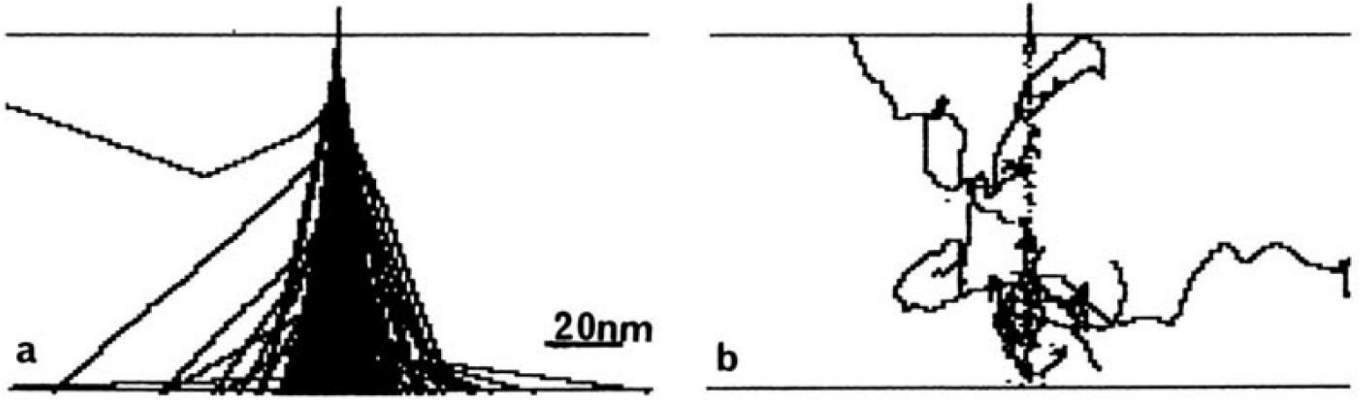


Fig.1 (a) Primary and (b) Fast Secondary trajectories in Almandine at 100kv

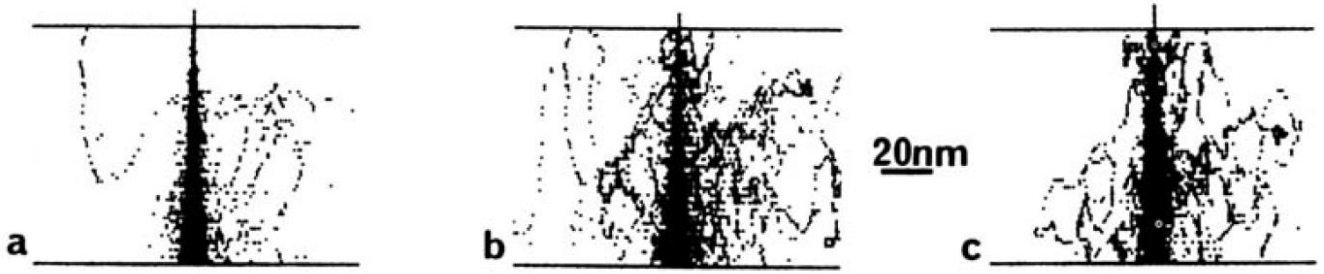


Fig.2 Corresponding Xray dot maps for (a) Fe K, (b) Si K, (c) O K lines

# Effect of Fast Secondary Electrons on X-Ray Microanalysis

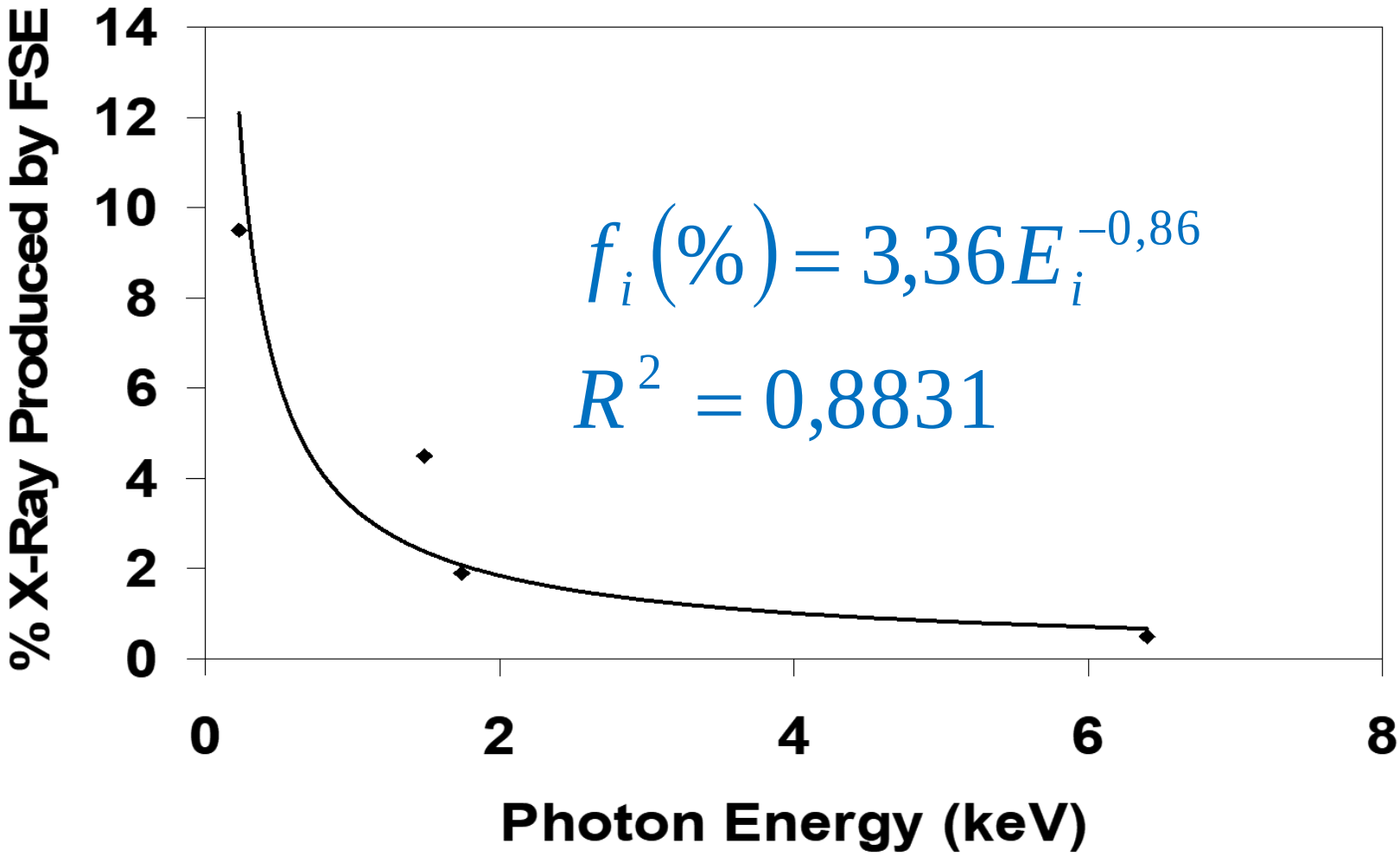


Joy, Newbury & Myklebust (1982), Journal of Microscopy, 128, RP1 – RP2

# Effect of FSE on $K_{AB}$

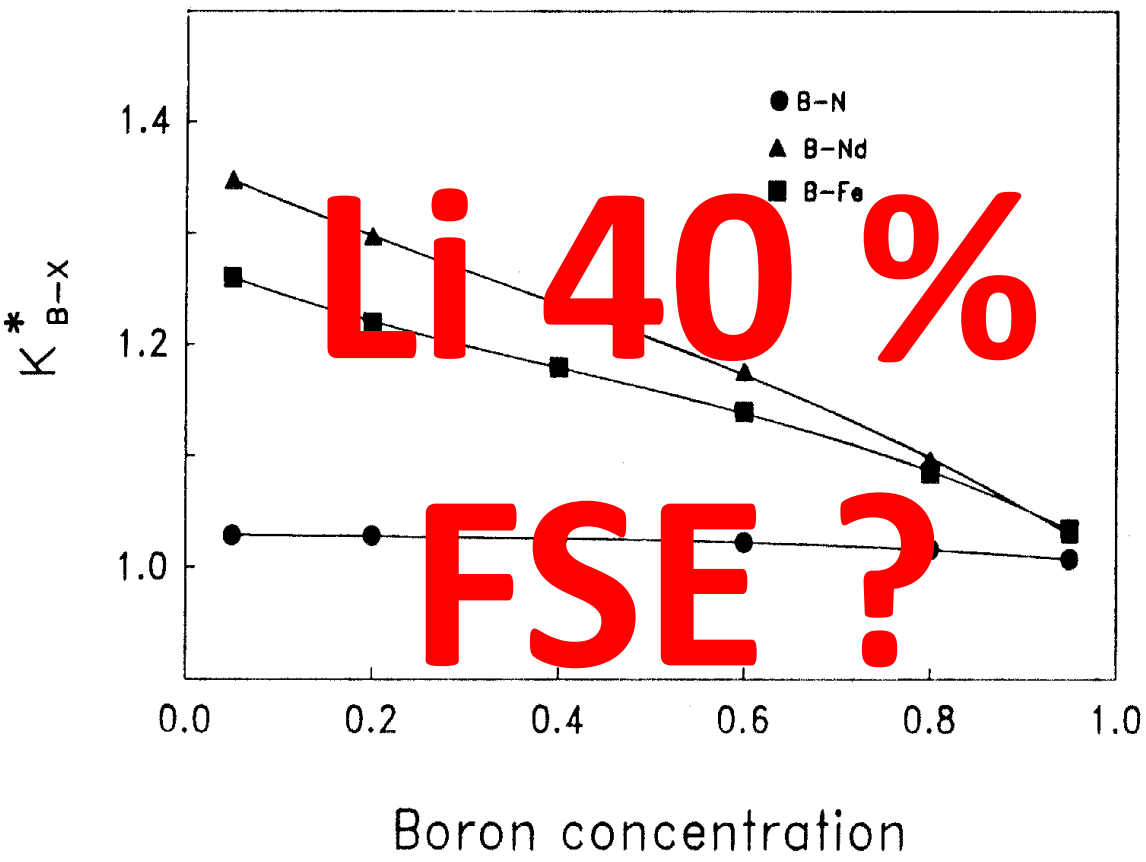


Li 40 %

FSE ?

$$K^*_{AB} = \frac{K_{AB}(e_P)}{K_{AB}(e_P + e_S)} = \frac{1 - f_B}{1 - f_A}$$

*R. Gauvin and G. L'Espérance (1992), Journal of Microscopy, Vol. 168, pt. 2, pp. 153-167*

# X-Ray Emitted by Auger Electrons

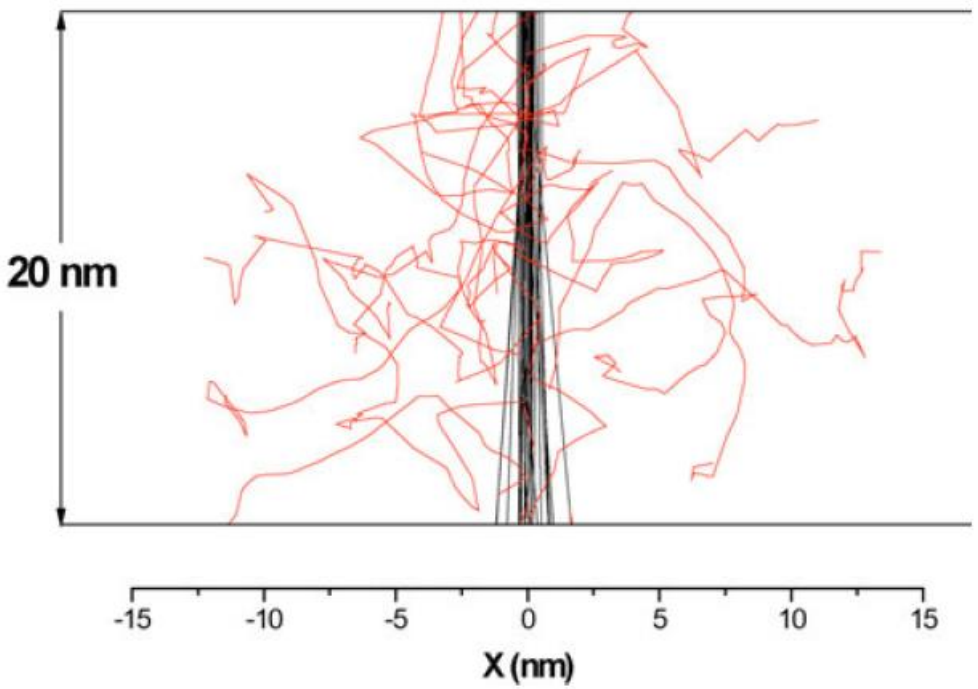


**Figure 21.** Trajectories of the primary and Auger Au $M_4N_{67}N_{67}$ electrons in a 20 nm thick foil of an Au–1% (at.) B alloy for $E_0$ = 100 keV. Taken from Gauvin (2007*b*).

# Effect of Auger Electrons on Li Emission

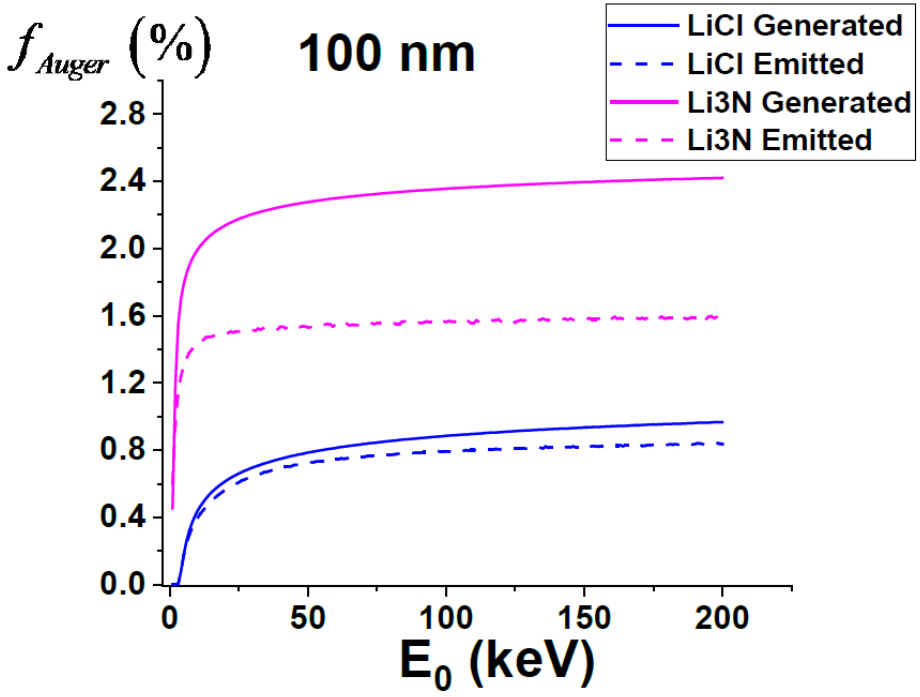


**Figure 2.** Percentage of X-Ray generated by the Auger Electrons the $K_\alpha$ line of Lithium in LiCl and $Li_3N$ for a 100 nm thin foil as a function of accelerating voltage. For $Li_3N$, the x-ray for Li is generated by the 0.38 keV KLL Auger electron of N and for LiCl, Li x-rays are generated by the 2.25 keV KLL Auger electron of Cl.

R. Gauvin et al. (2021), Microscopy & Microanalysis.

# The EELS Detector

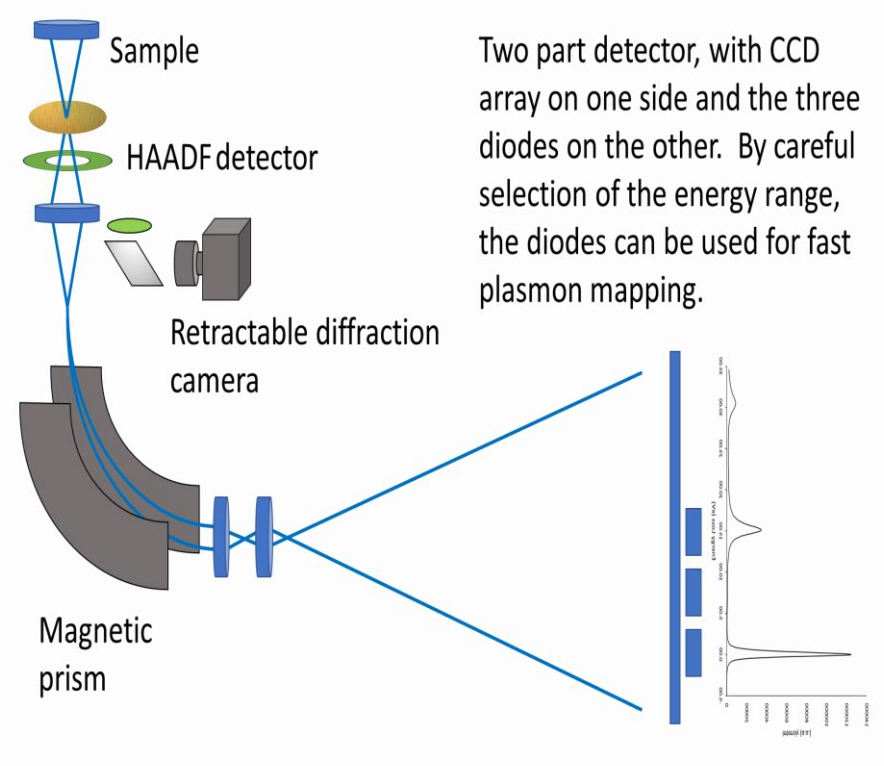


Figure 1: Simplified diagram of the microscope, showing the HAADF detector, the diffraction camera and the dual mode EELS/EF-STEM detector.

# Li Detection in $LiO_2$

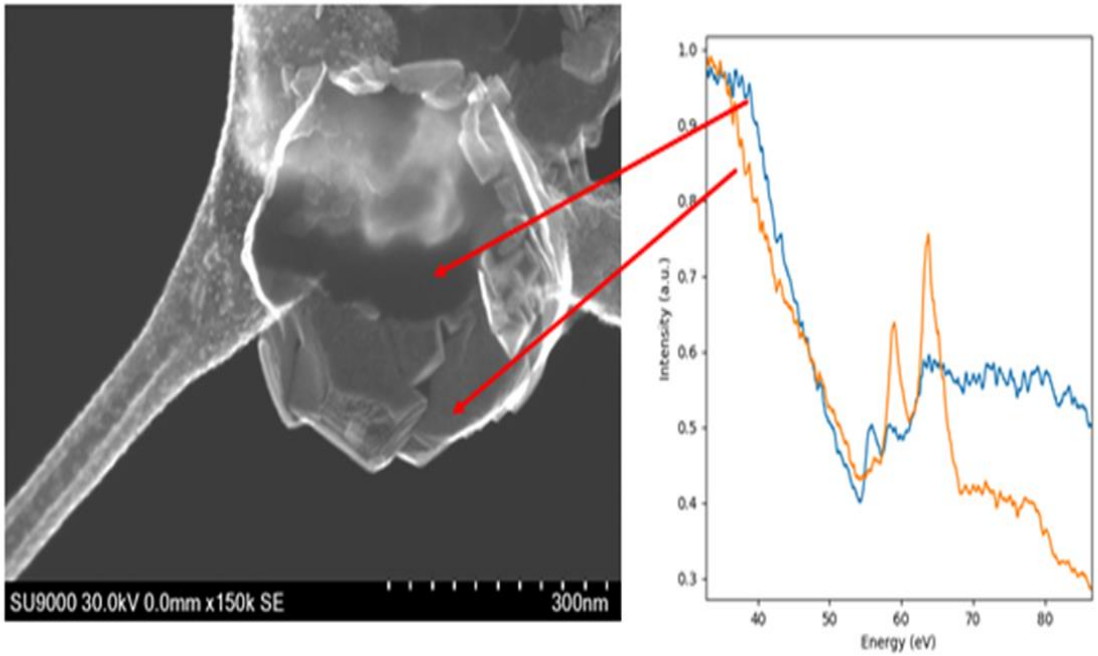

# Chemical Analysis with STEM-EELS at Low Voltage (SU-9000) $Li_2FeSiO_4$ (LFS) – Low-Loss

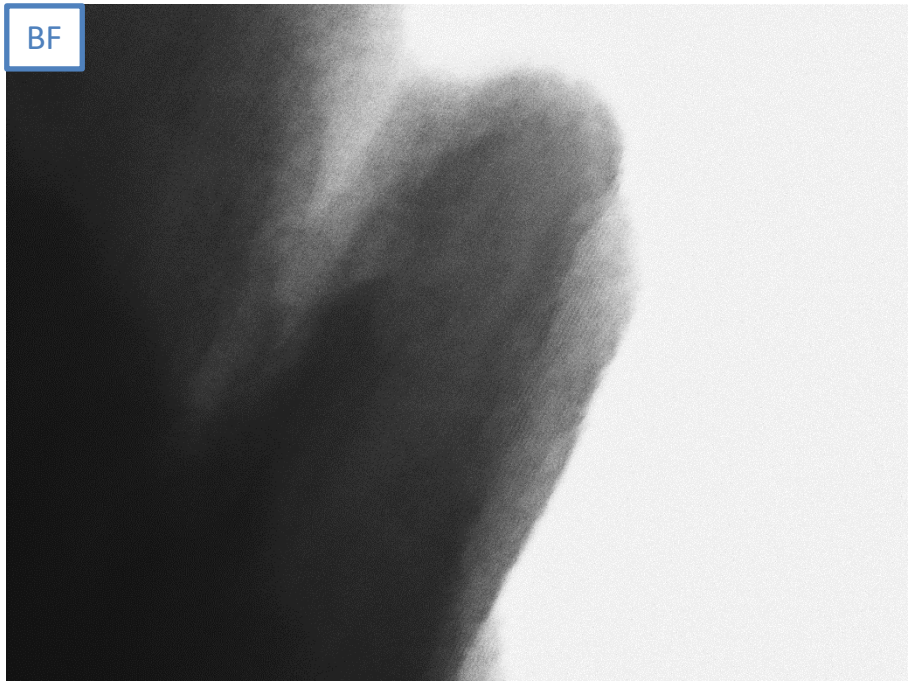


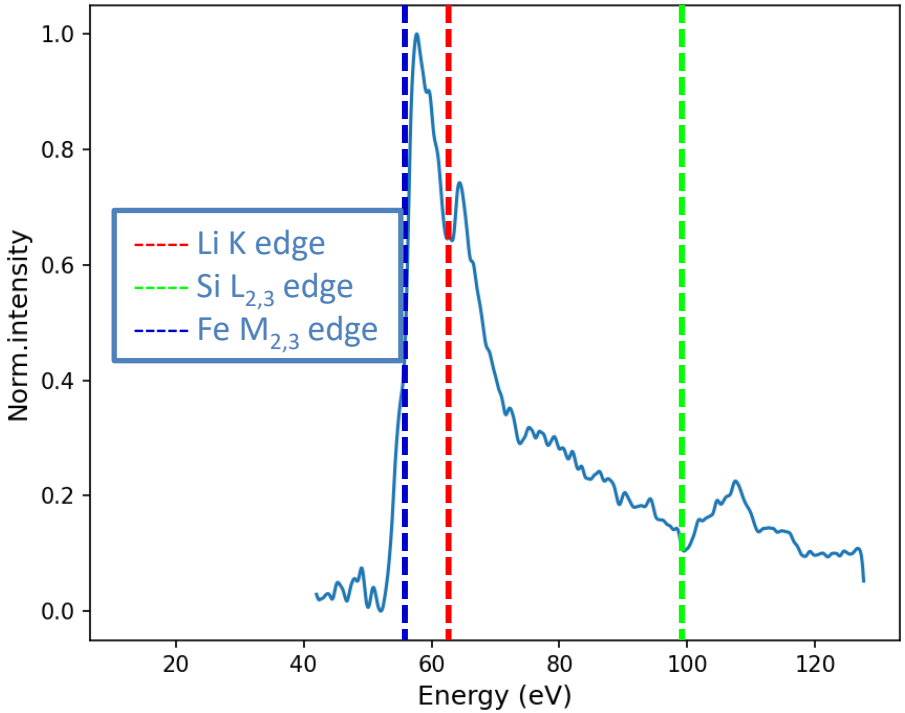

# AA 2099

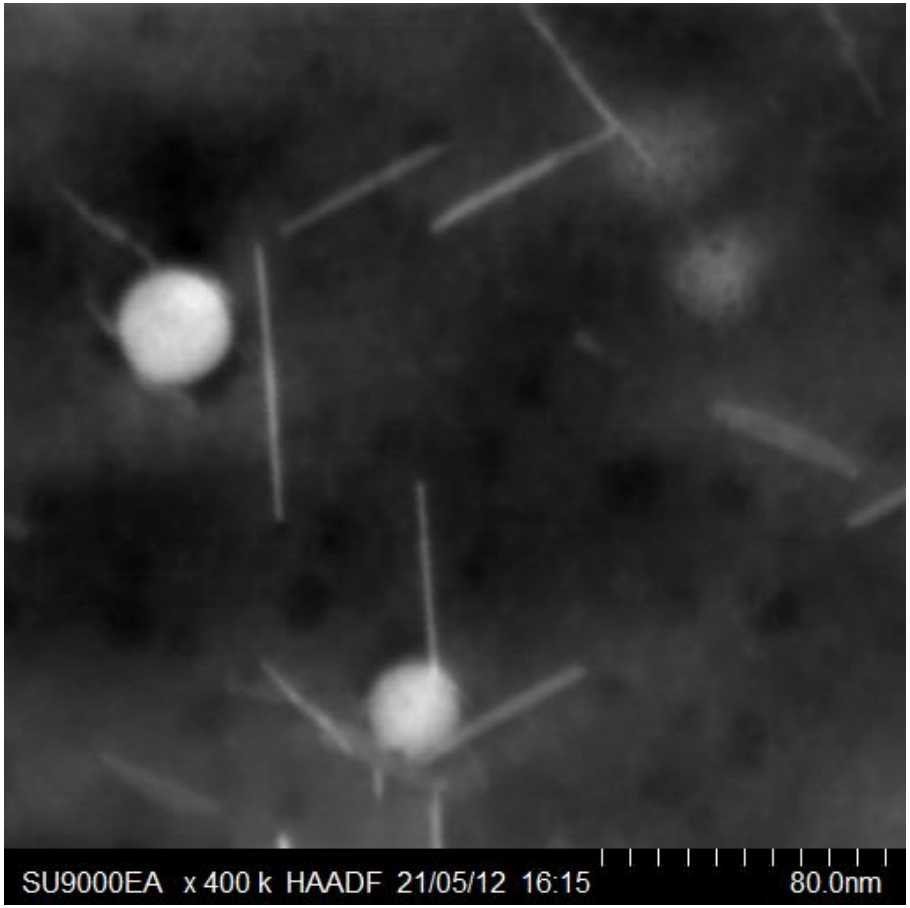


HAADF

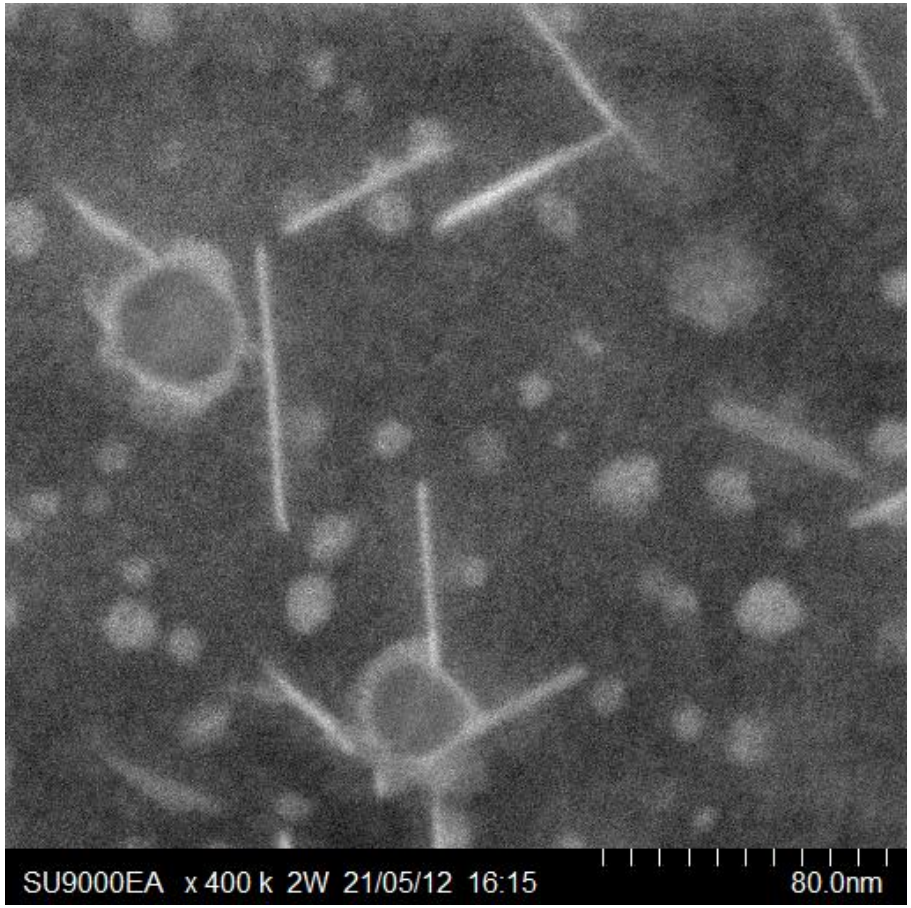


Li Jump Ratio

# Ethos NX-5000 Triple Beam FIB - 2020

# Épaisseur Film Mince – EELS
# Malis, Cheng, Egerton (1988)

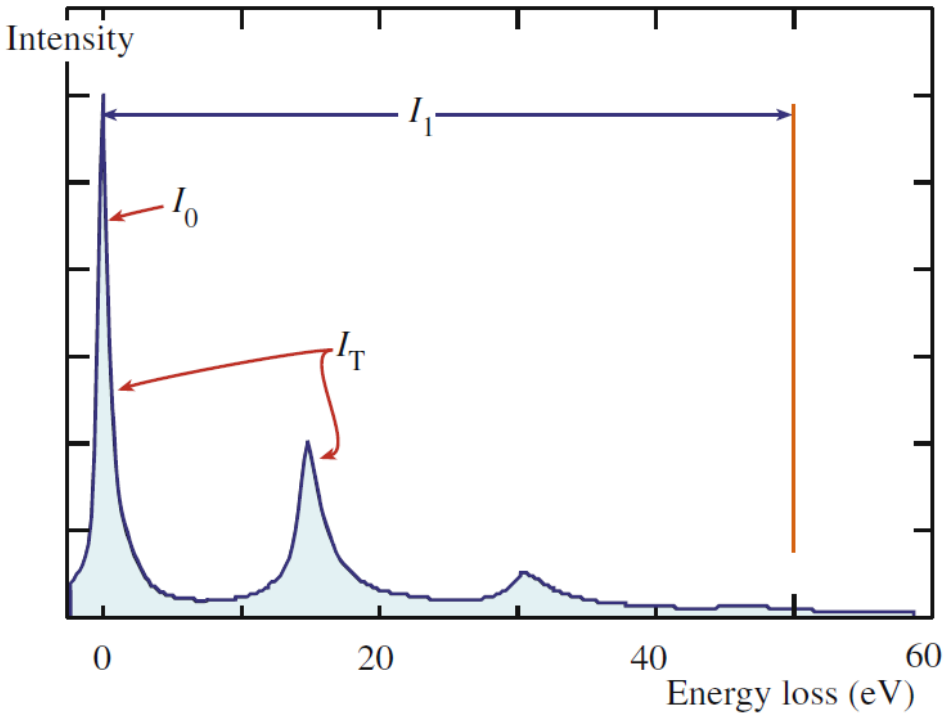


$$t = \lambda ln\left(\frac{I_T}{I_0}\right)$$

$$\lambda = \frac{106\,F\,(E_0/E_m)}{ln(2\beta\,E_0/E_m)}$$

$$E_m = 7.6Z^{0.36}$$

$$F = \frac{1 + E_0/1022}{(1 + E_0/511)^2}$$

# Si FIB lamella

## SU9000 at 30keV

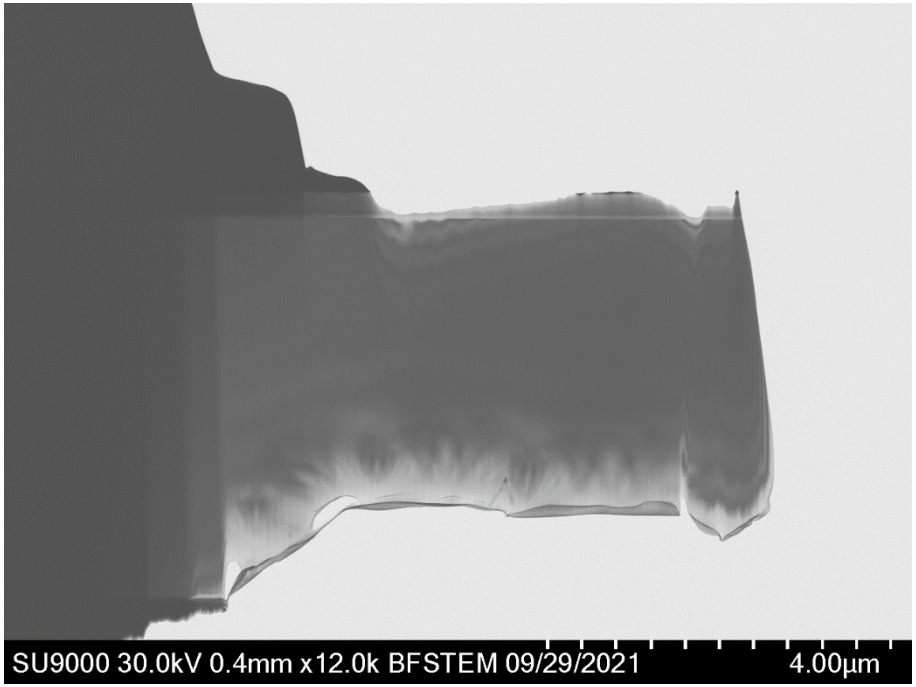


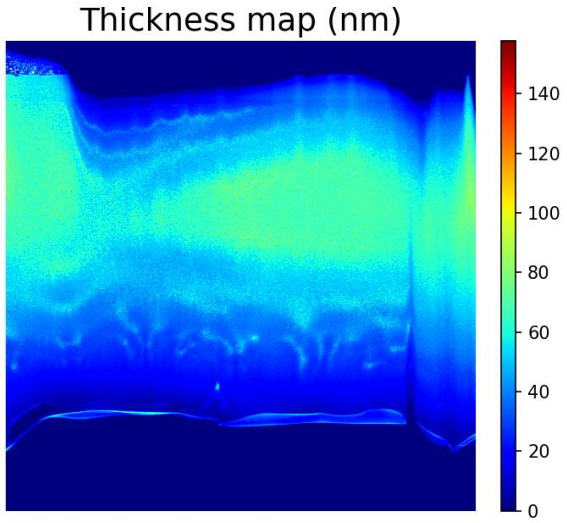

# Si FIB lamella

## SU9000 at 30keV
## (111) 0,34 nm

CBED

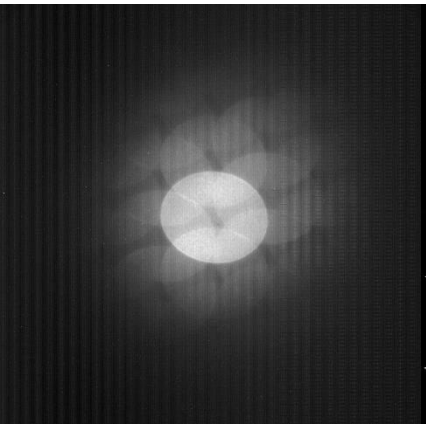

Indexed FFT

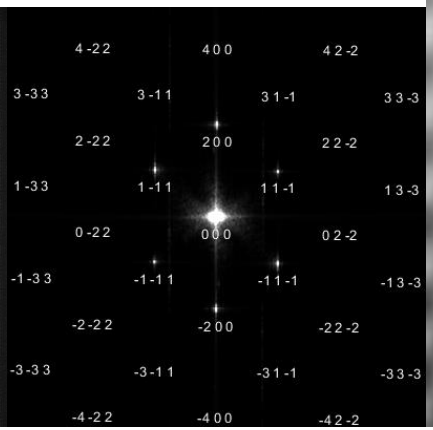


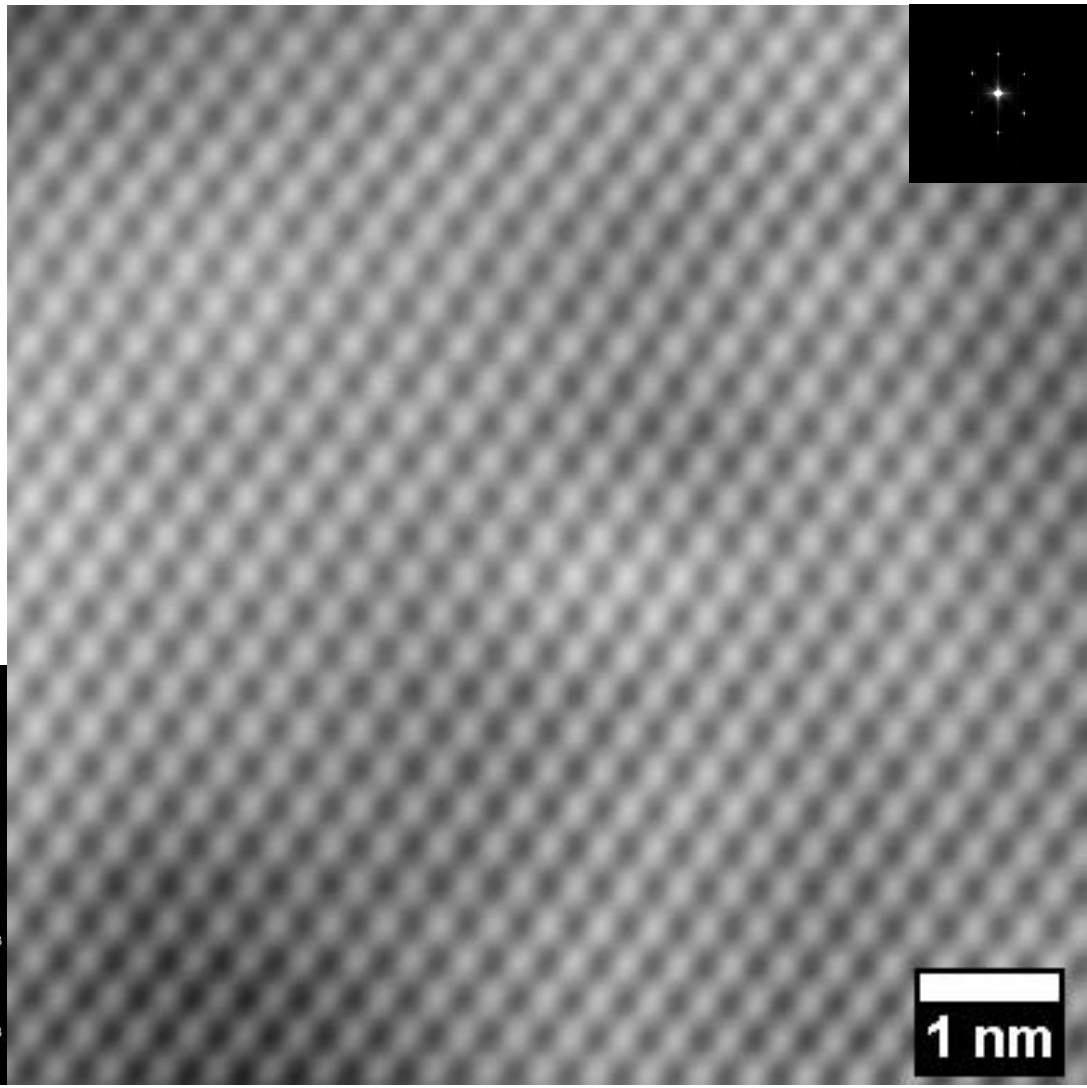

# Field Emission Scanning Electron Microscopy
# New Perspectives for Materials Characterization

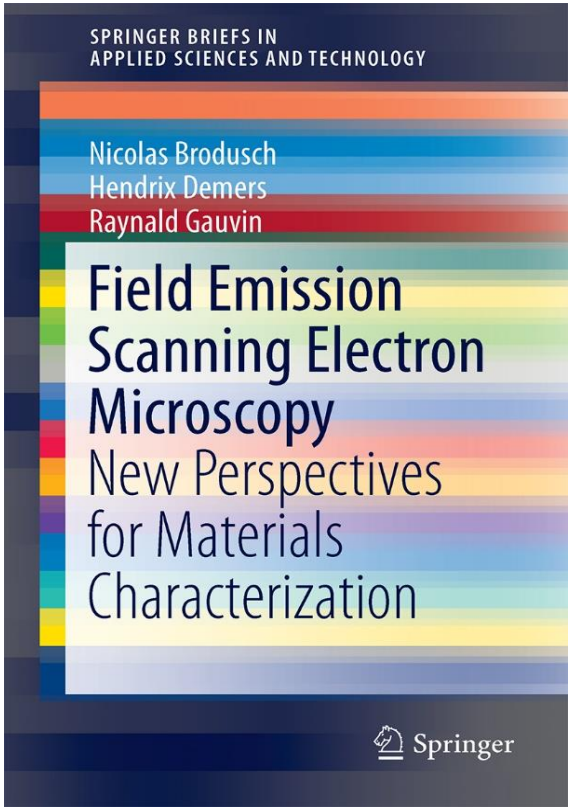


- Authors
  - Nicolas Brodusch
  - Hendrix Demers
  - Raynald Gauvin
- Available now at Springer or Amazon

http://www.springer.com/gp/book/9789811044328


memrg.com

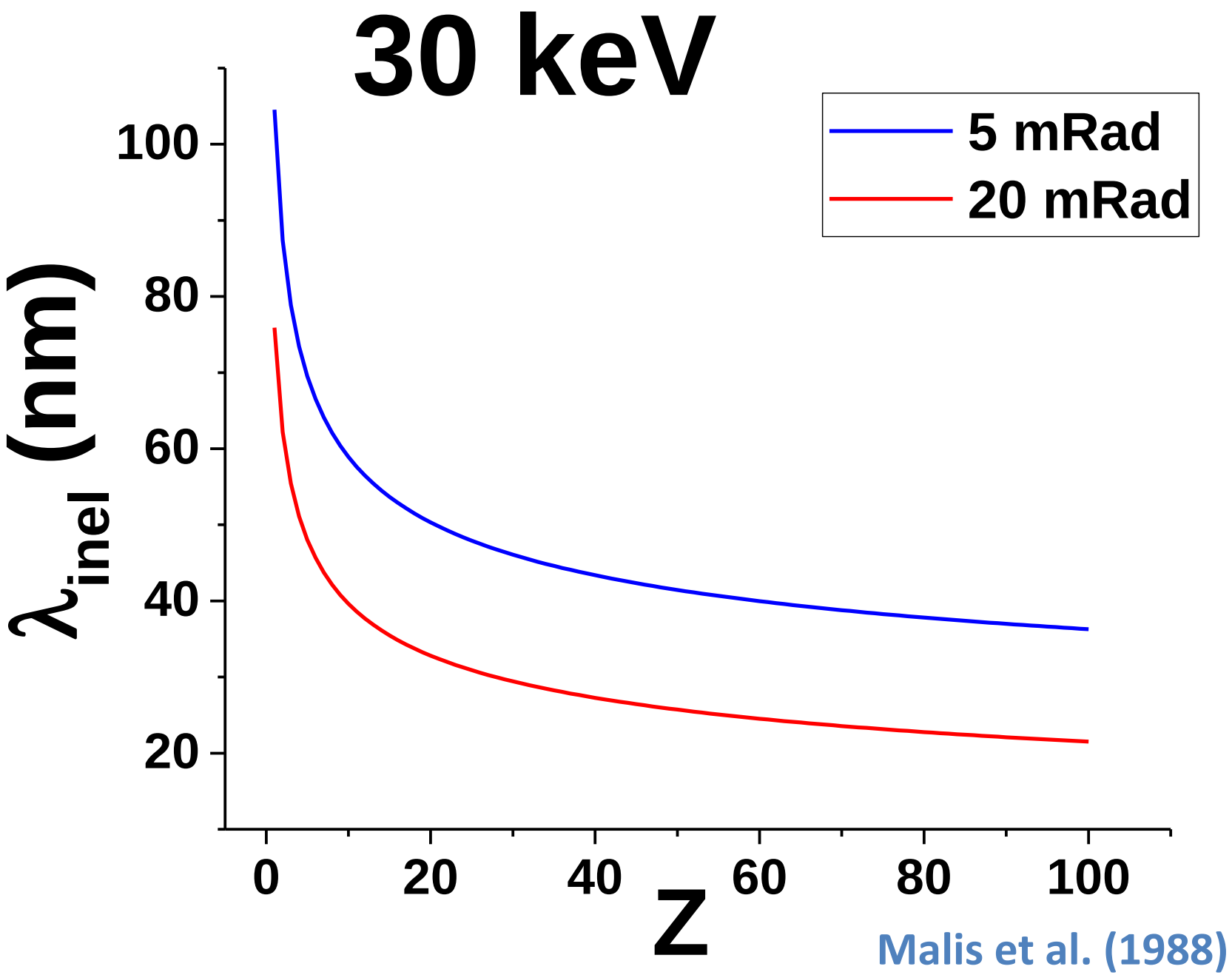


Malis et al. (1988)

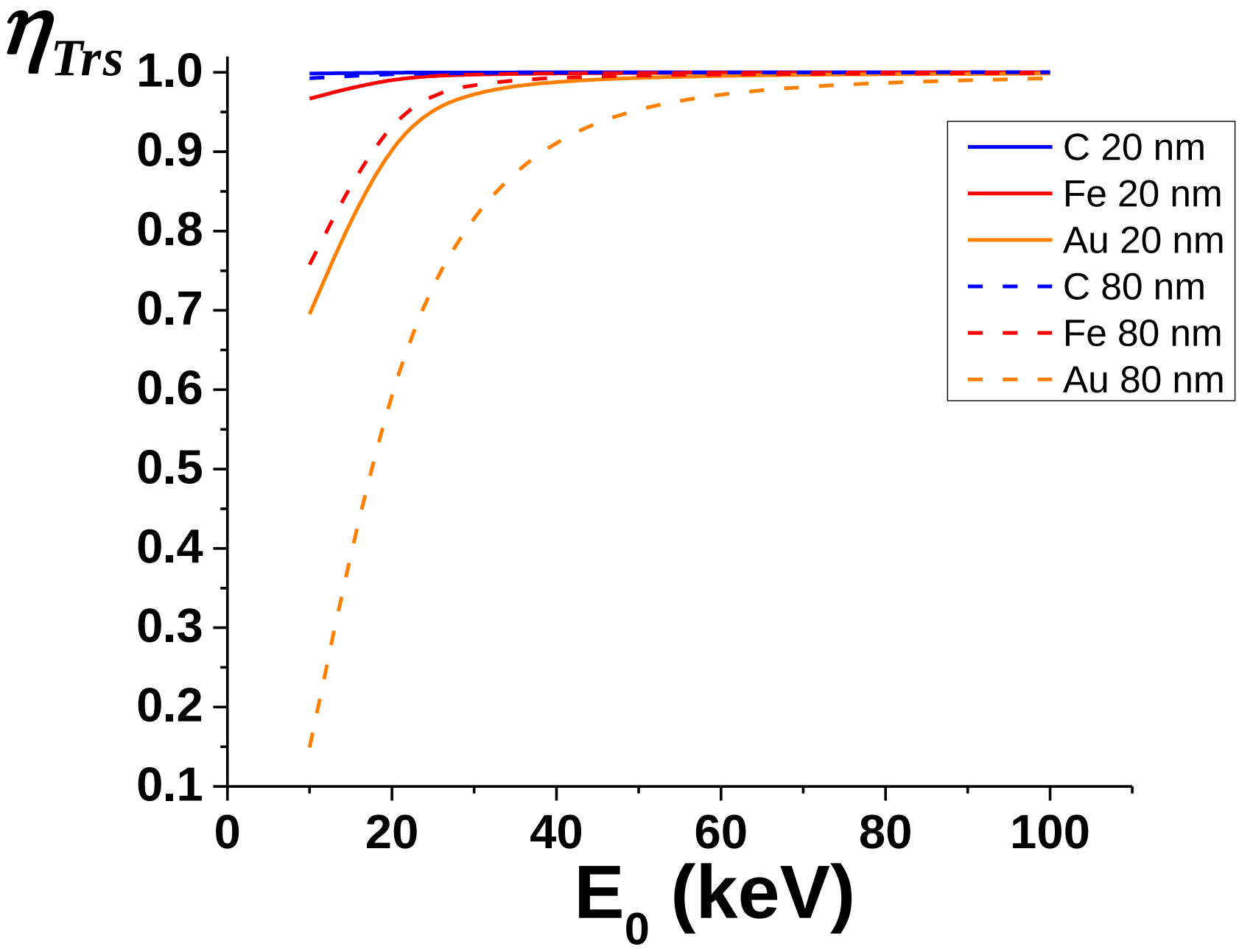
$\eta_{Trs}$
1.0
0.9
0.8
0.7
0.6
0.5
0.4
0.3
0.2
0.1
0
20
40
60
80
100
$E_0$ (keV)
C 20 nm
Fe 20 nm
Au 20 nm
C 80 nm
Fe 80 nm
Au 80 nm

# Alloy 2099 T83 – 80 nm Thin Film FIB performed with Hitachi NB-5000 2011

**HD – 2700 200 kV**

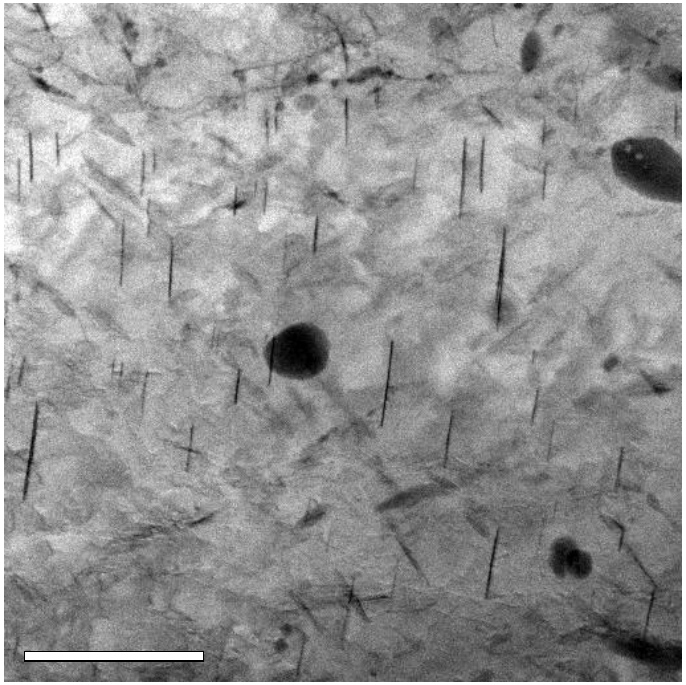

**SU-8000 30 kV**

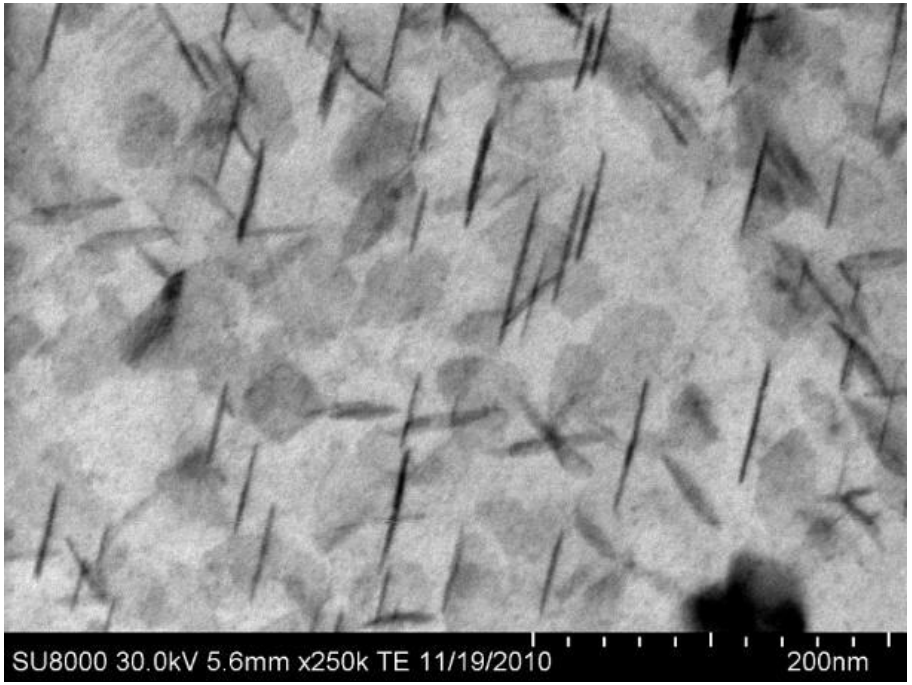

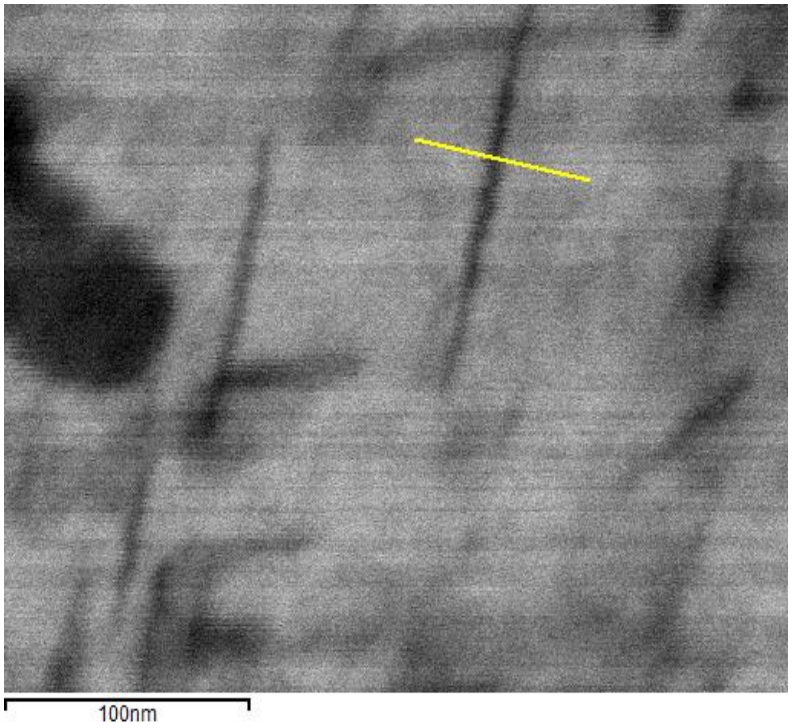


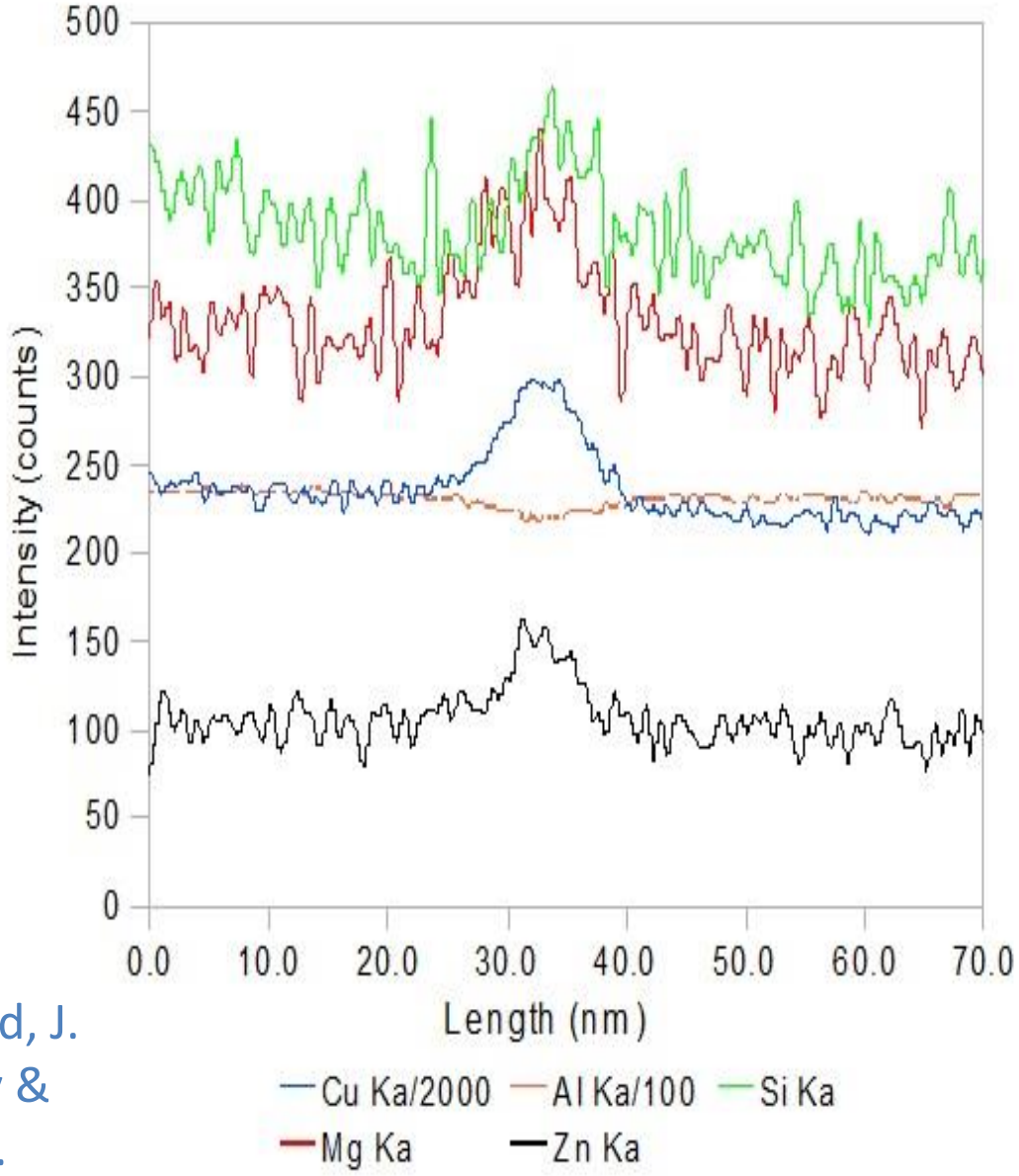


N. Brodush, M. L. Trudeau, P. Michaud, J. Boselli, R. Gauvin (2012), Microscopy & Microanalysis, 18, 6, pp. 1393 - 1409.

# X B 100-X Fe, 30 keV, 50 nm, 10 000 000 e

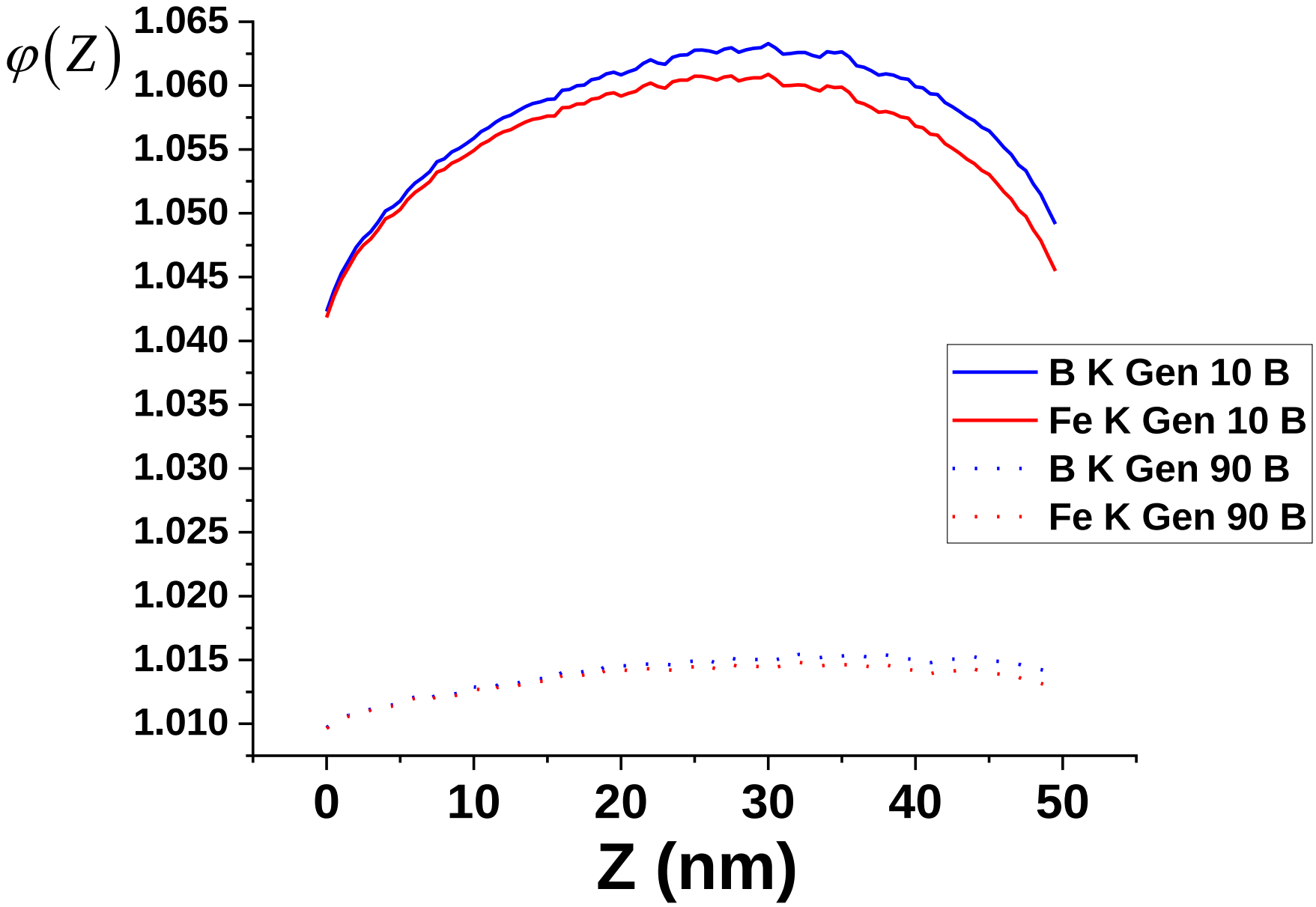

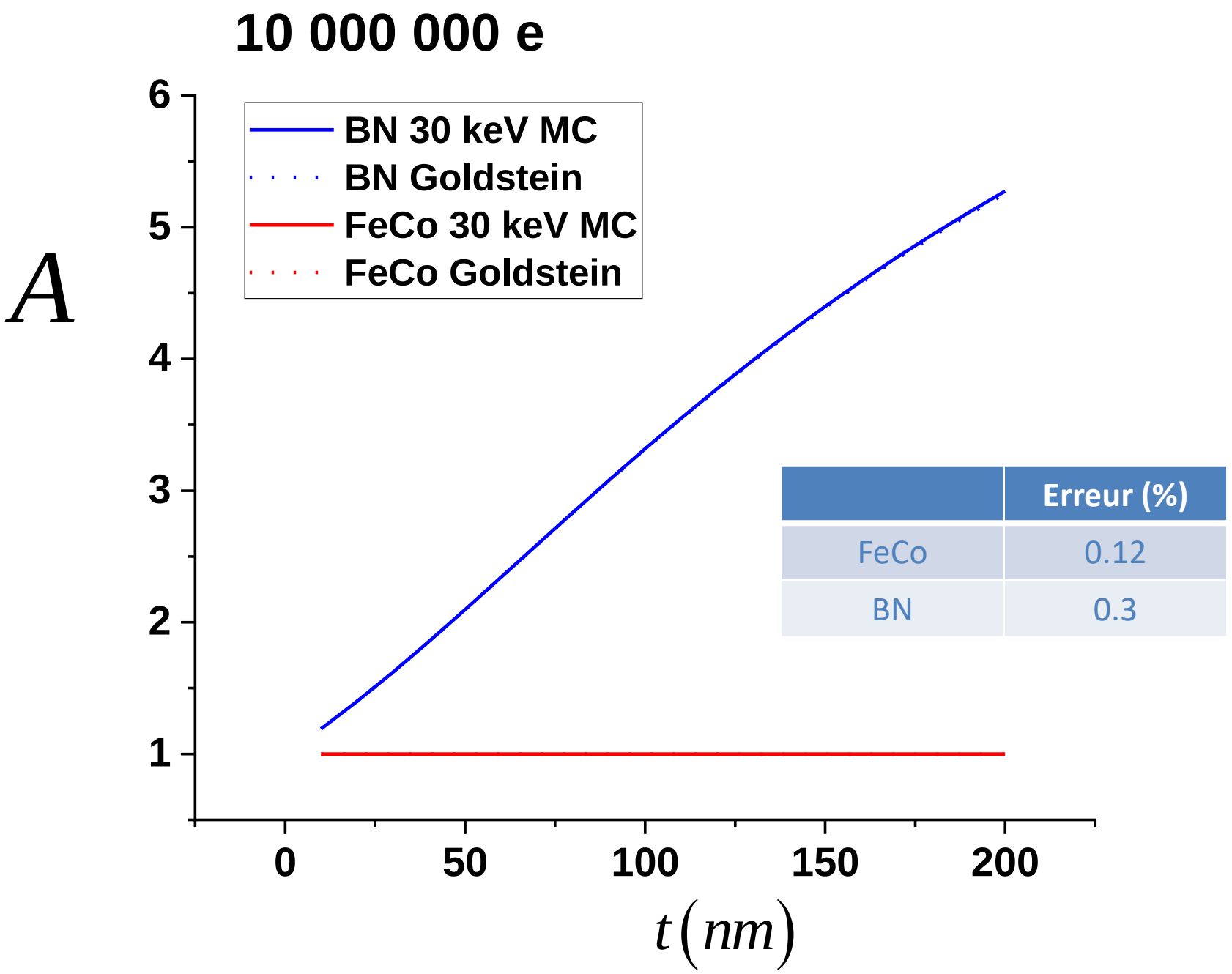


| | Erreur (%) |
|---|---|
| FeCo | 0.12 |
| BN | 0.3 |

# Conversion of graphite to graphene oxide

CBED

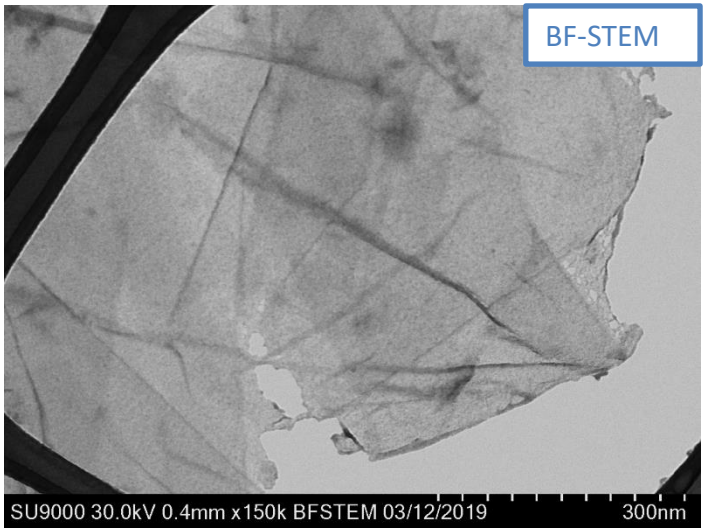


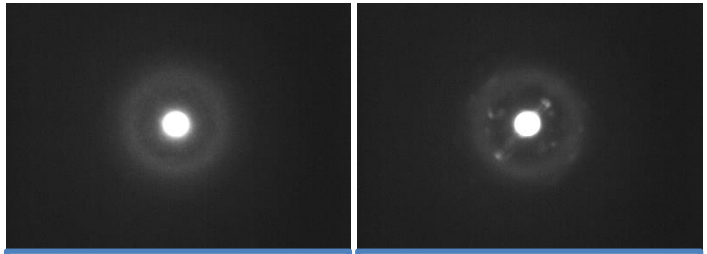

amorphous region | semi-crystalline region

EELS

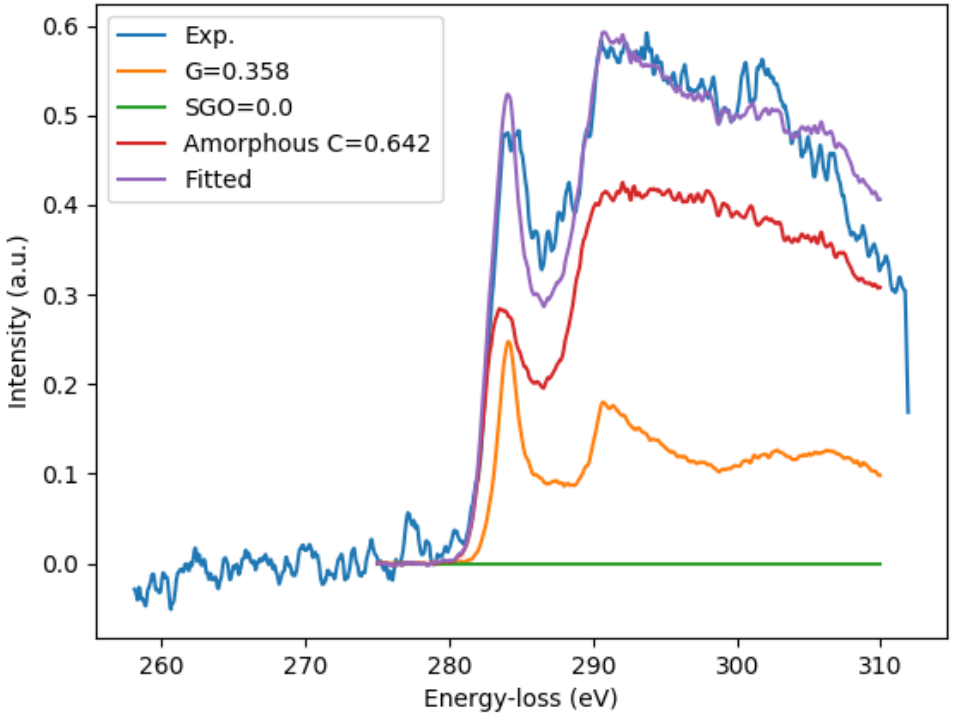


***EELS C K edge profile fitting***

# Three-windows mode on Al NPs
# Low-loss EELS – Plasmon imaging

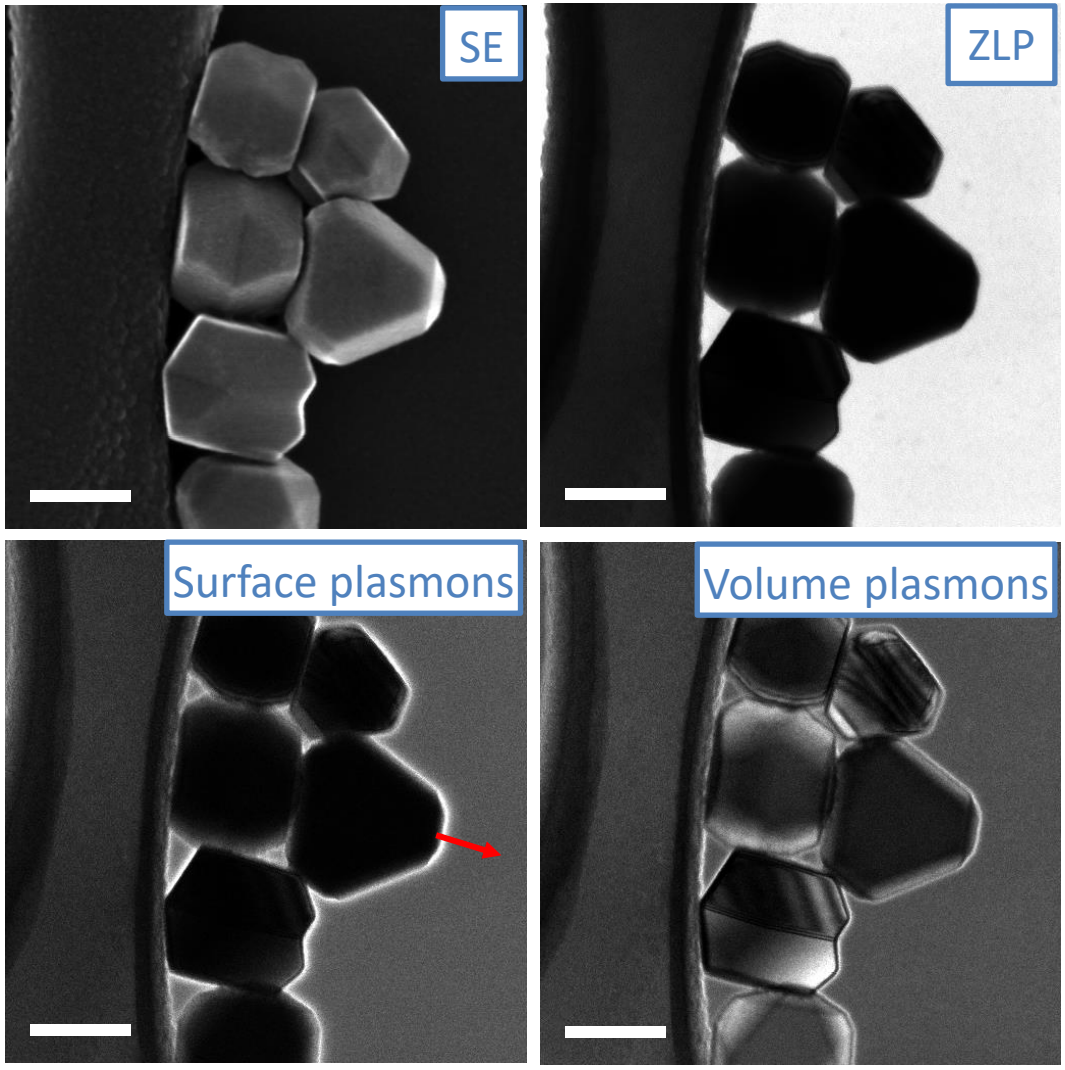


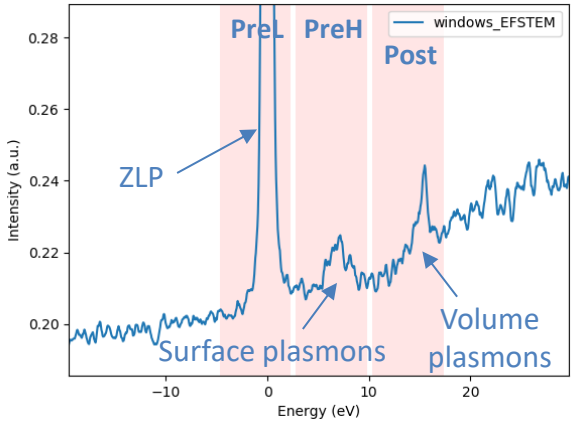


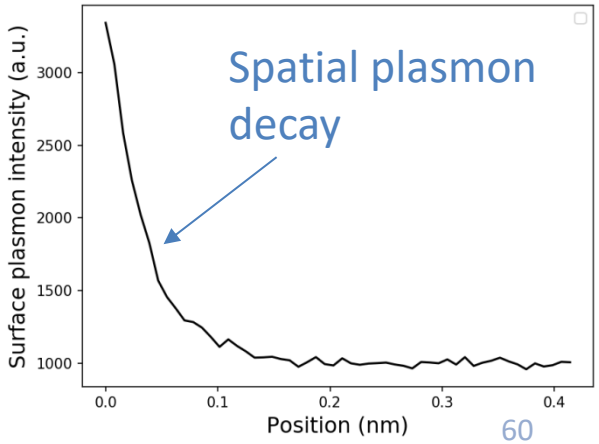

# Quantitative X-Ray Microanalysis
# The f Ratio Method

$$f_A = \frac{I_A}{I_A + I_B}$$

$$f_A = \frac{1}{1 + \Lambda_{A-B} K_{A-B} \frac{\int \varphi_B(\rho z) e^{\chi_B \rho z} d\rho z}{\int \varphi_A(\rho z) e^{\chi_A \rho z} d\rho z} \frac{F_B}{F_A} \frac{c_B}{c_A}}$$

P. Horny, E. Lifshin, H. Campbell and R. Gauvin (2010), "Development of a New Quantitative X-Ray Microanalysis Method for Electron Microscopy", Microscopy & Microanalysis, Vol. 16, No. 6, pp. 821-830.

# 50 B - 50 Fe (%At.), 10 000 000 e

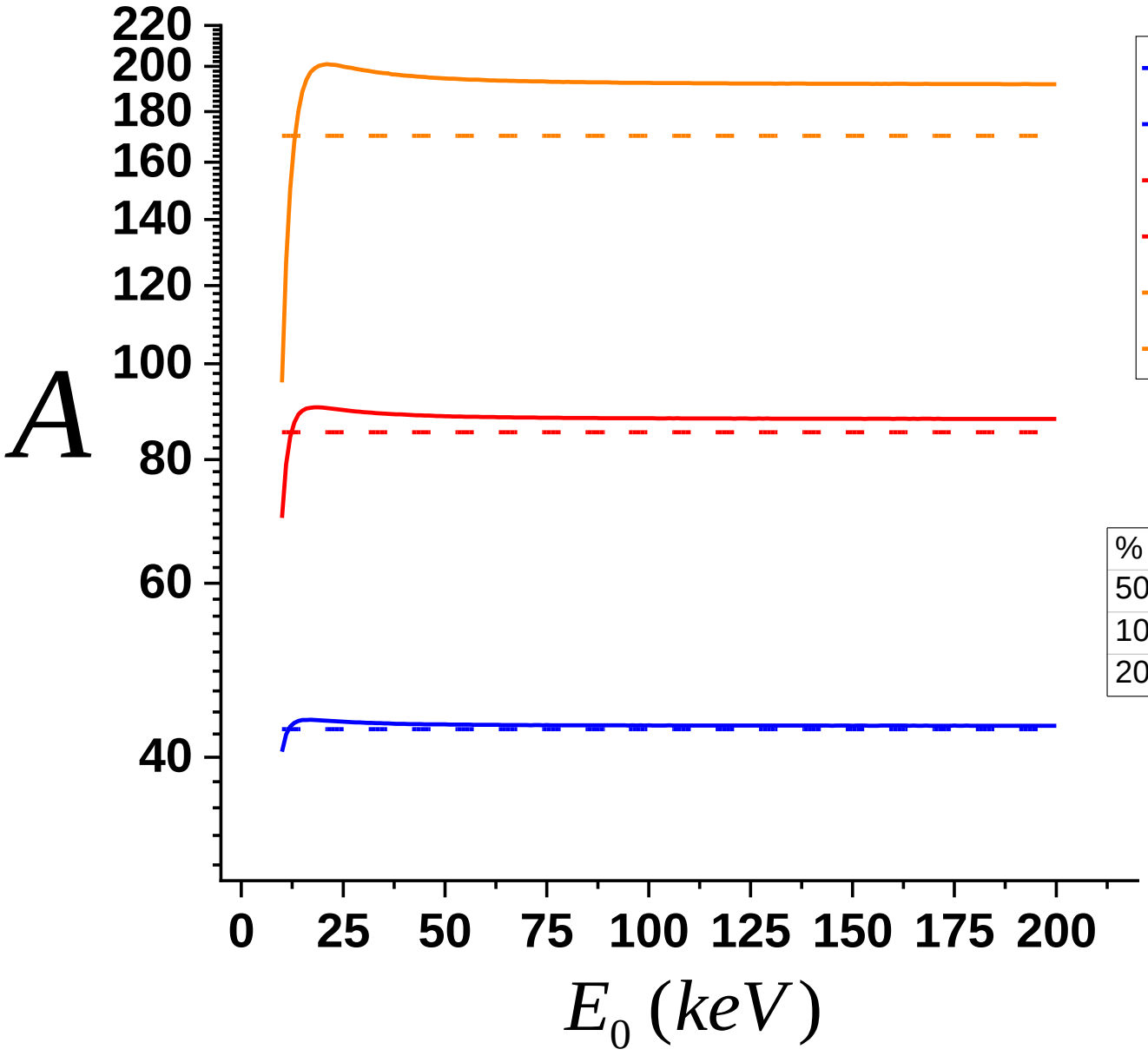


| % erreur | 30 keV | 200 keV |
|---|---|---|
| 50 nm | 1.5 | 0.8 |
| 100 nm | 4.8 | 3.2 |
| 200 nm | 16.5 | 12.8 |

# Microanalyse des Films Minces

- Tixier et Philibert (1968) ont développé une méthode de ratio des intensités de films minces mais avec une correction ZAF avec des témoins massifs.
- Duncumb (1968)

# Fast Secondary Electrons
# Bulk Oxygen, 100 keV

**R. Gauvin (1990), Ph.D. Thesis**

# Imaging of nanomaterials with EDS at 30 kV (windowless EDS detector)

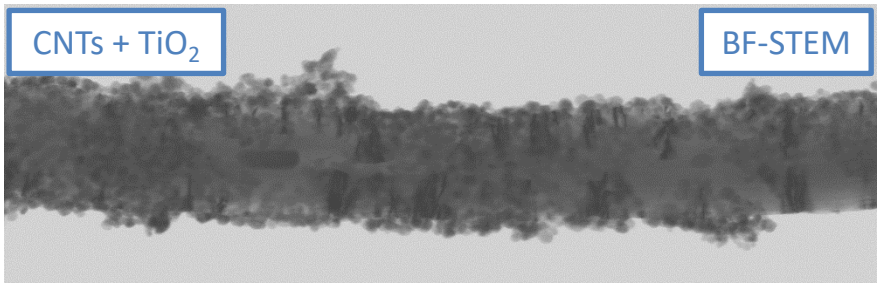


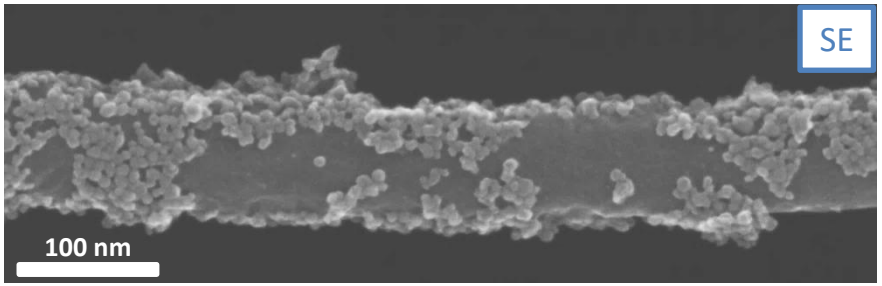


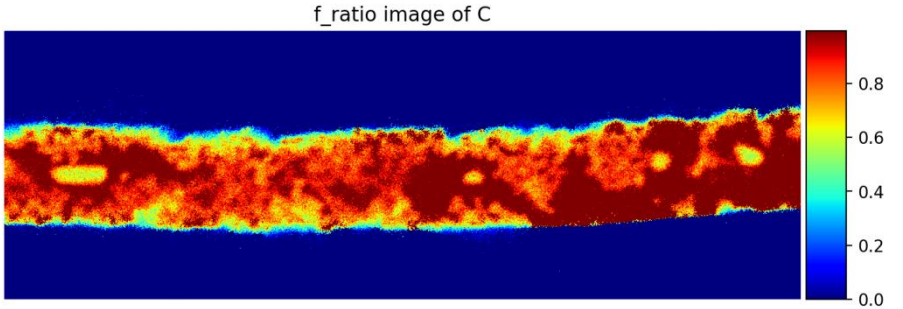


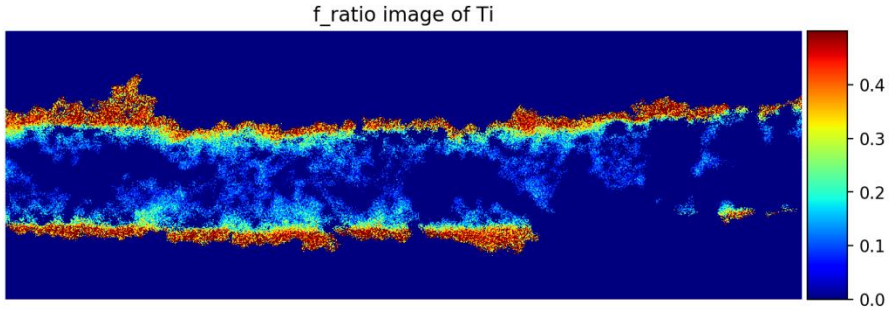


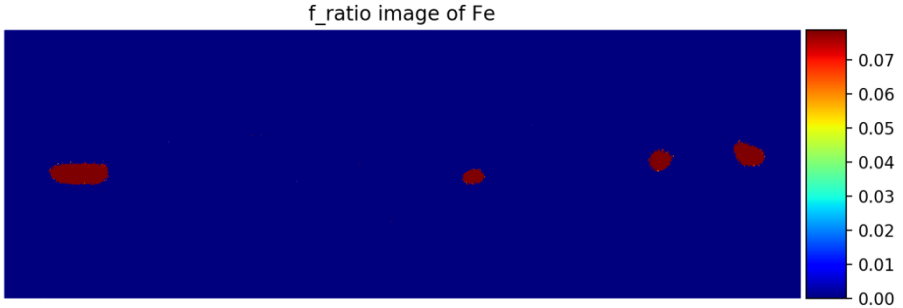


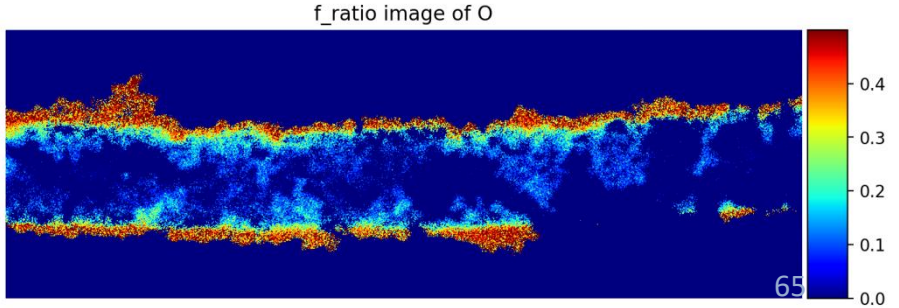

# $Li_2CoSiO_4$ (LCS, precursor: $CoCl_2$): Low Voltage (3 kV) X-ray Imaging (SU-9000)

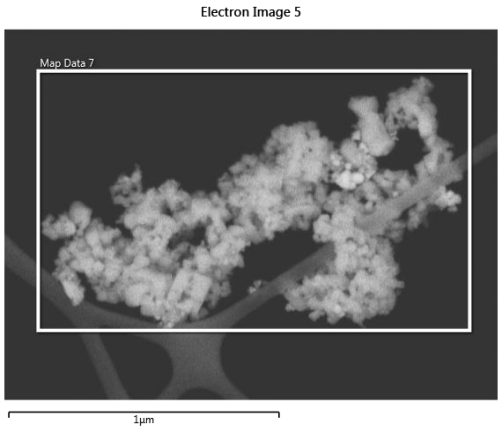


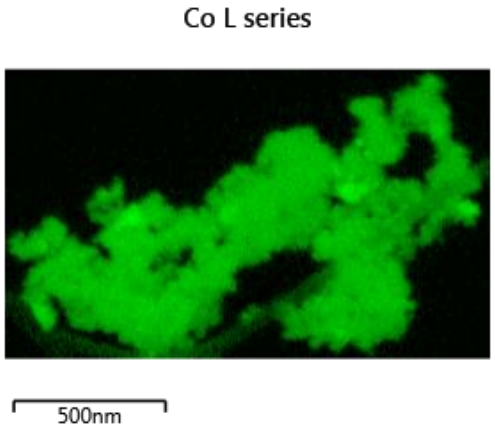


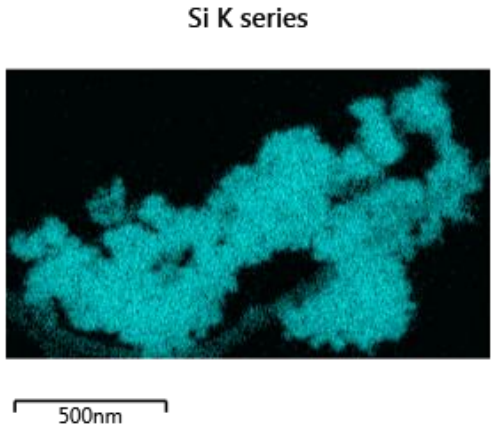


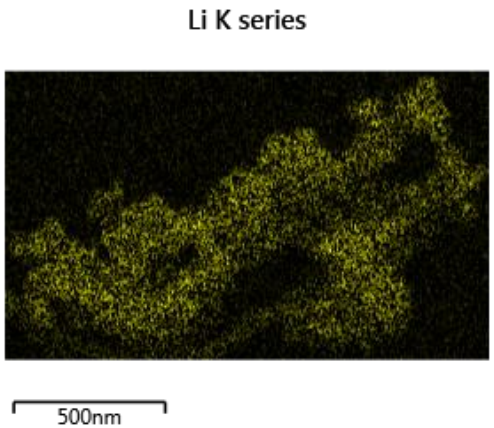


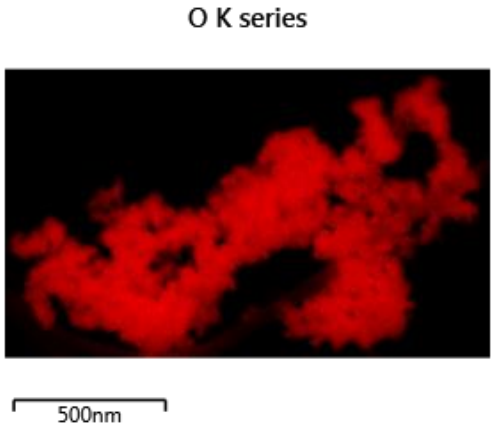


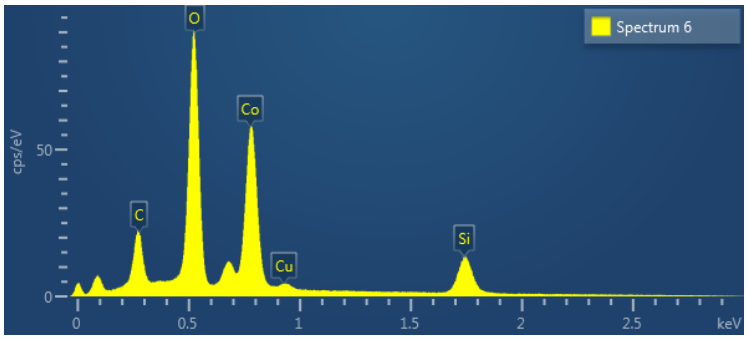

STEM-BF

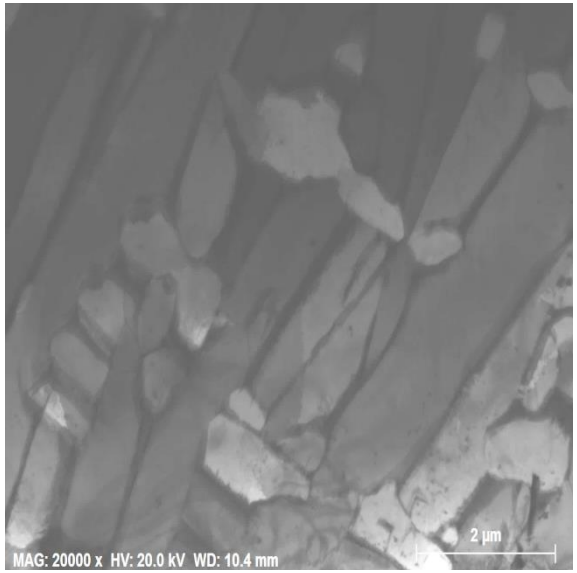


Ti Kα - Net

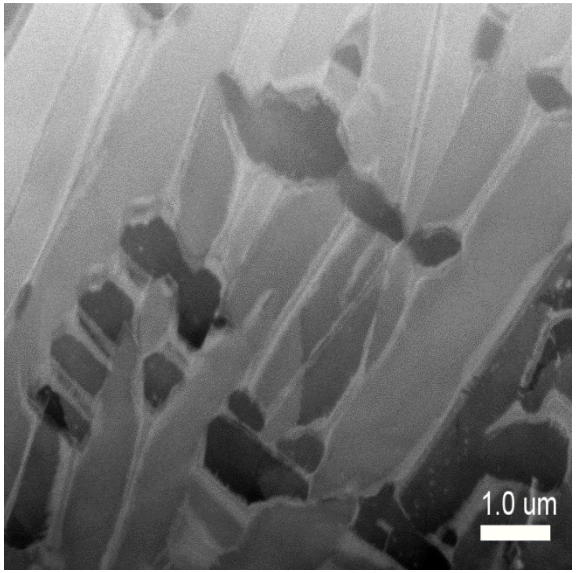


Ti Kα – f_ratio

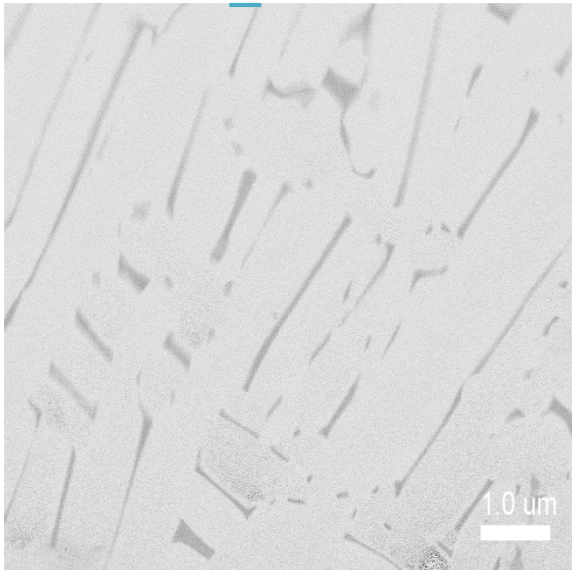


a

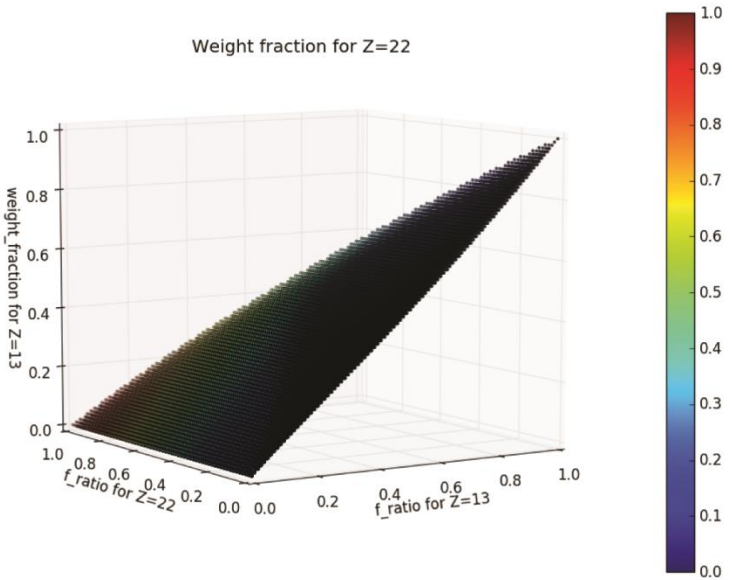


b Al

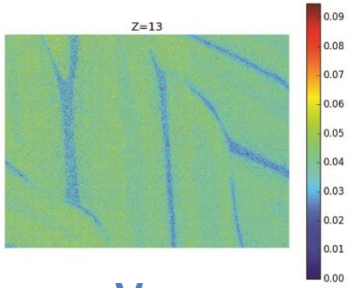


c Ti

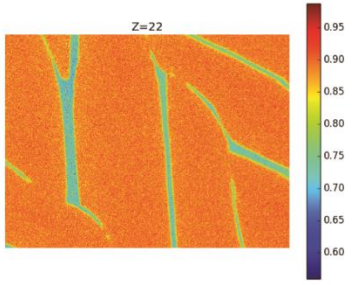


d V

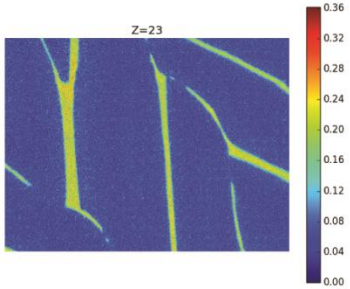


e Fe

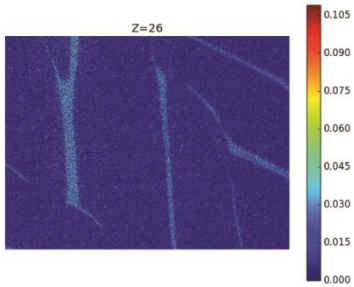

# Mg-Ca-Zn alloy
# STEM 30kV – Bright-field Imaging

**0 % Mn**

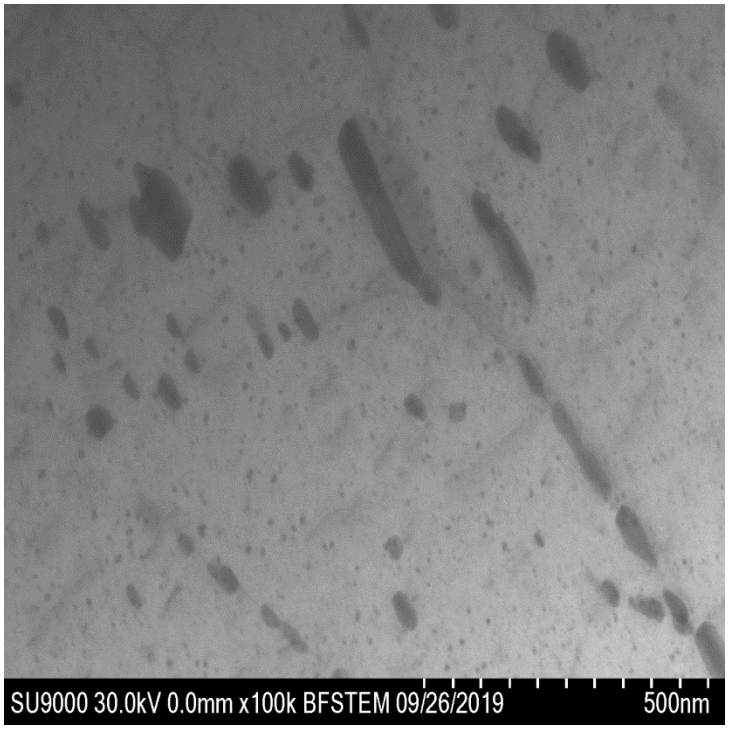


**0.3 % Mn**

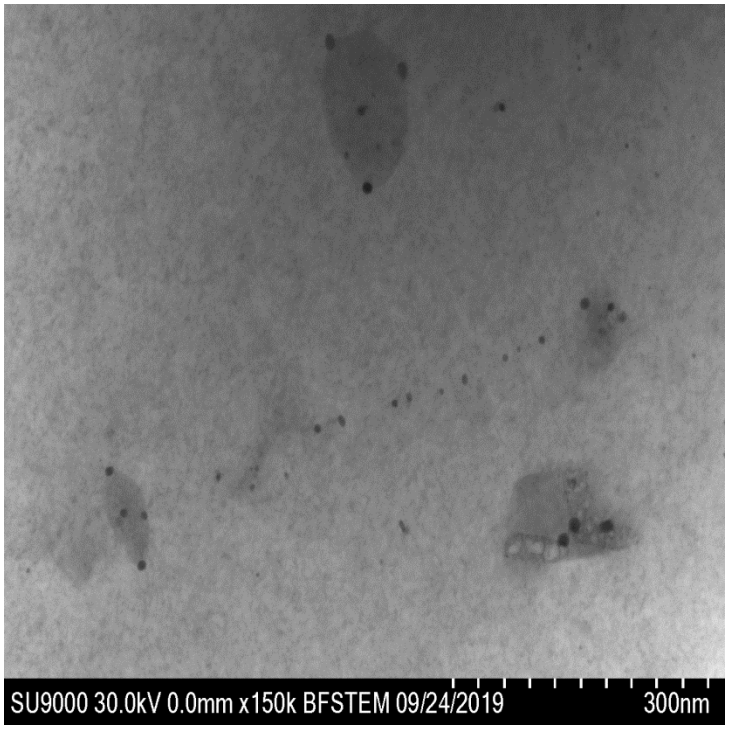

# STEM 30kV – EDS mapping (Extreme detector)

**0 % Mn**

**0.3 % Mn**

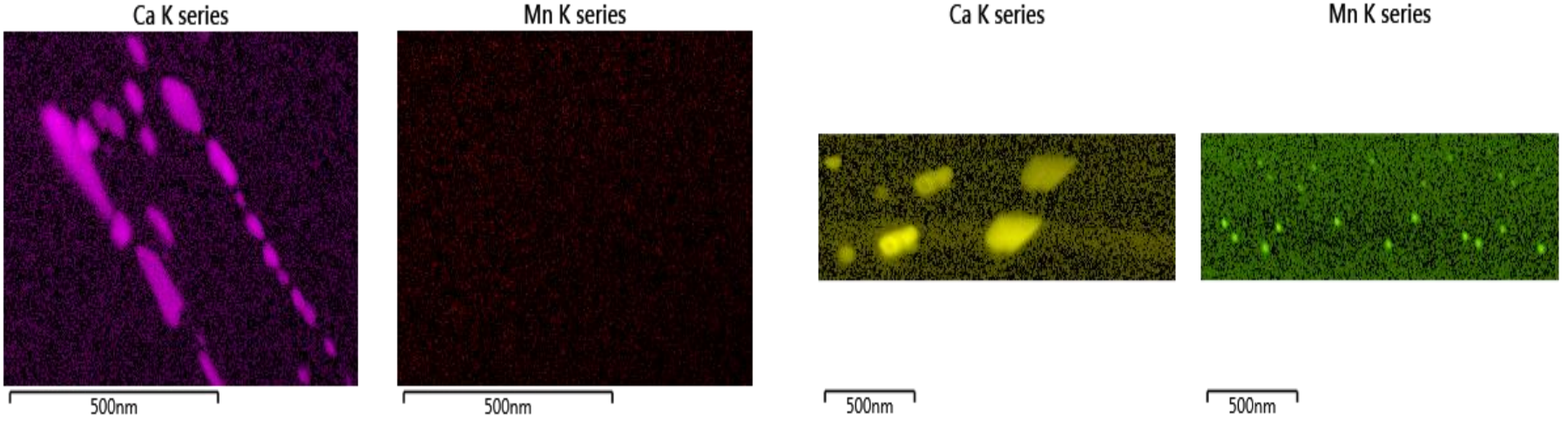

# STEM 30kV – EELS Elemental mapping

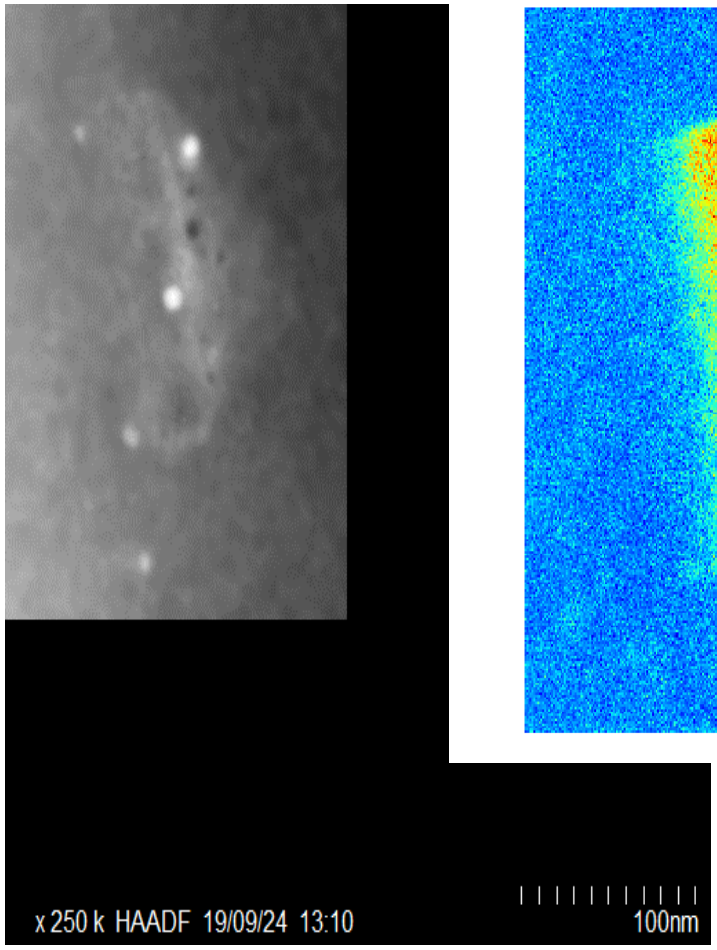


Jump ratio map for Ca L edge

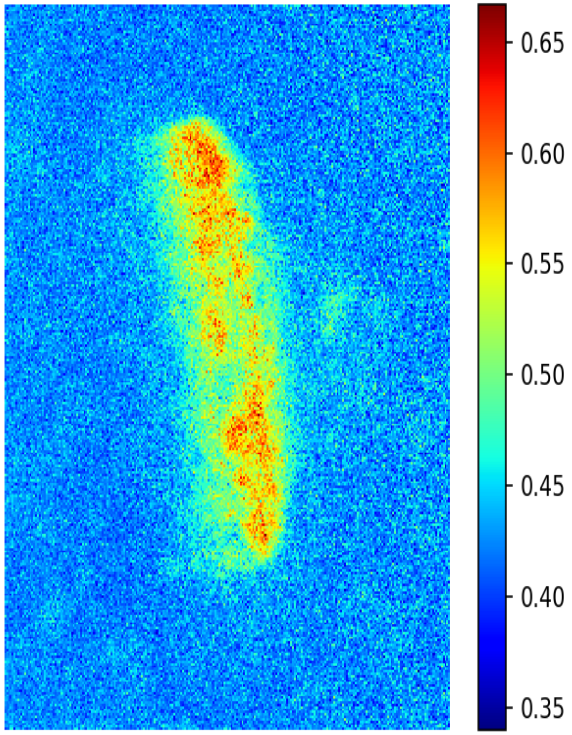


Jump ratio map for Mn L edge

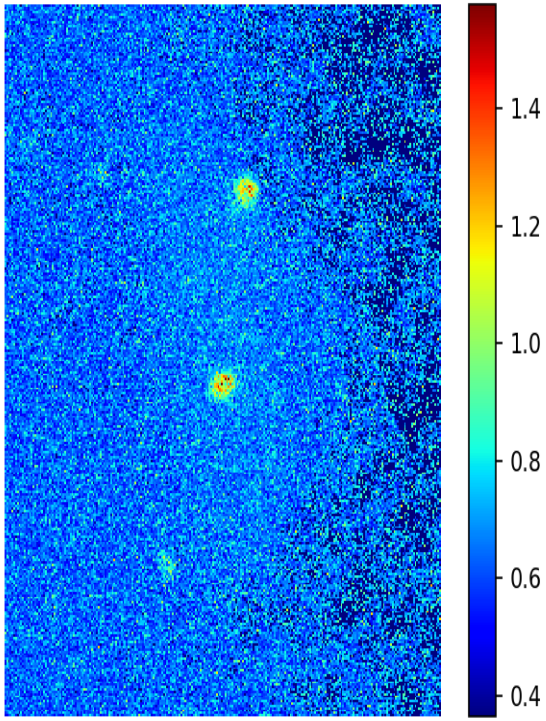

# Lithium X-ray production

- Maximum emission at low voltage ($E_0$ < 5 kV)
- Different intensity for similar Li weight fractions
- Complex emission process

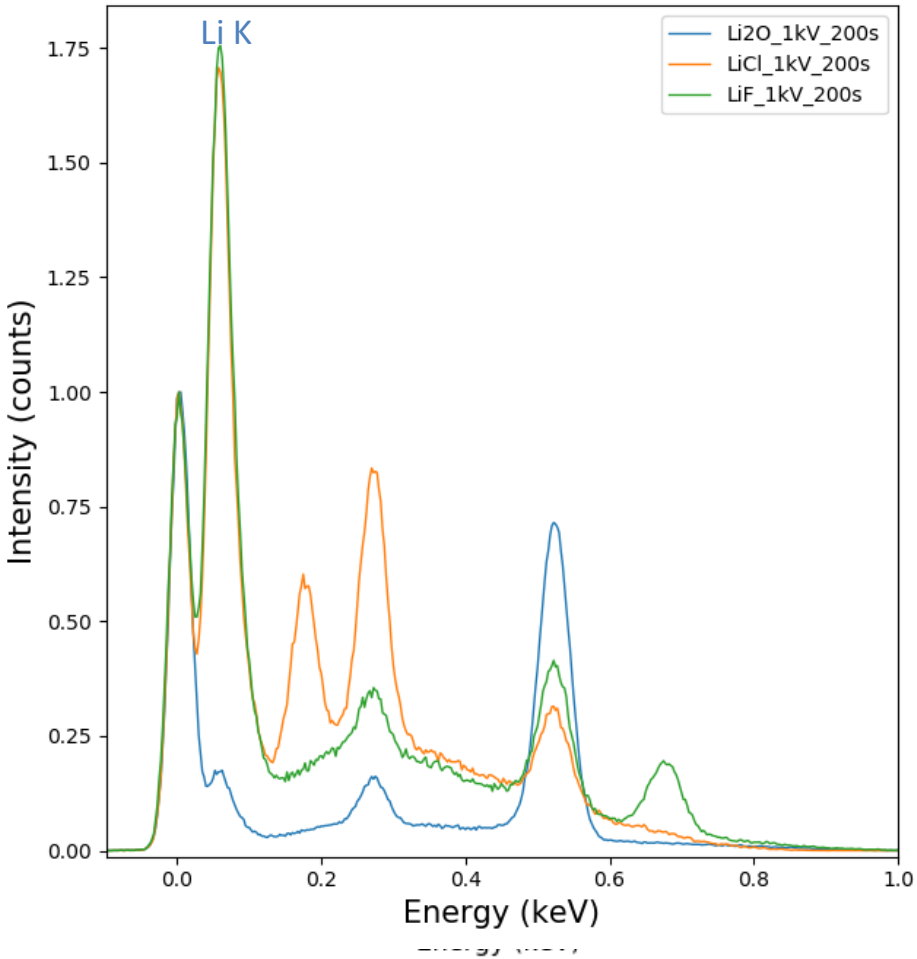


| Compound | Theoretical Lithium minimum weight fraction |
|---|---|
| $LiO_2$ | 0.1782 |
| LiF | 0.2676 |
| LiCl | 0.1637 |

# $Al_{64}Mg_{36}$ powder

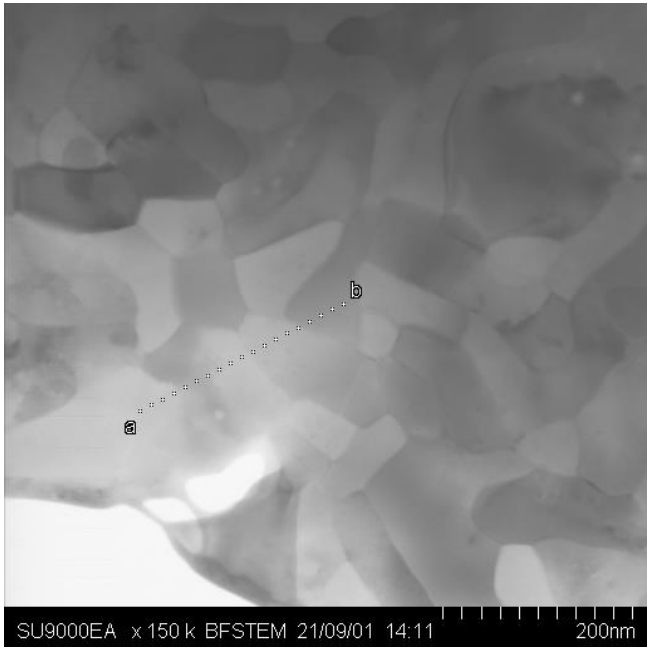


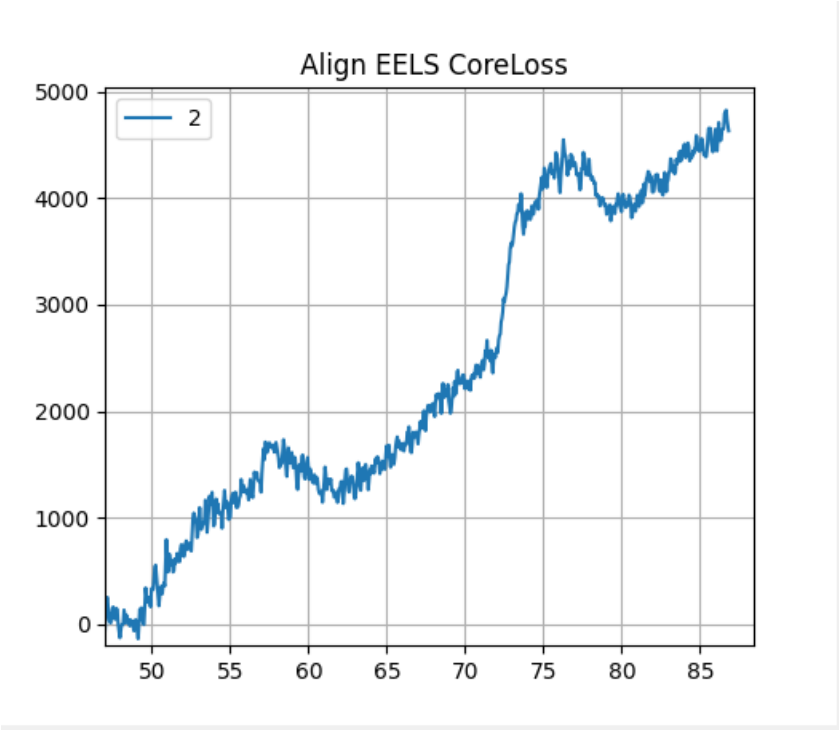

# SEM et STEM à Bas Voltage

Moins cher que TEM
à Haute Énergie

Plus de Temps de
Microscopie

Pour les mêmes dollars

# h - BN

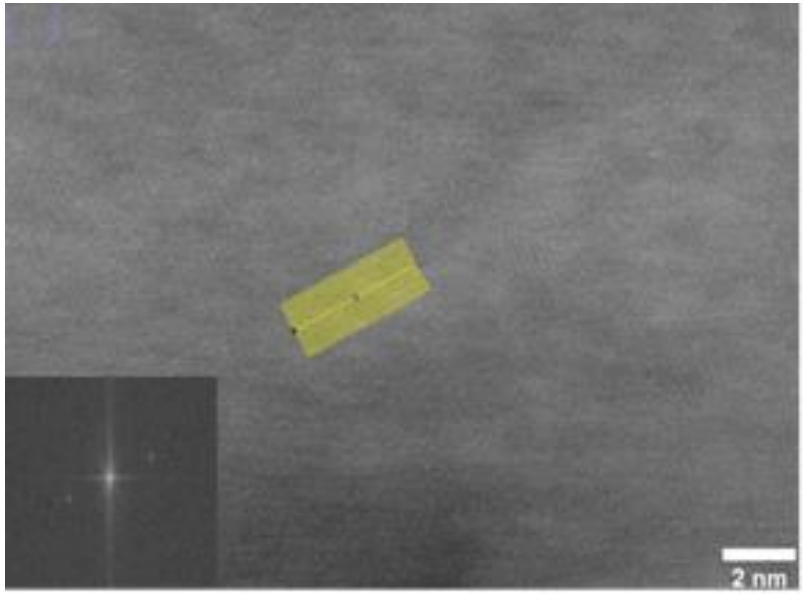
2 nm

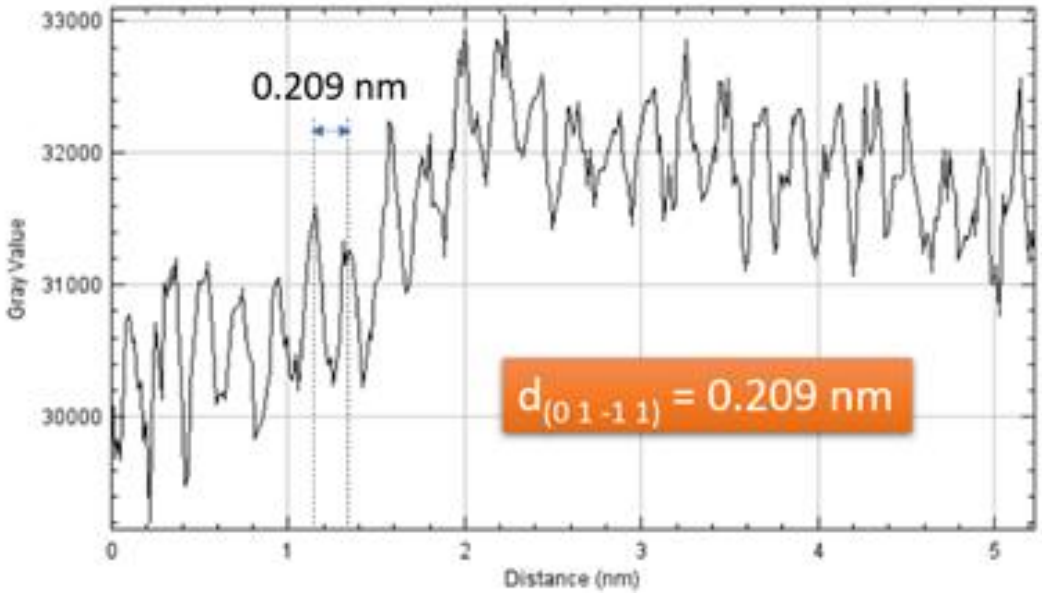
0.209 nm
$d_{(0\,1\,-1\,1)}$ = 0.209 nm
Gray Value
33000
32000
31000
30000
0
1
2
3
4
5
Distance (nm)

# Si FIB lamella

## SU9000 at 30keV

HAADF raw

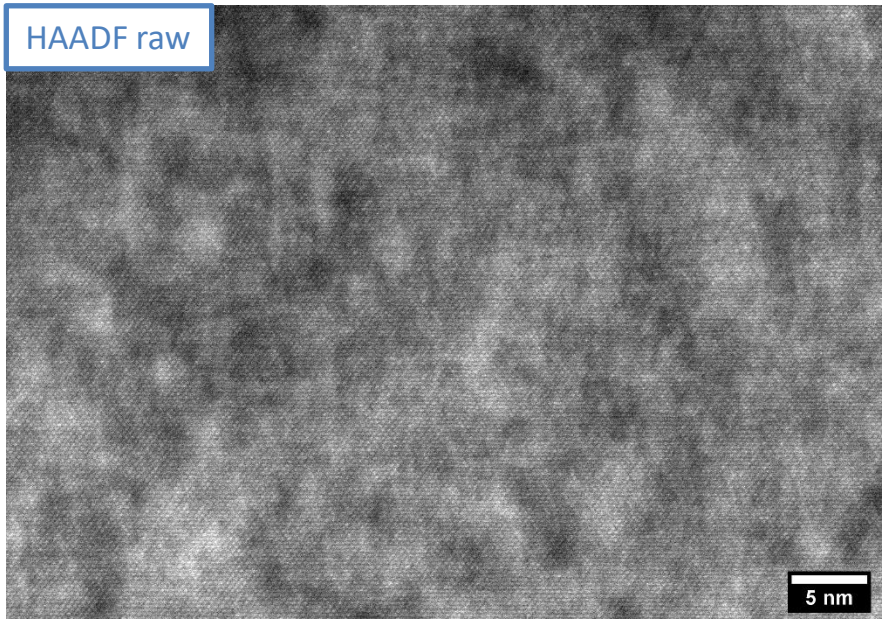


HAADF processed

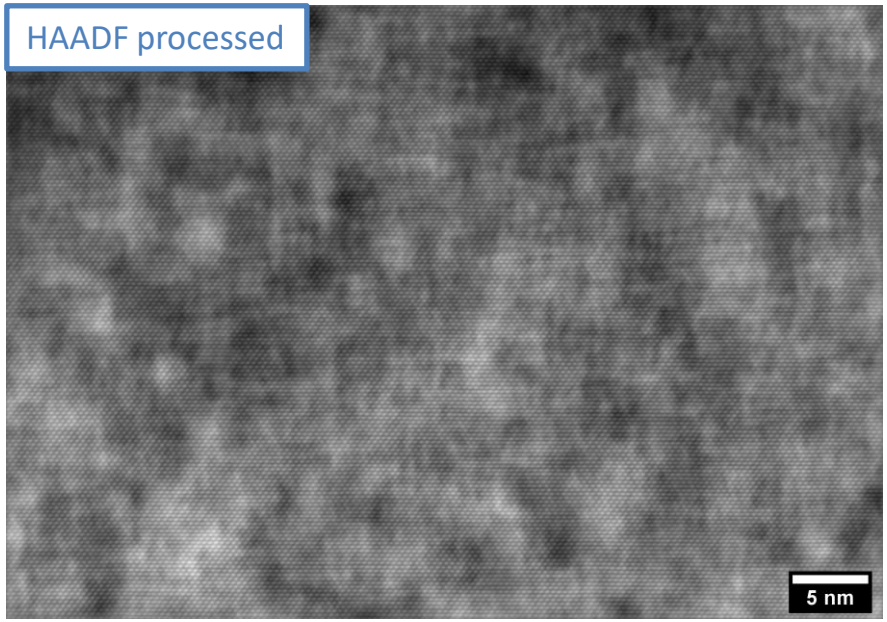

# Dual – Beam FIB

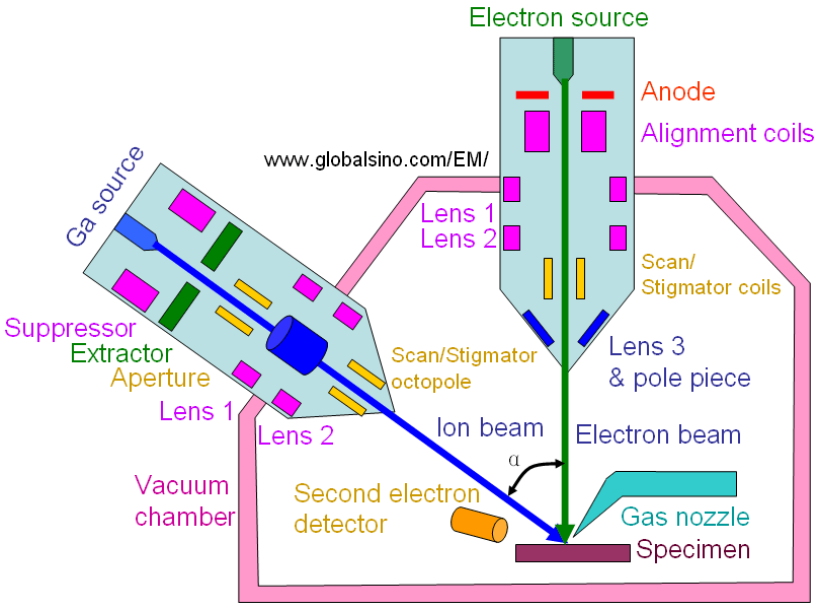


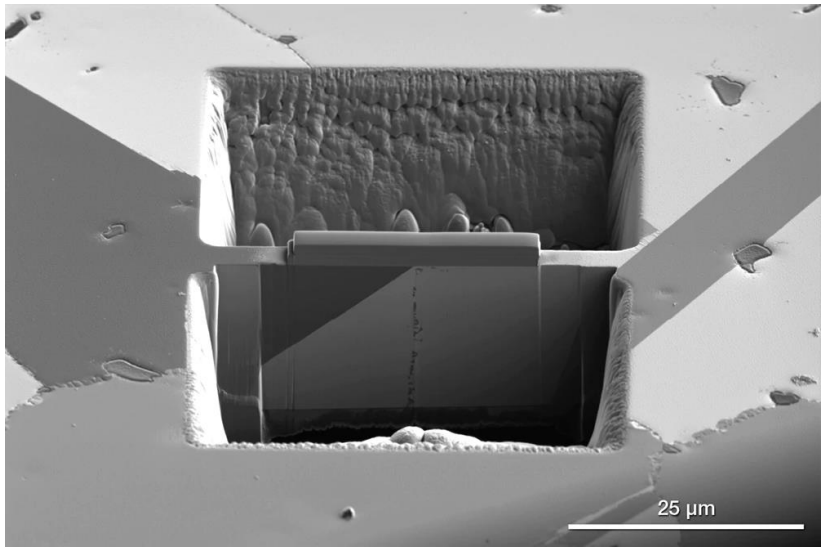


- TEM thin film preparation
- 3D Imaging
- Nano fabrication

# Applications : Bulk lift-out for ECCI microstructure Imaging of localized subsurface features

- Lift-out of thick lamellas to transfer in other SEMs for further analysis

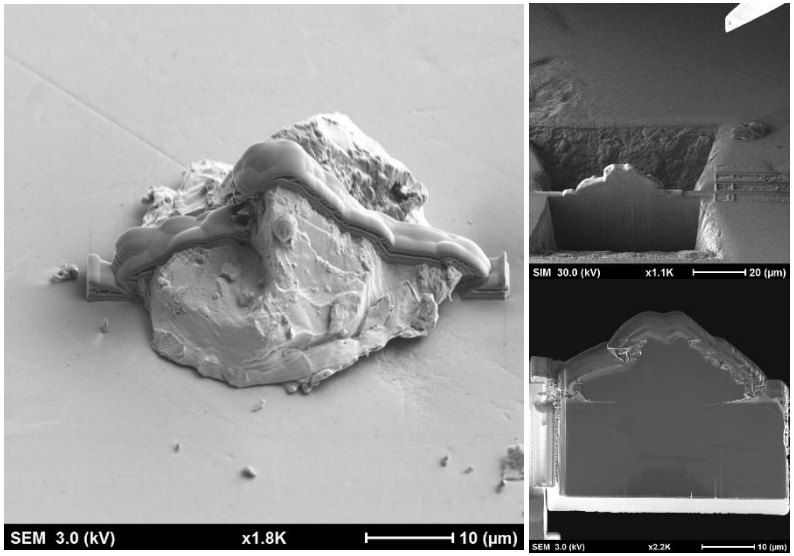


In the FIB-SEM system: liftout and fine polishing

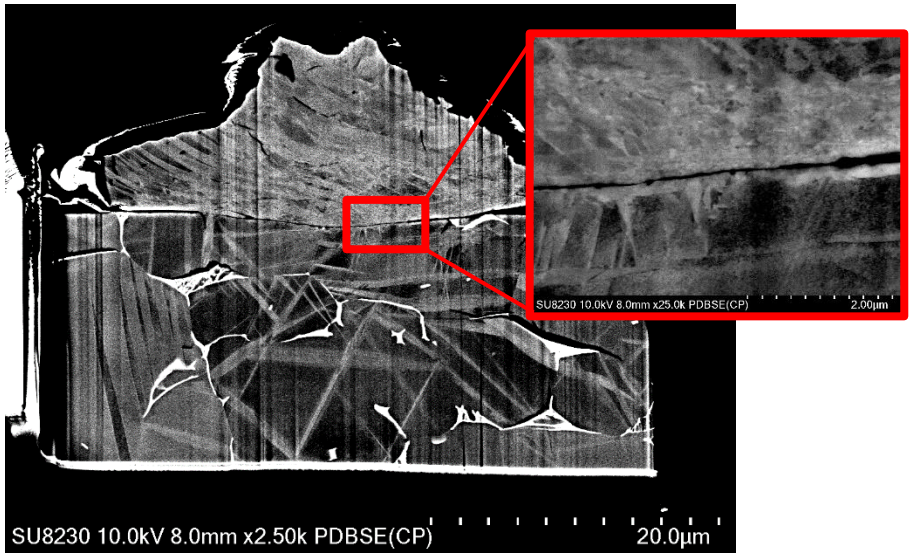


Transfer to SEM for imaging (ECCI) and or further analyses (EDS, EBSD etc)

*Specimen: Courtesy of Sima Alidokht, Prof. Richard Chromik Group*
*Acquisition : Stéphanie Bessette*

# Pr. Jinhyuk Lee's Cathode

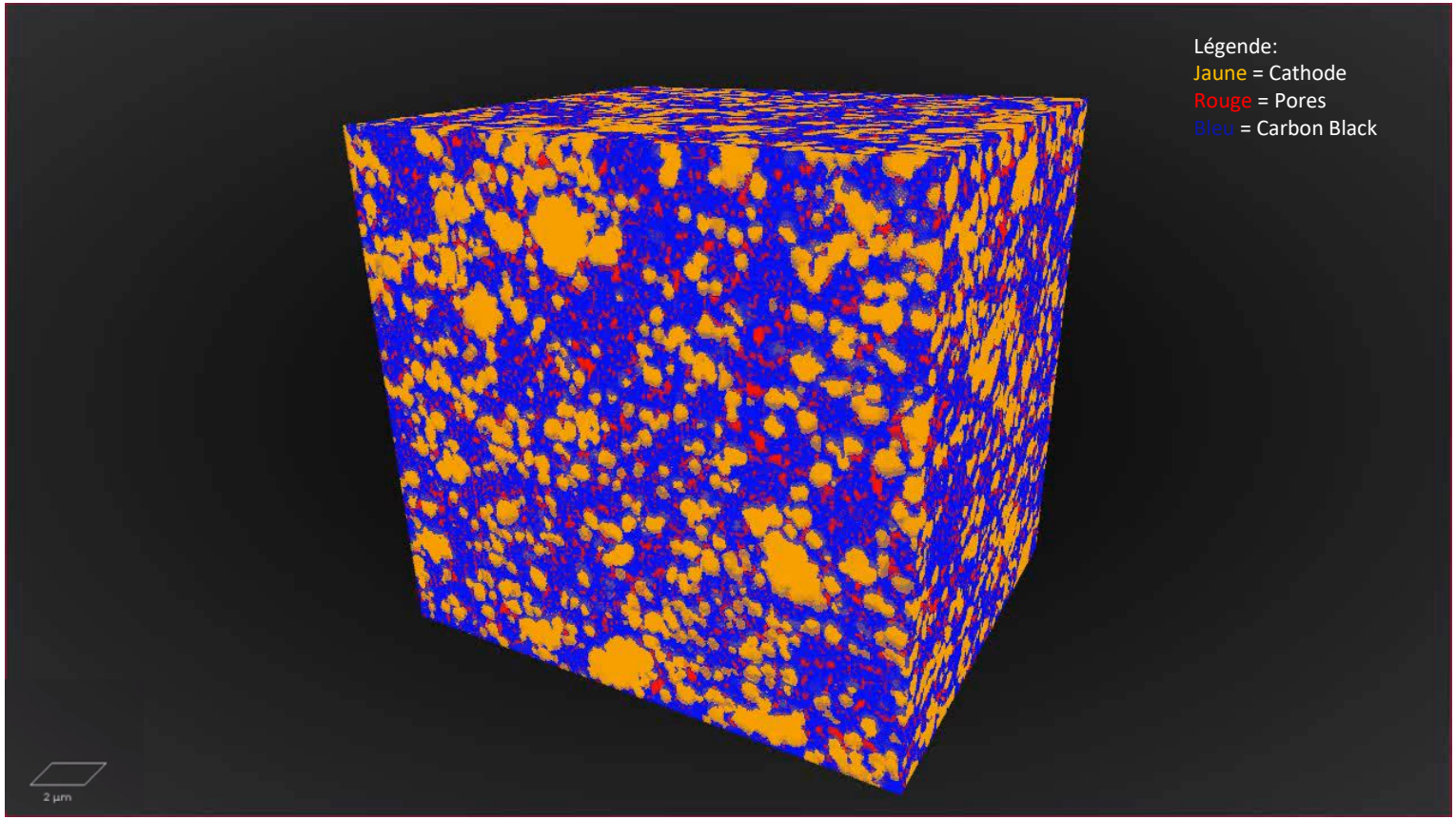


Superimposed SEM signal : BSE L+U (composition contrast)

We use Deep Learning to improve image segmentation with DragonFly. Stéphanie Bessette FIB + DragonFly.

# Pores

*m = 2.68*
*D = 0.60*

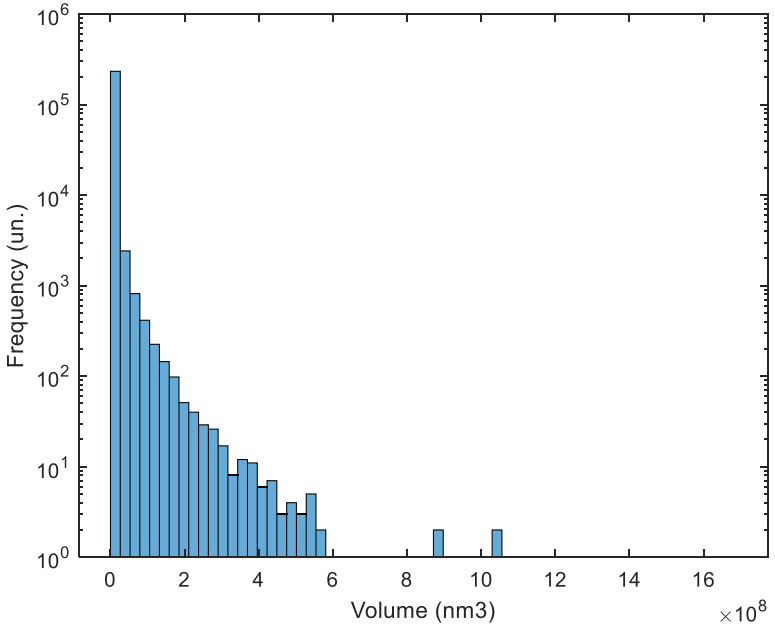


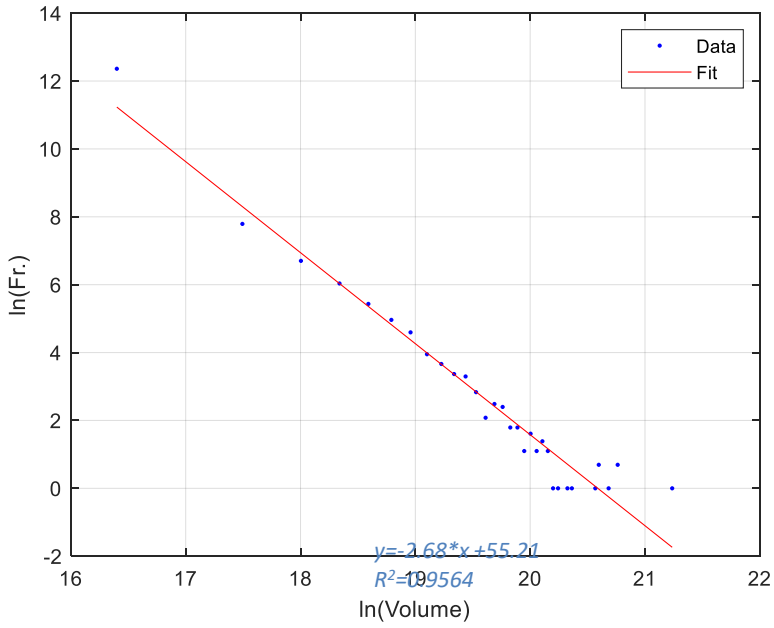


$$f(r) = Kr^{-(1+D)} \propto r^{-m}$$

$$r \propto V^{1/D}$$

$$D = \frac{1}{m-1}$$

# First Results FIB
# Low C Martensitic Steel. Pr. Yue
# 100 nm thin film – 30 keV

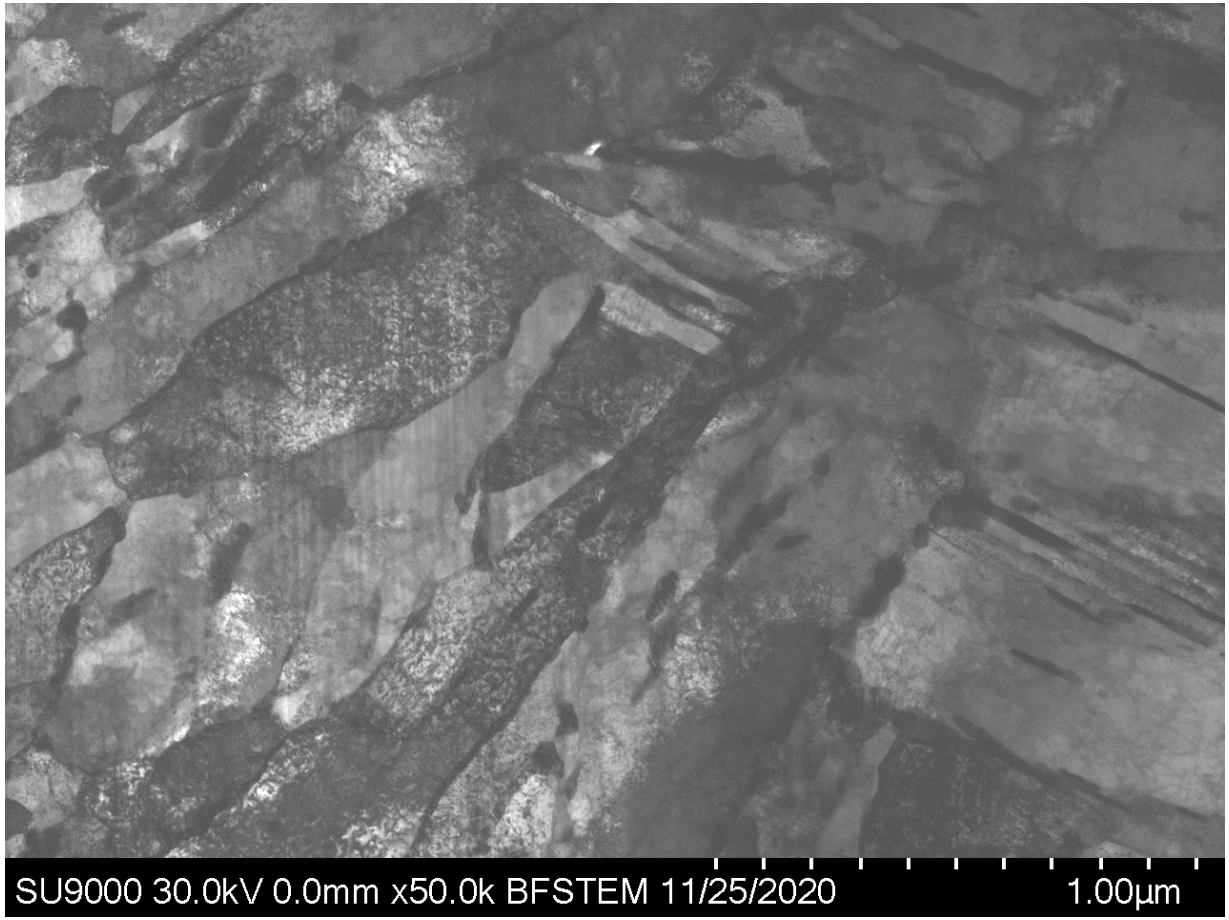

# SU – 8230 EBSD in Transmission

TKD map on low carbon martensitic steel
(T. Das / S. Yue)

DF (colorized)

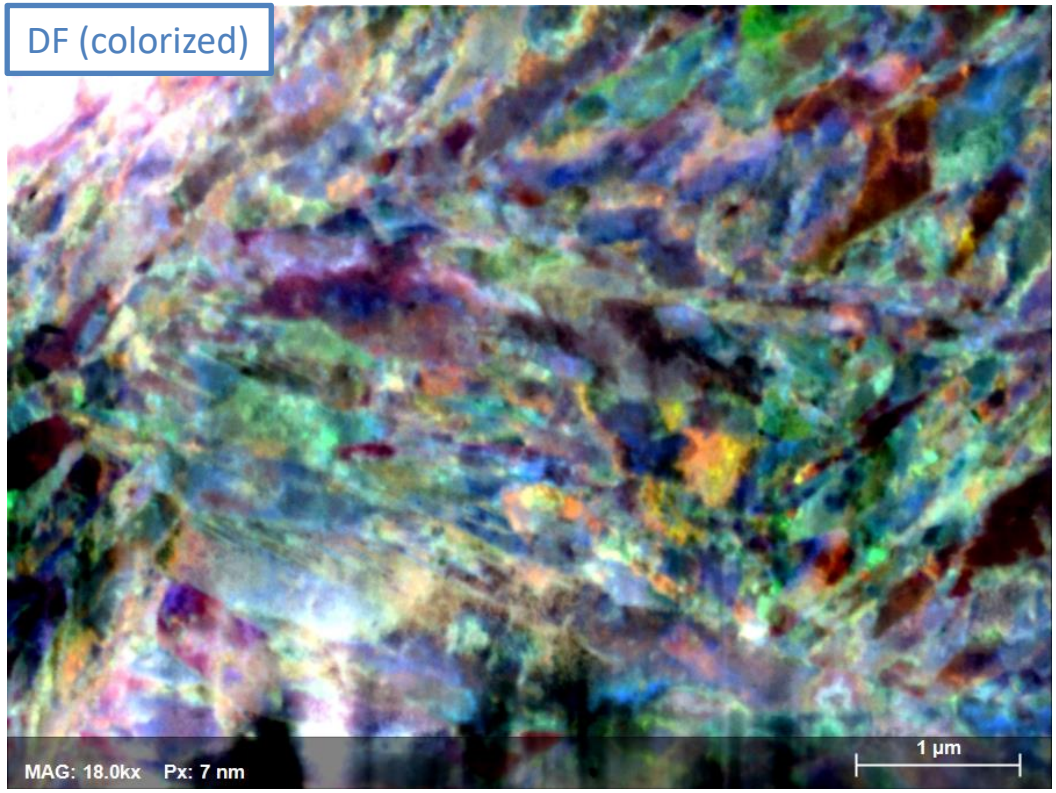


Band contrast map

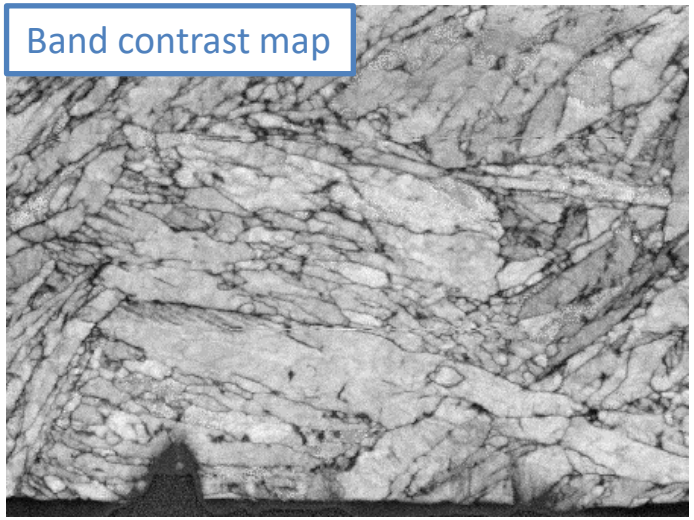

Grain map

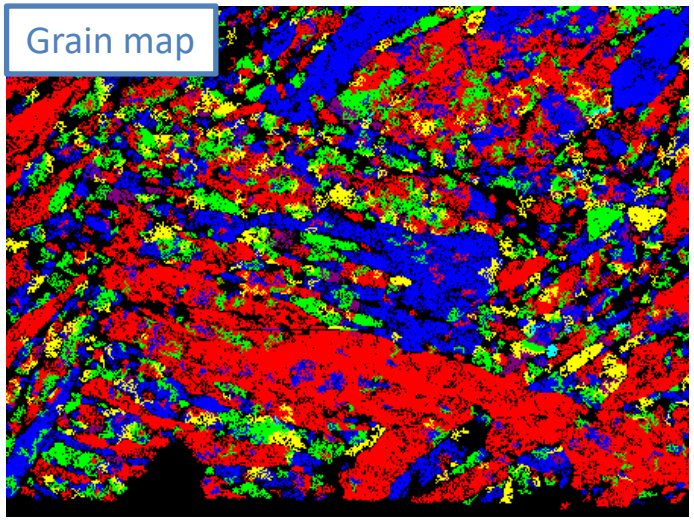

**Smallest grains 10 – 15 nm**

# Increased ionization damage (radiolysis) at low accelerating voltage

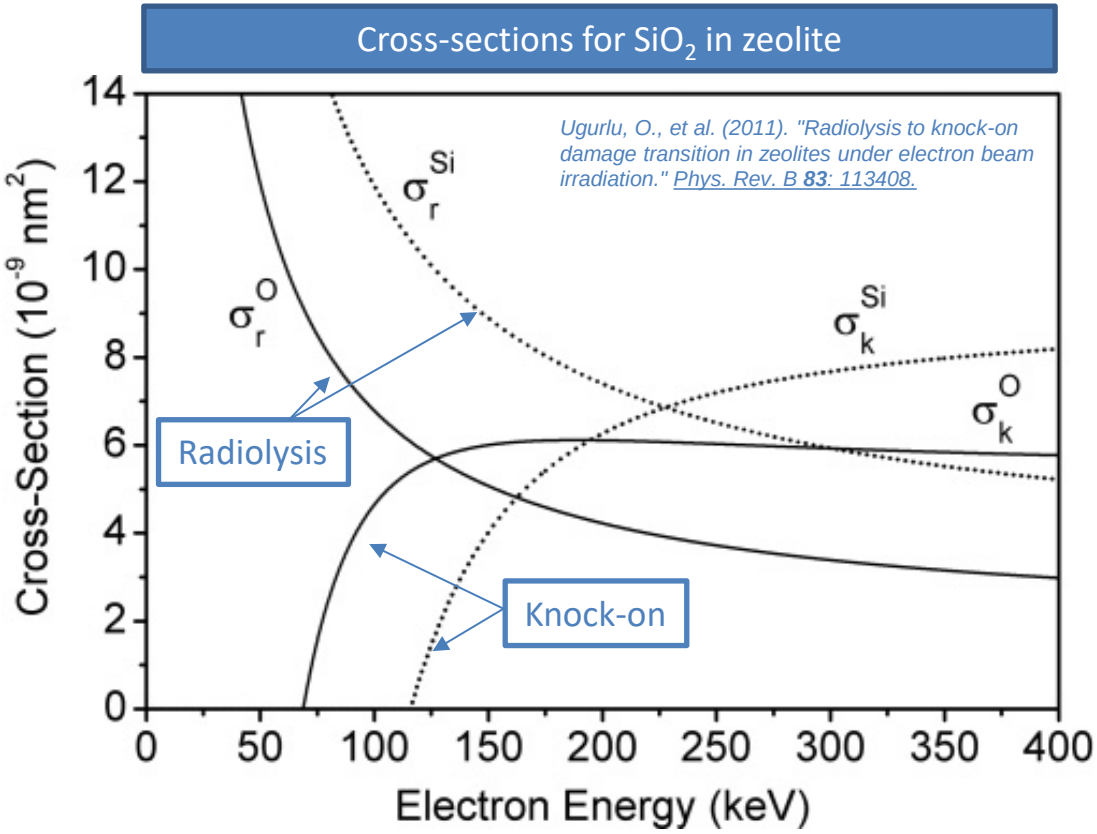


- Radiolysis dramatically increased for $E_0$ < 100 kV
- Limitation for electron sensitive materials

# CRYO TRANSFER HOLDER

Model 200: DUAL AUTOGRID CRYO TRANSFER HOLDER; THERMOFISHER/FEI

Model 205: DUAL GRID CRYO TRANSFER HOLDER; THERMOFISHER/FEI

Model 210: DUAL AUTOGRID CRYO TRANSFER HOLDER; JEOL

Model 215: DUAL GRID CRYO TRANSFER HOLDER; JEOL

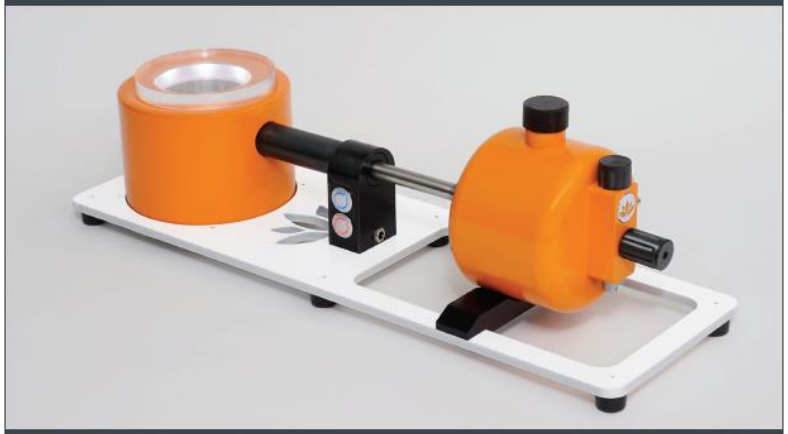

The newly designed Cryo Transfer Holder allows for 10 hours of high quality data acquisition with your Transmission Electron Microscope

SIMPLE ORIGIN

OPTIMIZE YOUR RESEARCH

# Elemental imaging mode of EELS

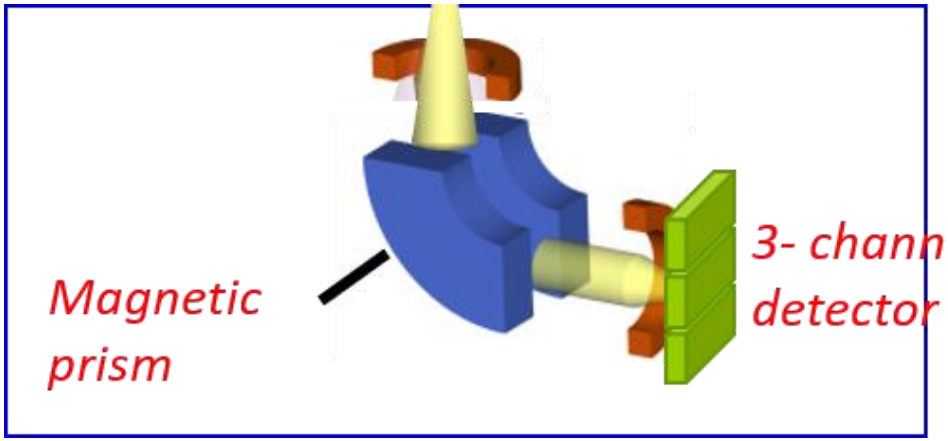


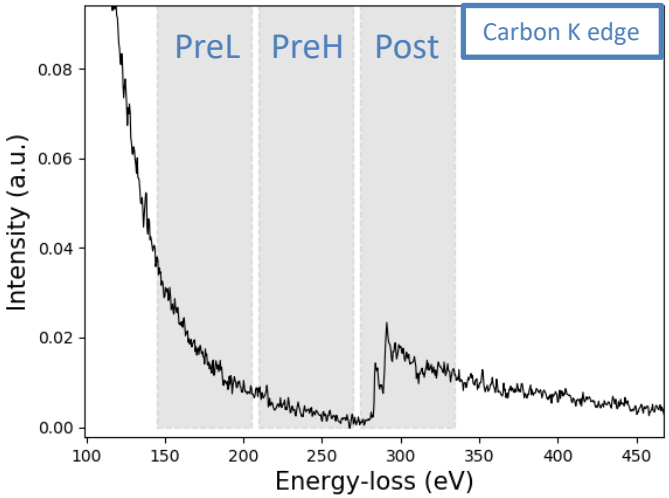


## Elemental map (3-windows)

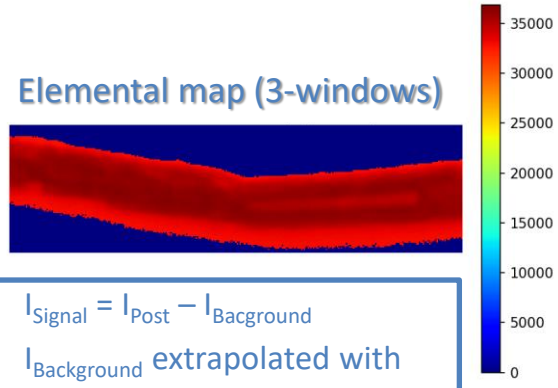


- $I_{Signal} = I_{Post} - I_{Bacground}$
- $I_{Background}$ extrapolated with preL and PreH windows

## Jump ratio map (2-windows)

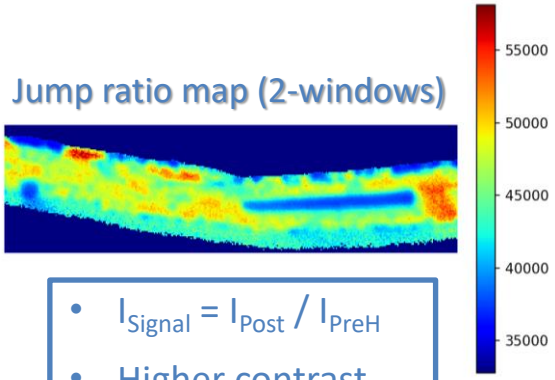


- $I_{Signal} = I_{Post} / I_{PreH}$
- Higher contrast
- Only qualitative

# Thin film preparation $Al_{36}Mg_{64}$ powder

Procedure steps :

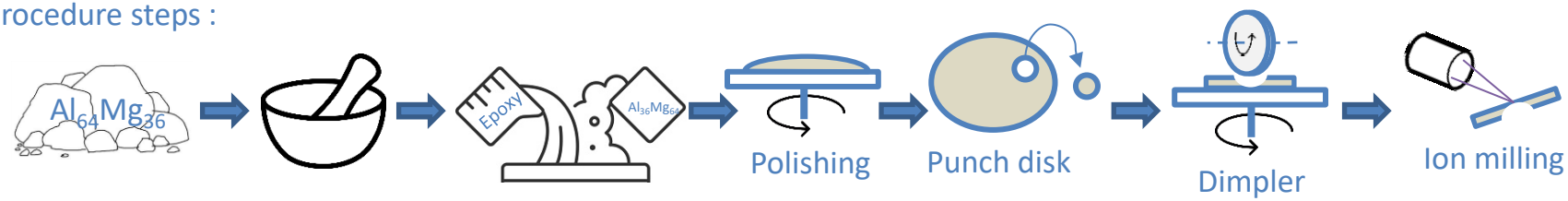


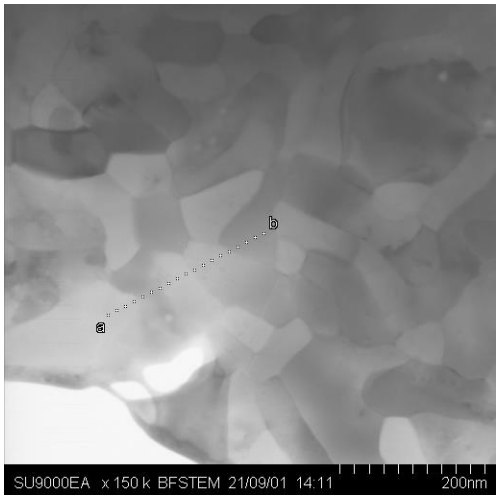


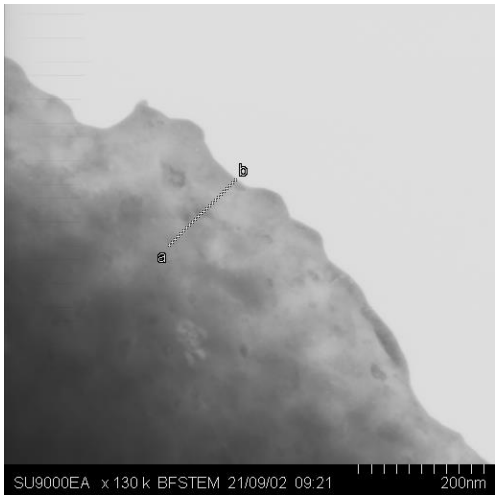


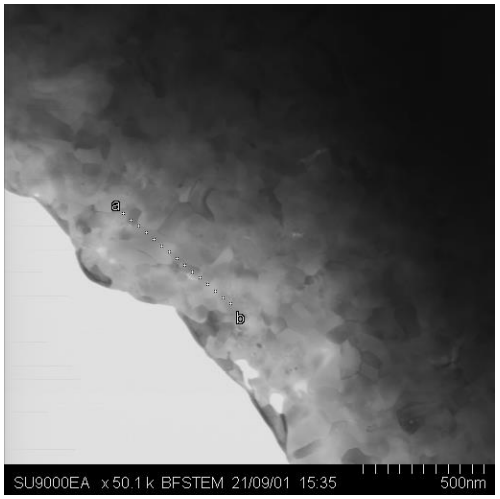

One point of the line scan spectrum

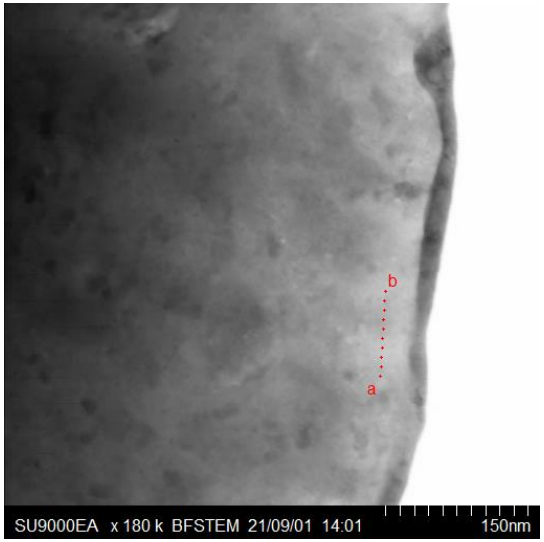


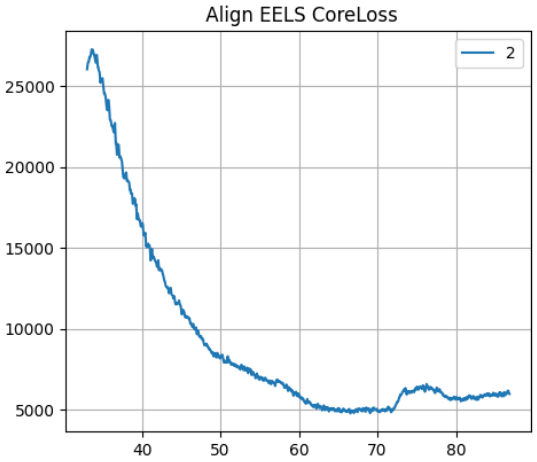


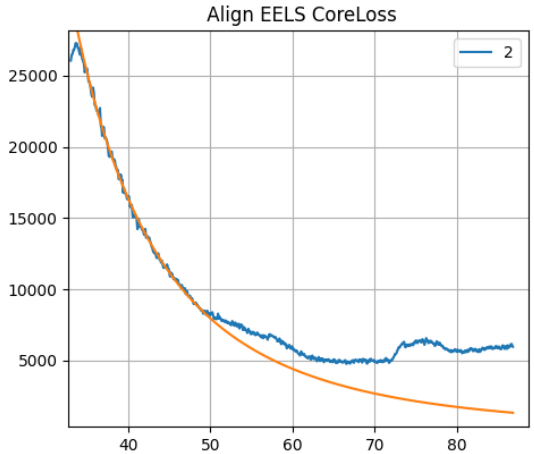


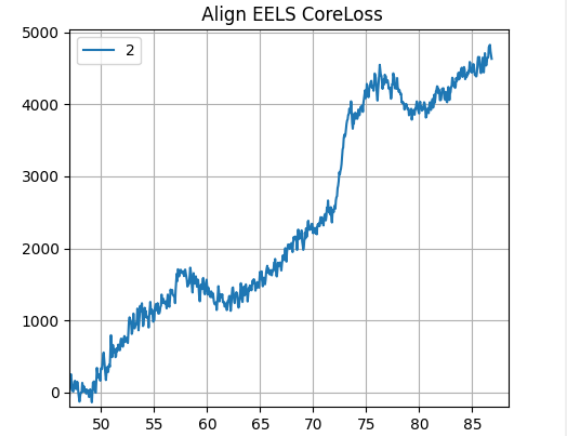


Background subtraction function ($y = Ax^{-r}$)
Is good for near low-loss ?

# Electron diffraction in the SEM/STEM (semi-immersion type)

- Convergent beam diffraction (on-axis TKD set-up)

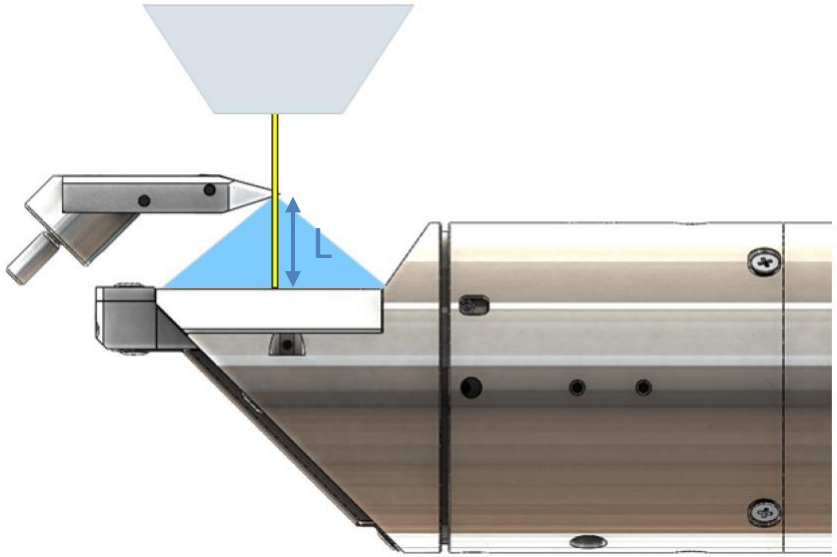


- High sensitivity
- Large collection angle
- Adjustable camera length (L)
- Mapping capability of the EBSD system
- Allows TKD and CBED

# Electron diffraction in the SEM/STEM (semi-immersion type)

- Convergent beam diffraction (on-axis TKD set-up)

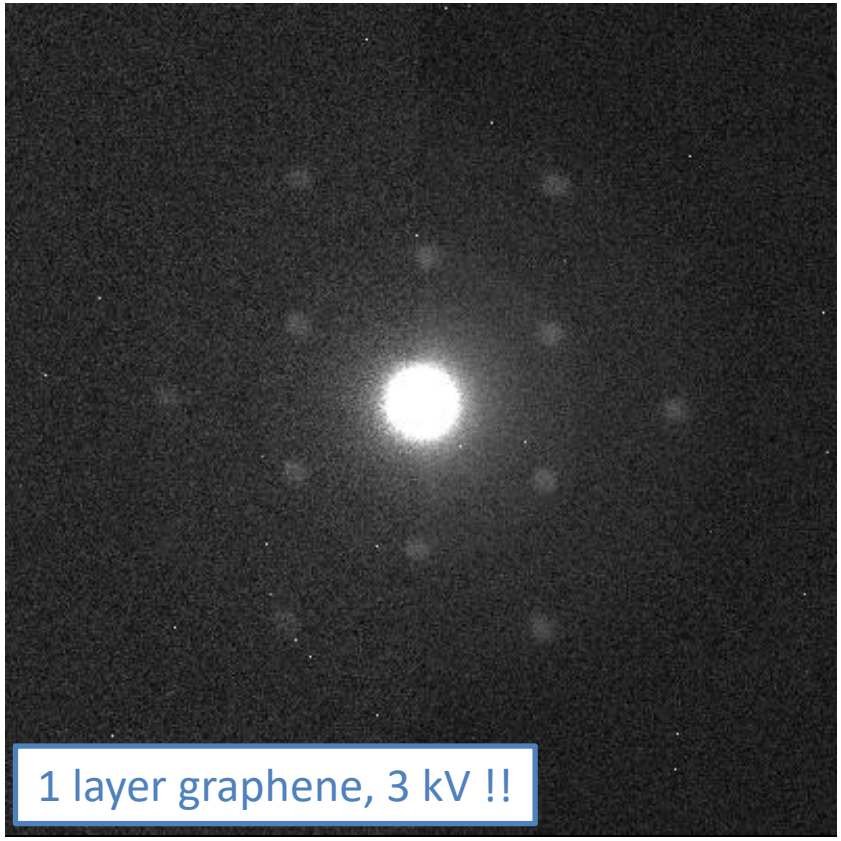

# Lattice Imaging of Ni-Pt CNT

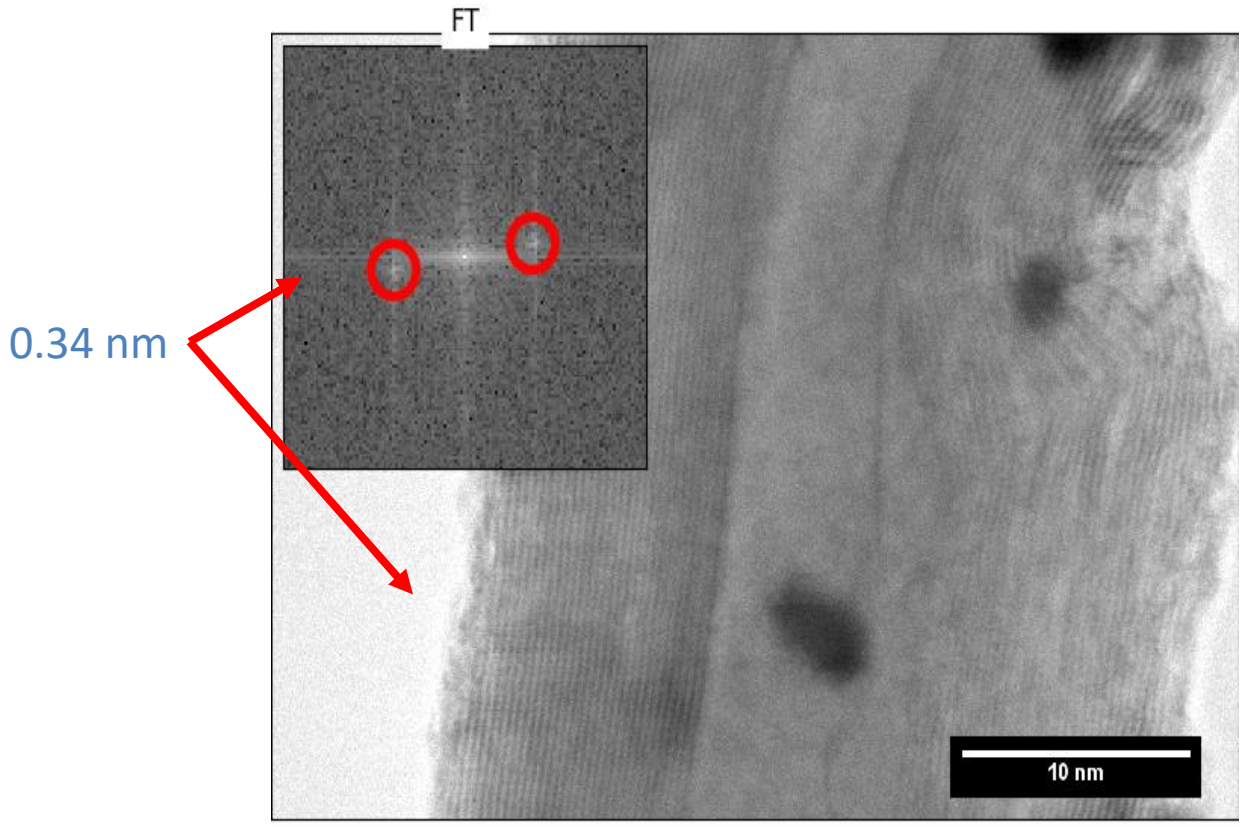

# Electron diffraction in the SEM/STEM (immersion type)

- Convergent beam diffraction

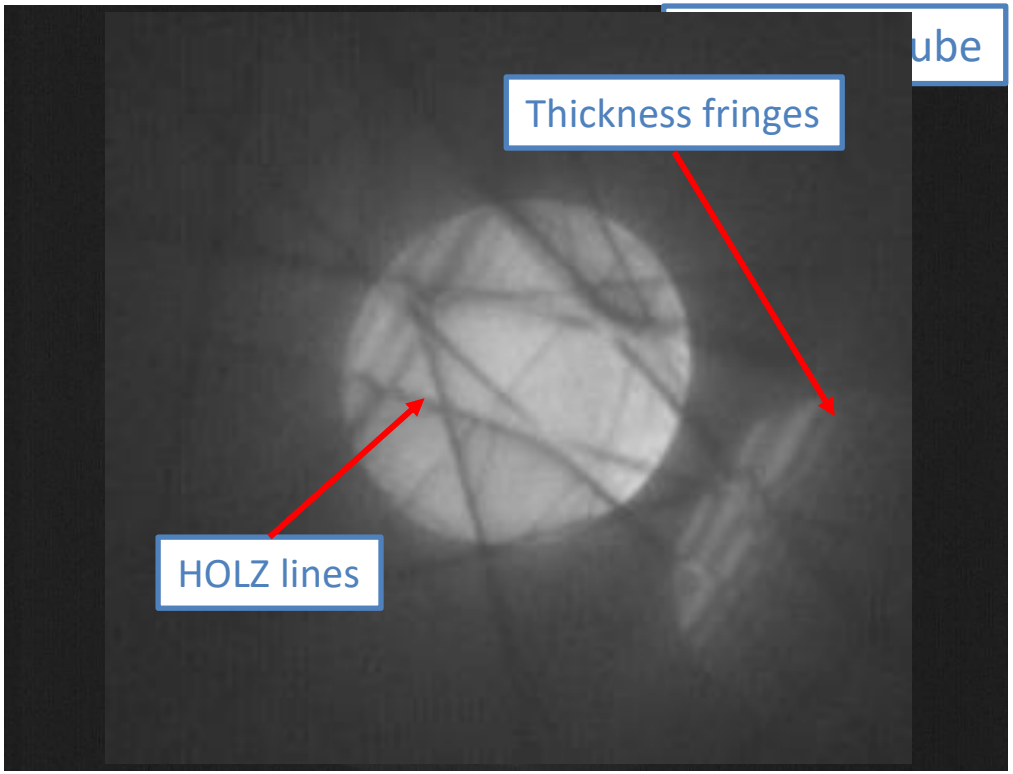


- Thickness measurement
- Lattice constant
- Strain measurement

# Graphene Spot Diffraction

**1 Layer**

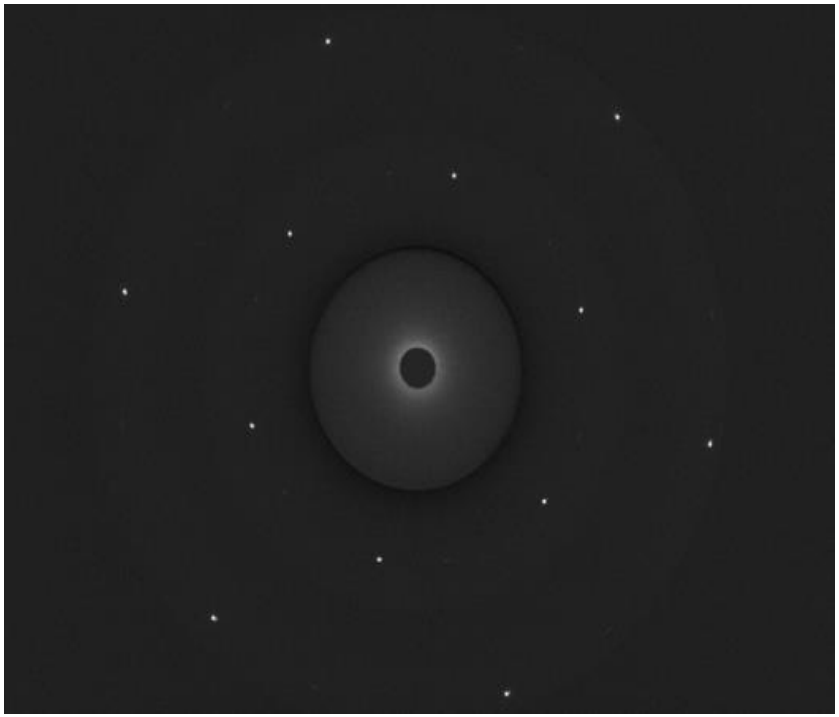

**2 Layers**

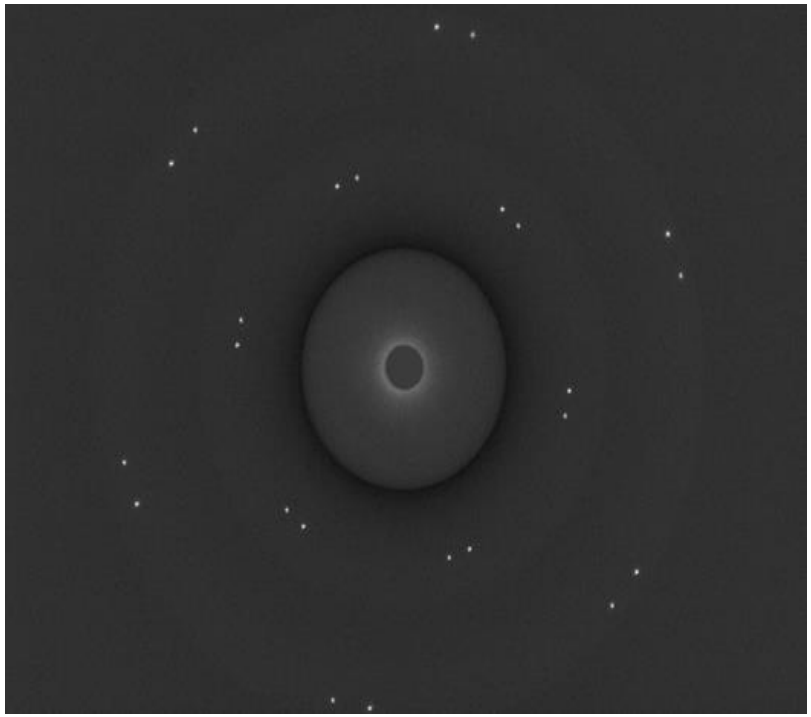

# High Resolution Imaging
# Control of Convergence Angle

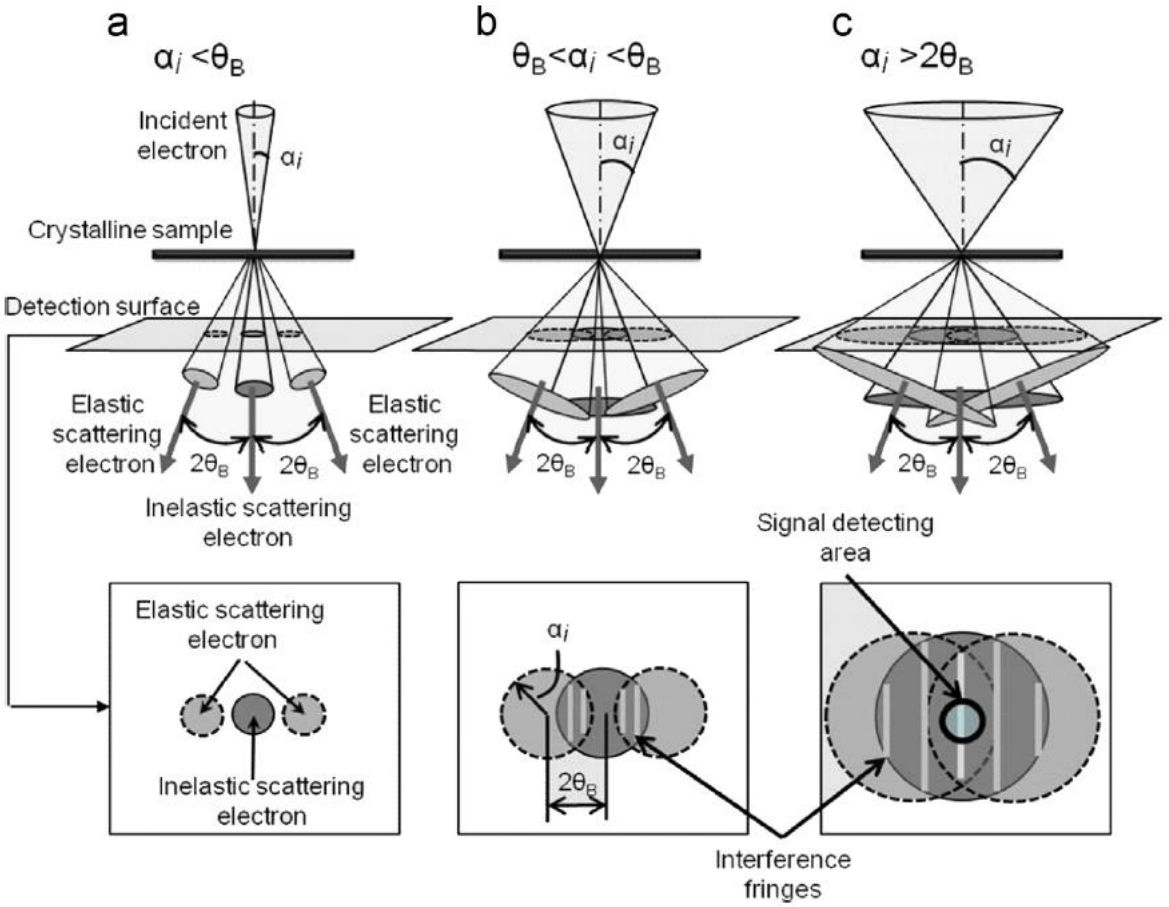

# $Li_2FeSiO_4$

Tecnai 12 BioTwin
TEM at 200 kV

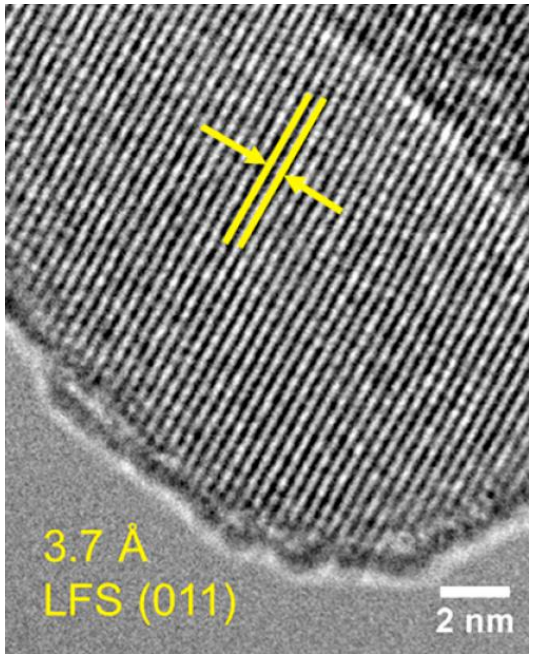


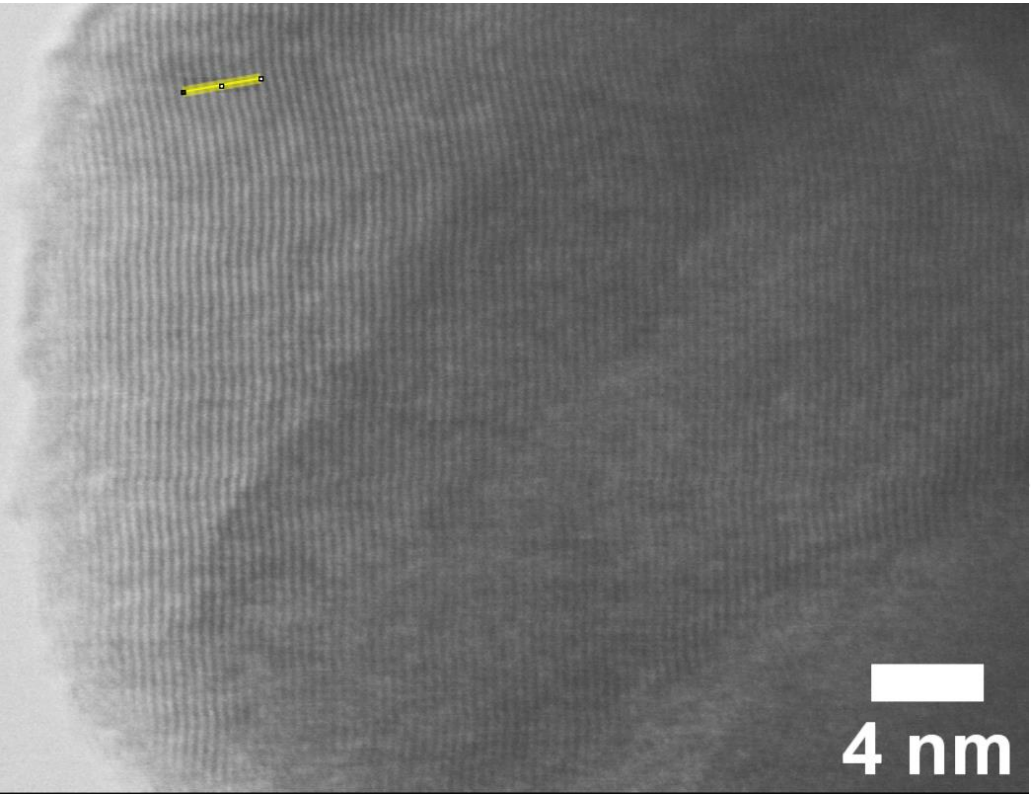


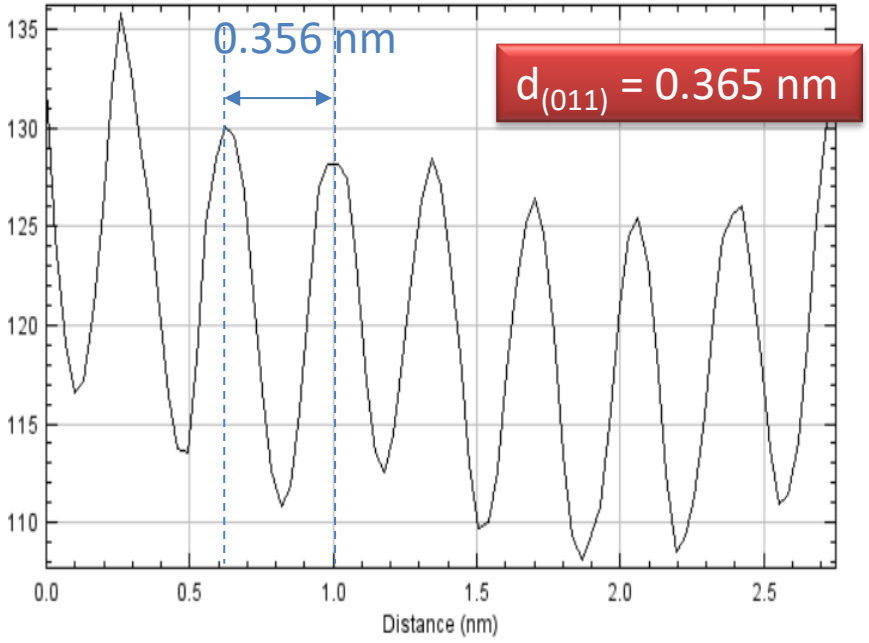

# Al 2099, 30 keV, BF